



Contents lists available at SciVerse ScienceDirect

Annals of Physics

journal homepage: www.elsevier.com/locate/aop



Non-abelian symmetries in tensor networks: A quantum symmetry space approach

Andreas Weichselbaum

Department of Physics, Arnold Sommerfeld Center for Theoretical Physics, and Center for NanoScience, Ludwig-Maximilians-Universität, 80333 Munich, Germany

ARTICLE INFO

Article history:

Received 10 March 2012

Accepted 8 July 2012

Available online 24 July 2012

Keywords:

Non-abelian symmetries

Clebsch–Gordan coefficients

Lie algebra

Numerical renormalization group

Density matrix renormalization group

Tensor networks

ABSTRACT

A general framework for non-abelian symmetries is presented for matrix-product and tensor-network states in the presence of well-defined orthonormal local as well as effective basis sets. The two crucial ingredients, the Clebsch–Gordan algebra for multiplet spaces as well as the Wigner–Eckart theorem for operators, are accounted for in a natural, well-organized, and computationally straightforward way. The unifying tensor-representation for quantum symmetry spaces, dubbed QSpace, is particularly suitable to deal with standard renormalization group algorithms such as the numerical renormalization group (NRG), the density matrix renormalization group (DMRG), or also more general tensor networks such as the multi-scale entanglement renormalization ansatz (MERA). In this paper, the focus is on the application of the non-abelian framework within the NRG. A detailed analysis is presented for a fully screened spin-3/2 three-channel Anderson impurity model in the presence of conservation of total spin, particle–hole symmetry, and SU(3) channel symmetry. The same system is analyzed using several alternative symmetry scenarios based on combinations of U(1)_{charge}, SU(2)_{spin}, SU(2)_{charge}, SU(3)_{channel}, as well as the enveloping symplectic Sp(6) symmetry. These are compared in detail, including their respective dramatic gain in numerical efficiency. In the Appendix, finally, an extensive introduction to non-abelian symmetries is given for practical applications, together with simple self-contained numerical procedures to obtain Clebsch–Gordan coefficients and irreducible operators sets. The resulting QSpace tensors can deal with any set of abelian symmetries together with arbitrary non-abelian symmetries with compact, *i.e.* finite-dimensional, semi-simple Lie algebras.

© 2012 Elsevier Inc. All rights reserved.

E-mail address: Andreas.Weichselbaum@physik.lmu.de.

Contents

1. Introduction	2973
2. MPS implementation of non-abelian symmetries	2976
2.1. General quantum space representation (<i>QSpaces</i>)	2978
2.2. A-tensors and operators	2980
2.3. Multiplicity	2981
2.4. Contractions	2984
2.5. Scalar operators	2985
2.6. Operator matrix elements	2986
2.7. Density matrix and backward update	2987
3. Implications for DMRG and beyond	2988
3.1. Generalized A-tensor for tensor networks	2989
3.2. Two-site treatment	2990
3.3. State space truncation	2991
3.4. Wave function prediction	2992
4. Correlation functions	2992
5. The numerical renormalization group	2994
5.1. Full density matrix	2994
5.2. Model: symmetric three-channel system	2995
6. NRG results	2997
6.1. Spectral functions	2999
6.2. Detailed comparison of symmetry settings	3001
7. Summary and outlook	3002
Acknowledgments	3003
Appendix A. Non-abelian symmetries 101	3003
A.1. Simple example: rotational symmetry	3004
A.2. SU(2) spin algebra	3005
A.3. Generators and symmetry labels	3007
A.4. Example SU(N)	3011
A.5. Decomposition into irreducible representations	3013
A.6. Tensor product spaces	3014
A.7. Irreducible operator sets and Wigner–Eckart theorem	3015
A.8. Several independent symmetries	3017
A.9. Symmetries in physical systems	3017
A.10. The symplectic group Sp(2m)	3027
Appendix B. Numerical implementation	3033
B.1. Tensor product decomposition of symmetry spaces	3033
B.2. State space initialization and operator compactification	3035
Appendix C. Example <i>QSpaces</i>	3036
C.1. Fermionic site with $U(1)_{\text{charge}} \otimes SU(2)_{\text{spin}}$ symmetry	3037
C.2. Fermionic sites in the presence of particle–hole symmetry	3039
C.3. Three channels with $SU(3)$ channel symmetry	3041
References	3046

1. Introduction

Numerical methods for strongly correlated quantum-many-body systems are confronted with exponentially large Hilbert spaces. With a limited number of exact analytical solutions at hand and with perturbative treatments for low-energy or ground-state physics often insufficient, a certain systematic treatment with respect the Hilbert space is required. Besides quantum Monte Carlo approaches, that explore quantum systems in a stochastic way [1], a systematic state space decimation is provided by renormalization group (RG) techniques such as the density matrix renormalization group (DMRG) [2] or the numerical renormalization group (NRG) [3], both highly efficient for quasi-one-dimensional systems, and since non-perturbative, considered essentially exact.

Quantum-many-body Hilbert spaces are built from the direct product of the state spaces of the participating individual particles. As such particle statistics plays an essential role. While the

focus of this paper is on fermionic systems, generalizations to spin systems are straightforward. The treatment of bosonic systems, on the other hand, comes with the additional hurdle that even a single local bosonic degree of freedom already has an infinite state space of its own which must be truncated for numerical treatment. Nevertheless, assuming that the bosonic state spaces can be properly categorized in symmetry sectors, the complications deriving from their infinite dimensionality are considered separate from the issues regarding the description of pure symmetries of the Hamiltonian. In the case of two-dimensional systems finally, more exotic types of particles exist that are neither fermions nor bosons, but anyons. Much attention has been paid to these recently within the framework of tensor networks [4–9]. While the treatment of particles with non-abelian statistics is nicely complimentary to the work presented here, this shall not be pursued any further in what follows.

Methods such as the DMRG or the NRG then, are based on the same algebraic structure of matrix product states (MPSs) [10,11]. Initially introduced for one-dimensional systems with MPS owing its name to this case, a wide range of activity has emerged within recent years to generalize MPSs to tensor-networks for two- or higher-dimensional systems [8,12–14]. While clearly appealing from the point of view of area laws for entanglement-entropy [15–17], tensor network states (TNSs) often share the same disadvantage as linear systems with periodic boundary conditions within the DMRG, namely that state spaces become intrinsically non-orthogonal. Therefore also the unique association of symmetry labels with each index in a tensor is compromised. This, however, can be circumvented by introducing an emerging extra-dimension, which is at the basis of the recently developed multi-scale entanglement renormalization ansatz (MERA) [18,19]. Nevertheless, the *traditional* DMRG approach applied to 2D systems [20] with open or cylindrical boundary conditions yet with long-range interactions has continued to provide a highly competitive, extremely well-controlled, even though numerically expensive approach.

Within both, traditional DMRG as well as NRG, state spaces of entire blocks are built iteratively by adding and merging one site at a time. Clearly, the single index describing an effective basis for the entire block or site can be chosen orthogonal. In addition, basis states can be labeled in terms of the symmetries of the underlying Hamiltonian. Operators written as matrix elements in this very same basis therefore also share the same well-defined partitioning in terms of symmetry sectors. By grouping symmetry state spaces together, the Hamiltonian becomes block-diagonal, while more general operators usually obey well-defined selection rules between symmetry sectors. Consequently, the sparsity of these operators due to symmetry can be efficiently and exactly included in the numerical description, such that usually only a few dense data blocks with non-zero matrix elements remain, given the symmetry constraints. While this well represents the advantage of implementing generic abelian symmetries in a calculation, the presence of non-abelian symmetries offers yet another strong simplification: many of the non-zero matrix elements are actually *not independent* of each other, bearing in mind, for example, the Wigner–Eckart theorem. Therefore going beyond abelian symmetries, non-abelian symmetries allow to significantly *compress* the non-zero blocks in terms of multiplet spaces [21–23]. In particular, this removes the mixing of symmetry sectors, had only abelian symmetries be used, instead. With the Clebsch–Gordan coefficient spaces factorizing [8,9,24], they can be split off systematically in terms of a tensor-product and dealt with separately.

An MPS is optimal for one-dimensional systems. When exploring systems that are not strictly one dimensional but acquire *width*, such as ladders of several rungs in DMRG or multi-channel models in NRG, the price to be paid for orthonormal state spaces is that one must represent the system as a one-dimensional MPS nevertheless. This introduces longer-range interactions to the mapped 1D system, with the effect that the typically required dimensions of the state spaces to be kept in a calculation, grow roughly exponentially with system width. The number of symmetries then that (i) are available and (ii) are also be exploited in practice, decides whether or not a calculation is feasible. Abelian symmetries such as particle (charge Q) or spin (S_z) conservation are usually implemented in DMRG calculations. However, only very few groups have implemented non-abelian symmetries, and these are also constrained to SU(2) symmetries only [21,22], due to its complexity in the actual implementation. General treatment of non-abelian symmetries within the MERA, on the other hand, is currently under development [8,25]. NRG, in contrast, had been set up including non-abelian SU(2) spin symmetry from its very beginning [3], dictated by limited numerical resources. So

far, however, only a very few isolated attempts including more complex non-abelian settings exist within the NRG [26], while to our knowledge there exists no general realization yet of arbitrary non-abelian symmetries in either method.

This paper focuses on the systematic description and implementation of non-abelian symmetries of a given Hamiltonian within the generalized MPS framework through explicit evaluation to Clebsch–Gordan coefficients. This naturally also includes the description of abelian symmetries, as they can be trivially written in terms of Clebsch–Gordan coefficients. While the focus within non-abelian symmetries belongs to $SU(N)$ and the symplectic group $Sp(2n)$, the generalization to other non-abelian symmetries or also point groups is straightforward once their particular Clebsch–Gordan coefficients are worked out. In contrast to the well-known $SU(2)$ then, general non-abelian symmetries, such as $SU(N \geq 3)$, represent a significant increase in algorithmic complexity, in that they can and routinely do exhibit inner and outer multiplicity. The latter, for example, implies that in the decomposition of the tensor-product of two irreducible representations (IREPs) into a direct sum of IREPs, the same IREP may occur *multiple* times. Nevertheless, this can be dealt with properly on the algorithmic level, as will be shown in detail in this paper.

While the presented non-abelian framework for general tensors is straightforwardly applicable to traditional DMRG as well as NRG, the paper focuses on the application within the NRG. Detailed results are presented for a fully screened spin-3/2 Anderson impurity model with $SU(3)$ channel-symmetry [*i.e.* see Hamiltonian in Eq. (27)]. This model has been suggested as the effective microscopic Kondo model for iron impurities in gold or silver [27], historically the first system where Kondo physics was observed experimentally [28,29]. Being a true three-channel system, this cannot be trivially rotated into a simpler configuration of fewer relevant channels. The result is an extremely challenging calculation within the NRG that requires non-abelian symmetries for fully converged numerical results for reasonable coarse-graining of the continuous bath. The non-abelian symmetries present in the model considered are (i) particle–hole symmetry in each of the three channels, $SU(2)_{\text{charge}}^{\otimes 3}$, (ii) total spin symmetry, $SU(2)_{\text{spin}}$, and (iii) channel symmetry, $SU(3)_{\text{channel}}$. The non-abelian particle–hole $SU(2)$ symmetry, however, does *not* commute with the channel $SU(3)$ symmetry, while the plain abelian charge $U(1)$ symmetry does commute. Overall, this suggests a larger enveloping symmetry, which turns out to be the symplectic symmetry $Sp(6)$ [30] [for an introduction to $Sp(2n)$, see Appendix A.10]. With this, the following symmetry scenarios are considered and compared in detail,

$$\begin{aligned} & SU(2)_{\text{spin}} \otimes SU(2)_{\text{charge}}^{\otimes 3}, \\ & SU(2)_{\text{spin}} \otimes U(1)_{\text{charge}} \otimes SU(3)_{\text{channel}}, \quad \text{and} \\ & SU(2)_{\text{spin}} \otimes Sp(6). \end{aligned}$$

While the first setting represents a more traditional setup based on multiple sets of plain $SU(2)$ symmetries only, the second setting already includes the larger channel $SU(3)$ symmetry. Both of these symmetries do not capture the full symmetry of the model, which finally is achieved by using the enveloping $Sp(6)$ symmetry.

Due to the internal two-dimensional structure of the $SU(3)$ symmetry based on the fact that $SU(3)$ has two commuting generators, *i.e.* is of rank 2, its multiplets have significantly larger internal dimension, in practice, up to over a hundred. Therefore despite the reduction of the particle–hole symmetry to a plain abelian symmetry, the second setting with the $SU(3)$ channel symmetry allows to outperform the more traditional setup based on $SU(2)$ symmetries only. Similarly, with $Sp(6)$ a rank-3 symmetry, multiplets then easily reach dimensions of several thousands there, which allows to reduce multiplet spaces significantly further still. A detailed analysis of this is provided in this paper, with a more general self-contained introduction to non-abelian symmetries considered given in the Appendix [cf. Appendix C.3].

From an NRG point of view [31], a few essential steps are required. These are (i) the evaluation of relevant operator matrix elements required to construct the Hamiltonian, (ii) the generic setup of an iteration, adding one site to the so-called Wilson chain, and finally, for thermodynamical properties (iii) also the treatment of the full thermal density matrix [31]. All of these steps are simple in principle, yet come with the essential challenge to have a flexible transparent framework for the treatment

of non-abelian symmetries in practice. In this paper, such a framework is presented in terms of generalized contractions of tensors in the presence of symmetry spaces, introduced as QSpaces below.

The paper is thus organized as follows. Section 2 describes the MPS implementation of non-abelian symmetries in terms of QSpaces. Section 3 points out specific implications for DMRG and more general tensor networks. Section 4 describes the implications for calculating correlation functions in the presence of irreducible operator sets. Section 5 gives a short review of the NRG together with specialties related to non-abelian symmetries, such as calculating reduced density matrices. This section also introduces the model Hamiltonian of a fully symmetric 3-channel Anderson model. Section 6 then presents explicit NRG results, followed by summary and outlook. Finally, also an extended Appendix has been added to the paper. The latter is intended to provide a more general pedagogical self-contained introduction to non-abelian symmetries as they occur in fermionic lattice models, together with their actual implementation in practice in terms of QSpaces.

2. MPS implementation of non-abelian symmetries

Consider some Hamiltonian \hat{H} that is invariant under a set of n_s symmetries,

$$\mathcal{S} \equiv \bigotimes_{\lambda=1}^{n_s} \mathcal{S}^\lambda, \quad (1)$$

that is, $[\hat{H}, \hat{S}_\alpha^\lambda] = 0$, where α identifies the generator \hat{S}_α^λ for the simple (non-abelian) symmetry \mathcal{S}^λ . To be specific, for example, $\mathcal{S} = \text{SU}(2)_\text{spin} \otimes \text{SU}(2)_\text{charge} \equiv \mathcal{S}^1 \otimes \mathcal{S}^2$ with $\lambda \in \{1, 2\}$ would stand for the combination of spin and charge SU(2) symmetry, respectively. The tensor-product notation in Eq. (1) indicates that the symmetries act independently of each other, that is $[\hat{S}_\alpha^\lambda, \hat{S}_{\alpha'}^{\lambda'}] = 0$ for $\lambda \neq \lambda'$.

Given the symmetries as in Eq. (1), this allows to organize the complete basis of eigenstates of \hat{H} in terms of the symmetry eigenbasis. Every state then belongs to a well-defined irreducible multiplet q^λ for each symmetry \mathcal{S}^λ . The multiplet itself has an internal state space structure that is described by the additional quantum labels q_z^λ . For example, in the case of $\mathcal{S}^\lambda = \text{SU}(2)$, q^λ (q_z^λ) corresponds to the spin multiplet S (the S_z label), respectively.

Thus all states in a given vector space can be categorized using the hierarchical label structure

$$|qn; q_z\rangle \quad (\text{state-space label structure}), \quad (2)$$

where

- (i) $q \equiv (q^1, q^2, \dots, q^{n_s})$, to be referred to as *q-labels* (quantum labels), references the irreducible representations (IREPs) for each symmetry \mathcal{S}^λ , $\lambda = 1, \dots, n_s$. All states in given Hilbert space with the same *q*-labels are *blocked* together, to be referred to as *symmetry block q*.
- (ii) Given a symmetry block q then, the multiplet index $n_{(q)}$ identifies a specific multiplet within this space. It is therefore a plain index associated with given symmetry space q . Together with the *q*-labels, this forms the *multiplet level* which is considered the topmost conceptual level. Using the composite notation (qn) to identify an arbitrary multiplet, the subscript q to the multiplet index $n_{(q)}$ is considered implicit and hence is dropped, for simplicity.
- (iii) Finally, the set of labels $q_z \equiv (q_z^1, q_z^2, \dots, q_z^{n_s})$, to be referred to as *z-labels*, resolves the internal structure of each multiplet in q . That is, for each IREP q^λ , referring to the symmetry \mathcal{S}^λ in q , q_z^λ labels its internal IREP space. As such, the *z*-labels are entirely defined by the symmetries considered. By construction, the eigenstates of the Hamiltonian \hat{H} are fully degenerate in the *z*-labels.

Here the symmetry labels q and q_z describe the combined record of labels derived from all symmetries considered. In practice, states can mostly be treated on the higher multiplet level, while the lower level in terms of the *z*-labels is split off and taken care of by Clebsch–Gordan algebra and the coefficient spaces derived from it.

When non-abelian symmetries are broken, they are often reduced to their abelian subalgebra. This can be easily implemented, nevertheless, consistent with the presented framework. In particular, in

the abelian case, the non-abelian multiplet labels q are absent, while the abelian q_z quantum numbers remain. Therefore the q_z labels can be promoted to the status of q -labels, $q := q_z$. As a consequence, the concept of the actual q_z labels becomes irrelevant (therefore subsequently, the q_z label space may simply be set to zero, $q_z := 0$). The corresponding Clebsch–Gordan coefficients are all trivial scalars, i.e. equal to 1. Yet these ‘‘Clebsch–Gordan coefficients for abelian symmetries’’ do maintain an important role, in that they take care of the proper addition rules that come with abelian symmetries, resulting in $\langle q_1; q_2 | q \rangle = 1 \cdot \delta_{q_1+q_2}$.

Given the MPS background of NRG or DMRG, states spaces are generated iteratively, in terms of a product-space of a given effective state space with a newly added local site. Operators, on the other hand, are typically represented in local state spaces, and starting from there, they can be written in terms of matrix elements in the effective global state spaces. With this in mind, the implementation of non-abelian symmetries within the MPS framework therefore is based on the following two basic observations with respect to state space and operator representations, respectively.

- (1) State spaces: consider two distinct state spaces, $|Qn; Q_z\rangle$ and $|ql; q_z\rangle$ that, for example, represent a large effective state space and a small new local state space, respectively. Assuming that both state spaces are well-categorized in terms of IREPs, then their tensor-product space can also be decomposed into a direct sum of new combined IREPs $|\tilde{Q}\tilde{n}; \tilde{Q}_z\rangle$ using Clebsch–Gordan coefficients (CGCs),

$$|\tilde{Q}\tilde{n}; \tilde{Q}_z\rangle = \sum_{Qn; Q_z} \sum_{ql; q_z} (A_{Q\tilde{Q}}^{[q]})_{n\tilde{n}}^{[l]} \cdot C_{Q_z \tilde{Q}_z}^{[q_z]} |Qn; Q_z\rangle |ql; q_z\rangle. \quad (3)$$

Note that the Clebsch–Gordan coefficients given by $C_{Q_z \tilde{Q}_z}^{[q_z]} \equiv \langle QQ_z; qq_z | \tilde{Q}\tilde{Q}_z \rangle$ (i) fully define the internal multiplet space as specified by the Lie algebra, and (ii) determine the splitting, i.e. which output multiplets \tilde{Q} occur for given multiplets Q and q . On the multiplet level, on the other hand, where $(A_{Q\tilde{Q}}^{[q]})_{n\tilde{n}}^{[l]}$ combines the multiplets Qn and ql into the multiplet $\tilde{Q}\tilde{n}$ consistent with the splitting provided by the CGCs, the coefficients $(A_{Q\tilde{Q}}^{[q]})_{n\tilde{n}}^{[l]}$ may encode an arbitrary unitary transformation within the \tilde{n} output space for each \tilde{Q} . The r.h.s. of Eq. (3) demonstrates, that the CGC spaces clearly factorize from the multiplet space $A_{Q\tilde{Q}}^{[q]}$ as a tensor product.

- (2) Operators: within some state space $|Qn; Q_z\rangle$, the matrix elements of an irreducible operator (IROP) set \hat{F}^q [i.e. a set of operators that transforms according to multiplets q for given symmetries; cf. Eq. (A.3b), or also Appendix A.7] can be written using the Wigner–Eckart theorem as [32]

$$\langle Q'n'; Q'_z | \hat{F}_{q_z}^q | Qn; Q_z \rangle = (F_{QQ'}^{[q]})_{nn'}^{[1]} \cdot C_{Q_z Q'_z}^{[q_z]}, \quad (4)$$

with $C_{Q_z Q'_z}^{[q_z]}$ again the Clebsch–Gordan coefficients as in Eq. (3). On the multiplet level, the reduced matrix elements $(F_{QQ'}^{[q]})_{nn'}^{[1]} \equiv \langle Q'n' | \hat{F}^q | Qn \rangle$ refer to the single irreducible operator set labeled by q , which is indicated by the superscript [1]. The Wigner–Eckart theorem thus allows to compactify the operator matrix elements on the l.h.s. of Eq. (4) as the tensor-product of reduced matrix elements and CGCs, as shown on the r.h.s. of Eq. (4).

Therefore in both cases above, i.e. in all tensor objects relevant for a numerical calculation, the CGC spaces factorize. This allows to strongly compress their size, and thus to drastically improve on overall numerical performance. Moreover, note that in both cases, Eq. (3) as well as Eq. (4) the underlying structure comprises tensors of rank-3 throughout. This rank-3 structure holds for both, the reduced multiplet space as well as the CGC spaces. Therefore, in either case, the final data structure of either state space decomposition as well as reduced operator sets is exactly the same. It is implemented, in practice, in terms of what will be referred to as QSpace for general tensors of arbitrary rank.

2.1. General quantum space representation (QSpaces)

The generic representation, used in practice to describe all symmetry related tensors B , is given by a listing of the following type,

$$B \equiv \left\{ \begin{array}{c|c|c} q\text{-labels} & \text{reduced space } \|B\| & \text{CGC spaces} \\ \hline \{Q\}_1 & B_1 & \{C\}_1 \\ \{Q\}_2 & B_2 & \{C\}_2 \\ \dots & \dots & \dots \end{array} \right\}. \quad (5)$$

By notational convention, an actual operator \hat{B} will be written with a hat, while its representation in terms of matrix elements in a specific basis will be written without the hat, hence the corresponding QSpace is referred to as QSpace B . Many explicit examples of QSpaces are introduced and discussed in detail in Appendix C. As an up-front illustration, consider, for example, the general Hamiltonian of a single spinful fermionic site in the presence of SU(2) symmetry in the spin (S) and charge sector (C), which can be written as the QSpace [see Eq. (C.8)]

$$H \equiv \left\{ \begin{array}{c|c|c|c} (S; C) & (S'; C') & \|H\| & \text{CGC spaces} \\ \hline \frac{1}{2}; 0 & \frac{1}{2}; 0 & h_{\frac{1}{2}, 0} & \mathbf{1}^{(2)} \quad 1. \\ 0; \frac{1}{2} & 0; \frac{1}{2} & h_{0, \frac{1}{2}} & 1. \quad \mathbf{1}^{(2)} \end{array} \right\}. \quad (6)$$

With every non-zero block listed as an individual row, one can see that the only two reduced matrix elements $\|H\|$ free to choose without compromising the $SU(2)_{SC}^{\otimes 2} \equiv SU(2)_{\text{spin}} \otimes SU(2)_{\text{charge}}$ symmetry are the parameters (numbers) $h_{1/2, 0}$ and $h_{0, 1/2}$. By definition, the Hamiltonian is a scalar operator, therefore it is the only operator within its IROP, hence can be written as plain rank-2 QSpace (the third dimension for this IROP would be a singleton dimension, hence can be dropped). Being a scalar operator, the Hamiltonian is block diagonal, which is reflected in equal symmetry sectors ($S; C$) and ($S'; C'$) in each row for the first and the second dimension, respectively. Moreover, in given case, the corresponding Clebsch–Gordan coefficient (CGC) spaces also result in trivial identities, with $\mathbf{1}^{(2)}$ the two-dimensional identity. Note that the full set of CGC spaces in each row needs to be interpreted as appearing in a tensor product with the multiplet space, here the reduced matrix elements $h_{1/2, 0}$ or $h_{0, 1/2}$ [e.g. see Eq. (8) below].

In general, the representation of a tensor B of arbitrary rank- r in the QSpace in Eq. (5) [with Eq. (6) an example for a rank-2 QSpace], only lists the non-zero, *i.e.* relevant symmetry combinations. Having r tensor dimensions, each of its r indices refers to its specific state space $|qn; q_z\rangle_i \equiv |(q_i)n_i; (q_z)_i\rangle$ with $i = 1, \dots, r$, and hence carries its own label structure as in Eq. (2). The q -labels $(q)_i \equiv \{q^\lambda\}_i$ already represent the *combined* set of n_S IREP labels from all symmetries δ^λ for the state space at tensor dimension i . In general, by convention, the internal order of the q -labels $(q)_i$ w.r.t. λ is fixed and follows the order of symmetries used in Eq. (1).

For a certain row v of the QSpace listing in Eq. (5) then, the set of r q -labels are grouped into

$$\{Q\}_v \equiv \{(q)_1, \dots, (q)_r\}_v. \quad (7a)$$

The reduced matrix elements are stored in the dense rank- r tensor B_v indexed by n_i with $i = 1, \dots, r$. This is a plain tensor, with the multiplet spaces possibly already rotated by arbitrary unitary transformations and truncated. This is also reflected in the fact that the indices n_i are plain indices, *i.e.* carry no further internal structure. Finally, for every one of the $\lambda = 1 \dots n_S$ symmetries included, the corresponding CGC space is stored in the sparse tensors $C_{\lambda, v}$, *each of which is also of rank r*. These CGC spaces are grouped into $\{C\}_v$ in the last column,

$$\{C\}_v \equiv \{C_{1, v}, \dots, C_{n_S, v}\}. \quad (7b)$$

As the q -labels $\{Q\}_v$ also define the z -labels, there is no explicit need to store the z -labels $(q_z)_{i, v}$. The internal running indices in $C_{\lambda, v}$, however, are uniquely associated with the z -labels. Note also the different index setting: in contrast to Eq. (7a), which contains a set of r q -labels, *i.e.* one for every

dimension of the rank- r tensor B , Eq. (7b) contains a set of n_s rank- r CGC spaces, i.e. one for every symmetry.

In addition to the QSpace listing in Eq. (5), also the type and order of symmetries considered is stored with a QSpace, cf. Eq. (1), even though this is usually the same throughout an entire calculation. Moreover, note that the row or record index v in Eq. (5) is purely for convenience without any specific meaning, as the order of records in a QSpace can be chosen arbitrarily. Nevertheless, it is required to refer to a specific entry in a QSpace.

For a given record v in the QSpace in Eq. (5) then, the reduced space and the CGC spaces are to be interpreted as an overall tensor-product,

$$B_v \otimes \{C\}_v \equiv B_v \otimes \left(\bigotimes_{s=1}^{n_s} C_{s;v} \right), \quad (8)$$

which, of course, is never explicitly reexpanded into a single full object at any step, in practice. Eq. (8) rather demonstrates the single most important motivation to implement non-abelian symmetries in a numerical computation. By splitting off the CGC spaces in terms of a tensor product, block dimensions can be *strongly* reduced for larger calculations with several symmetries present. For the models analyzed in this paper, for example, this was typically an average dimensional reduction from plain abelian symmetries by a factor of 10 up to several hundreds. Considering that both NRG and DMRG scale like $\mathcal{O}(D^3)$ with D the typical dimension of data blocks, this is an enormous gain in efficiency. The factorized CGC spaces, on the other hand, can be dealt with independently, as will be explained in detail later. Assuming that usually the dimensions of the reduced states spaces B_v still exceed by far the typical dimensions encountered for the CGC spaces, the latter bear little numerical overhead. Only for larger-rank symmetries, such as the symmetry $Sp(6)$ discussed later, multiplet dimensions can become large themselves such that one needs to pay more attention to an efficient treatment of their corresponding CGC spaces [see Appendix C.3.2].

For QSpaces where the CGC spaces in Eq. (5) exactly correspond to the standard Clebsch–Gordan coefficients for each symmetry, one may argue similar to the z -labels, that actually it is not explicitly necessary to store the CGC spaces together with the QSpace, since these are known. This is true, indeed, for these particular cases, and CGC spaces may simply be referenced then. Nevertheless, the explicit storage of the CGC spaces with a QSpace as in Eq. (5) has practical value. When combining QSpaces through contractions, i.e. sum over shared indices, for example, quite frequently *intermediate* objects can arise that do have rank different, in particular also larger than 3 [e.g. see the intermediate objects X indicated by the dashed boxes in Fig. 4]. These then elude a description in terms of standard rank-3 CGCs. In this case, the actual CGC spaces for intermediate QSpace are important, and even though they do not necessarily resemble the interpretation of the original standard rank-3 spaces of standard Clebsch–Gordan algebra anymore, these spaces will be referred to as CGC spaces nevertheless, owing to their origin.

Furthermore, for specific algorithms such as NRG and DMRG, on a global level one typically deals with simple scalar operators such as the Hamiltonian or a density matrix, apart from intermediate steps where complex CGC structures can arise. Therefore the full sequence of contractions on the CGC level [e.g. see Fig. 4] can be replaced by analytical expressions or sum rules for Clebsch–Gordan coefficients. In particular, in many situations the explicit knowledge of 3j- and 6j-symbols, or more general (3n)-j symbols, appears sufficient [7,22,24,33,34] with current applications in this direction again mainly restricted at most to SU(2). If the (3n)-j symbols were known for arbitrary non-abelian symmetry, the explicit storage of the CGC spaces with the QSpaces would no longer be required, indeed, and could be avoided altogether. Note, however, that (3n)-j symbols require specific contractions which must be implemented within the code dependent on the context. While vast literature exists on (3n)-j symbols, this is limited to an overwhelming extent on the relatively simple symmetry of SU(2), for which analytic expressions exist, indeed. For arbitrary non-abelian symmetries, however, the (3n)-j symbols may or may not be known [35]. For the QSpace as outlined in this paper, on the other hand, no special treatment is required for specific contractions, and no explicit knowledge of possibly symmetry dependent CGC sum rules is required. The QSpace approach solely relies on the correct construction of the standard CGC spaces to start with, with the subsequent

sums over CGC spaces performed explicitly numerically and not analytically through *exactly* the same contraction as on the reduced multiplet level, as discussed in more detail later.

Finally, the explicit inclusion of the CGC spaces allows to build in strong consistency checks in the actual numerical implementation. Imagine that the Hamiltonian is built by a sequence of complex contractions. The Hamiltonian eventually must be a scalar operator, *i.e.* it is block diagonal in the symmetries and the CGC spaces reduce to plain identities. This can simply be checked at the end of the calculation, which thus provides a strong check of whether the symmetries have been implemented correctly or not. At the stage of intermediate contraction, however, the CGC spaces guarantee the correct splitting and weight distribution between different emerging symmetry sectors.

2.2. A-tensors and operators

Consider the prototypical MPS scenario as in Eq. (3) that takes some previously constructed state space $|i\rangle \equiv |Qn; Q_z\rangle$ and adds a new local state space $|\sigma\rangle \equiv |ql; q_z\rangle$, *e.g.* a new physical site. The state spaces are thus combined in a product-space described in terms of the IREPs $|j\rangle \equiv |\tilde{Q}\tilde{n}; \tilde{Q}_z\rangle$. Here the states i , σ , and j are introduced as notational shorthand for better readability. The product space then is spanned by $|i\sigma\rangle \equiv |\sigma\rangle|i\rangle$. The order of states in the latter product emphasizes that state $|\sigma\rangle$ is typically added *after* and thus onto the existing state $|i\rangle$, which is of particular importance for fermionic systems. In general, the combined states [36,37]

$$|j\rangle = \sum_{l\sigma} |i\sigma\rangle \underbrace{\langle i\sigma|j\rangle}_{=A_{ij}^{[\sigma]}}, \quad (9)$$

are described in terms of linear superpositions of the product space $|i\sigma\rangle$ given by the coefficients $A_{ij}^{[\sigma]}$, henceforth called *A-tensor* (rank-3) or $A^{[\sigma]}$ -matrices (rank-2). Without truncation, $A_{ij}^{[\sigma]}$ denotes a full unitary matrix $U_{(i\sigma),j}$ where the round bracket indicates that the indices i and σ have been *fused*, *i.e.* combined into an effective single index. The presence of symmetry and the proper categorization of state spaces, however, imposes certain constraints on this unitary matrix, as pointed out already with Eq. (3). In particular, the fully determined CGC spaces $C_{Q_z \tilde{Q}_z}^{[q_z]}$ factorize from the *A-tensor*, allowing an arbitrary rotation in the reduced multiplet space $A_{Q\tilde{Q}}^{[q]}$ only. For the specific case then, that the reduced multiplet spaces are identical to partitions of identity matrices with a clear one-to-one correspondence still of input and output multiplets, the corresponding *A-tensor* will be referred to as the *identity A-tensor* [see Fig. 2 later; for explicit examples, see Eq. (C.4) or Eq. (C.6)]. An identity *A-tensor* therefore represents the full state space still without any state space truncation, and is unique up to permutations in the combined output space. Its explicit construction is a convenient starting point, in practice, when merging new local state spaces with existing effective state spaces.

The entire construction of an *A-tensor* can be encoded compactly in terms of a rank-3 QSpace. Both coefficient spaces in Eq. (3), $C_{Q_z \tilde{Q}_z}^{[q_z]}$ as well as $A_{Q\tilde{Q}}^{[q]}$, directly enter the QSpace description in Eq. (5). A schematic pictorial representation of an *A-tensor* is given in Fig. 1. There the states i (j) represent the open composite index to the left (right), respectively, while σ refers to the open composite index at the bottom.

As already argued with Eq. (4), an irreducible operator shares exactly the same underlying CGC structure as an *A-tensor*. Thus also its representation in terms of a QSpace is *completely analogous*. Consider an IROP set $\hat{F}^q \equiv \{\hat{F}_{q_z}^q\}$, which transforms according to IREP q . Here, the composite index $\sigma \equiv (ql; q_z)$, for short, identifies the specific operators in the IROP set. As already indicated by the superscript [1] in Eq. (4), its associated multiplet index l has the trivial range $l = 1$, since, by definition, the IROP represents a single IREP on the operator level. With the states $|i\rangle \equiv |Q'n'; Q'_z\rangle$ and $|j\rangle \equiv |Qn; Q_z\rangle$ now representing the same state space within which the operator acts, with usually many multiplets and different symmetries, the operator representation of the IROP \hat{F}^q in the states $\langle i|$ and $|j\rangle$ is evaluated using the Wigner-Eckart theorem in Eq. (4). Similar to the *A-tensor* earlier, the resulting factorization of the CGC spaces $C_{Q_z \tilde{Q}_z}^{[q_z]}$ together with the remaining multiplet space $F_{Q\tilde{Q}}^{[q]}$ of reduced matrix elements directly enter the QSpace description in Eq. (5).

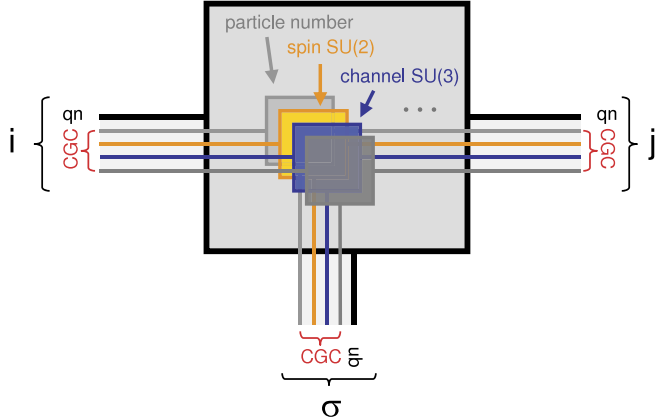


Fig. 1. (Color online) Schematic depiction of a rank-3 QSpace as an example for a basic building block for an MPS or a tensor network, where lines (boxes) represent indices (data spaces), respectively. Every index is assumed to refer to a state space with similar physical background, hence refers to the same global symmetries as in Eq. (1), and has the generic composite structure $|qn; q_z\rangle$ as in Eq. (2), where q_z specifies the states within the CGC spaces. The rank-3 QSpace depicted can be interpreted in two entirely different ways while sharing exactly the same underlying algebraic structure. These are (i) the state space decomposition into IREPs and (ii) operator representation for a given IROP in a given basis (see text). For the general interpretation of the QSpace depicted, consider for simplicity a single row v in Eq. (5). The set $\{Q\}_v$ defines the q -labels for all tensor dimensions (here a total of three). For given q -labels then, the corresponding multiplet indices n keep track of the reduced multiplet spaces. These are typically large still, as indicated by the thick black lines for each tensor dimension. The corresponding reduced rank-3 multiplet space A_v is depicted by the large gray box in the background. With the q -labels fixed, this also specifies the IREPs for every tensor dimension and every symmetry. The corresponding sparse CGC spaces are indicated by the small boxes around the center, with one box for every symmetry. Examples are abelian particle conservation, non-abelian spin SU(2), non-abelian channel SU(3), or other. By construction, all CGC spaces share the same rank as the underlying QSpace. Therefore each CGC space also has three lines attached, one for every tensor dimension. For non-abelian symmetries, in general the CGC spaces refer to finite multiplet dimensions, while for simpler symmetries, such as abelian symmetries, the CGC spaces actually become trivial, *i.e.* scalars. These, nevertheless, are also interpreted as having the same rank as the QSpace by using singleton dimensions wherever required.

So even though an operator is usually considered a rank-2 object, the fact that an IROP consists of an operator set indexed by σ , adds a *third* index to the QSpace. In contrast to the state interpretation of σ for the A -tensor above, however, here the “index” σ has a different interpretation in that it points to a specific operator in the IROP set. By convention, the operator index σ will always be listed as third tensor dimension in its QSpace representation. Given the three-dimensional representation of a general IROP, therefore its entire construction mimics the construction of an A -tensor in terms of a QSpace. As a consequence, Fig. 1 exactly also resembles the QSpace structure of an IROP. The states i (j) used for the calculation of the matrix element represent the open index to the left (right), respectively, while the operator index σ refers to the open index at the bottom.

Scalar operators, finally, such as the Hamiltonian of the system or density matrices, represent a special case, since there the IROP set contains just a single operator. Therefore the third index, *i.e.* the *operator index*, becomes a singleton and hence can simply be dropped [*e.g.* see Eq. (6)]. Scalar operators therefore are represented by rank-2 QSpaces. They are block-diagonal in their symmetries, and their CGC spaces are all equal to identity matrices, with an example already given in Eq. (6).

2.3. Multiplicity

For general non-abelian symmetries, frequently inner and outer multiplicity occur [38,39]. Both are absent in SU(2), yet do occur on a regular basis for $SU(N \geq 3)$. Inner multiplicity describes the situation where for a given IREP, several states may share exactly the *same* z -labels. Let m_z^q denote the number of times a specific z -label occurs within IREP q . Then the presence of inner multiplicity implies $m_z^q > 1$ for at least one z -label. Within such degenerate subspaces an arbitrary rotation

is allowed in principle. For global consistency, therefore the CGC spaces must adopt a well-defined internal convention on how to deal with inner multiplicity. This issue, however, is entirely contained within the CGC algebra, which is explored in more detail in the [Appendix A](#) [e.g. see discussion following Eq. [\(A.19\)](#), and [Appendix B.1](#)]. On the level of a QSpace, it is of no further importance otherwise. Essentially, the only implication of inner multiplicity is $q_z \rightarrow (q_z, \alpha_z)$ with $\alpha_z = 1, \dots, m_z^q$ [*cf.* Eq. [\(A.19\)](#)], where m_z^q depends on the multiplet q . With this minor adjustment, it is assumed throughout that the z -labels fully identify the internal multiplet space. Note that, in practice, the extra label α_z is never included explicitly. What is important, however, is a *consistent internal multiplet ordering* that respects multiplicity [see [Appendix B.1](#)].

Outer multiplicity, on the other hand, describes the situation where in the state space decomposition of a product-space of two IREPs, q_1 and q_2 , the *same* output IREP q may appear multiple times, the number of which is specified by $M_q^{[q_1, q_2]}$ [*cf.* Eqs. [\(A.35\)–\(A.38\)](#) and discussion]. Therefore outer multiplicity primarily also enters at the level of Clebsch–Gordan coefficients, as it is based on pure symmetry considerations. In contrast to inner multiplicity, however, outer multiplicity also affects the reduced multiplet space, as will be elaborated upon in what follows.

In the absence of outer multiplicity [*i.e.* $M_q^{[q_1, q_2]} \leq 1$ for all q_1, q_2 , and q of the symmetry, an example being $SU(N \leq 2)$], all rows in the QSpace in Eq. [\(5\)](#) must have *unique* $\{Q\}_v$. If this is not the case, then the rows can be made unique by combining the rows with the same $\{Q\}$. Assume, for example, $\{Q\}_v = \{Q\}_{v'}$ with $v \neq v'$: clearly, the $\{Q\}$'s are already the same. Having the *same* symmetry labels, this refers to the same set of IREPs, hence also the CGC spaces of these records must be identical, up to a possible global normalization factor which can be associated with the multiplet space, instead. Furthermore, given $\{Q\}_v = \{Q\}_{v'}$, the A_v and $A_{v'}$ data blocks do live in *exactly* the same vector spaces for each individual tensor dimension! Therefore A_v and $A_{v'}$ can be simply added up [here multiple contributions with the same $\{Q\}$ are considered additive, consistent with general conventions regarding sparse tensors; otherwise, say having given the same matrix element twice with different values, would immediately lead to contradictions].

In the presence of outer multiplicity, on the other hand, the uniqueness of the q -labels $\{Q\}_v$ in the QSpace in Eq. [\(5\)](#) has to be relaxed. The reason for this is as follows. Since outer multiplicity derives from the Clebsch–Gordan algebra as in Eq. [\(A.38\)](#), the CGC spaces

$$C_{Q_z \tilde{Q}_z}^{[q_z]} \rightarrow C_{Q_z \tilde{Q}_z, \alpha}^{[q_z]} \equiv \langle QQ_z; qq_z | \alpha \tilde{Q}, \tilde{Q}_z \rangle \quad (10)$$

acquire an additional label $\alpha = 1, \dots, M_{\tilde{Q}}^{[Q, q]}$ [different from the α_z used with inner multiplicity], where $M_{\tilde{Q}}^{[Q, q]}$ indicates the outer multiplicity in \tilde{Q} , given the product space of the IREPs Q and q . In terms of a QSpace object, one may therefore be tempted to enlarge the CGC space from rank-3 to rank-4, with the dimension of the 4th index being equal to $M_{\tilde{Q}}^{[Q, q]}$. This strategy alone, however, does not capture the full picture since outer multiplicity also *enlarges* and thus effects the multiplet space A_v of an A -tensor. By definition, outer multiplicity means that *different* multiplets with the same q can emerge. The only way they can be distinguished is through their Clebsch–Gordan coefficients. Therefore rather than enlarging the CGC space in a QSpace, $M_{\tilde{Q}}^{[Q, q]}$ records with the *same* $\{Q\}_v$ are allowed, instead. These records have CGC spaces of the same rank-3 dimensions, which, however, are clearly distinguishable, as they are orthogonal to each other [*cf.* Eq. [\(A.39\)](#)]. The $M_{\tilde{Q}}^{[Q, q]}$ sets of Clebsch–Gordan coefficients arising from outer multiplicity are thus spread over $M_{\tilde{Q}}^{[Q, q]}$ records within a QSpace object.

The situation in the multiplet space for an identity A -tensor is depicted schematically in [Fig. 2](#). In the absence of outer multiplicity, each symmetry combination $(q, q')_i$ can only contribute at most once to a given symmetry space q'' and gets its space allocated, as depicted, for example, for $(q, q')_4$ in [Fig. 2\(a\)](#), having only one non-zero block (shaded block) within the q'' output multiplet. The symmetry combinations $(q, q')_1$ and $(q, q')_2$, on the other hand, show outer multiplicity, in that they result twice in the same multiplet q'' , *i.e.* $M_{q''}^{[q, q']_1} = M_{q''}^{[q, q']_2} = 2$.

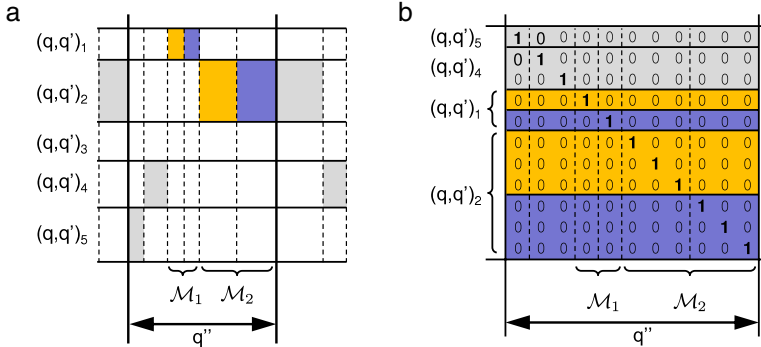


Fig. 2. Effect of outer multiplicity on multiplet space (A_v) in terms of an identity A -tensor—Panel (a) Schematic depiction of the state space decomposition of two input multiplet spaces with unique symmetry combinations (q, q') into combined multiplets q'' (rows and columns, respectively). State spaces of the same symmetry are grouped into blocks separated by solid lines (horizontally and vertically). For simplicity, an identity A -tensor is depicted, for which the individual sectors in q'' can be uniquely associated with the (q, q') they originate from. Hence each column, separated by solid lines, has exactly one shaded block considered non-zero, with all-zero blocks shown in white. Here vertical thin lines indicate sub-blocks that originate from different (q, q') , yet are eventually combined in the same block as they belong to the same symmetry q'' (separated by thick lines). Now, in the presence of outer multiplicity a specific (q, q') can contribute to the same q'' several times, as depicted schematically by the spaces \mathcal{M}_1 and \mathcal{M}_2 for the rows $(q, q')_1$ and $(q, q')_2$, respectively, both showing a multiplicity of $M_{q''} = 2$. Panel (b) depicts the *enlarged* multiplet space for the output multiplet q'' of panel (a) in order to accommodate the additional multiplets arising from outer multiplicity. Being an identity A -tensor, the entire block shown in panel (b) represents an identity matrix (in contrast to an arbitrary A -tensor, which may have an arbitrary unitary matrix in its place). The vertical lineup of (q, q') sectors is arbitrary, making the identity A -tensor unique up to permutations. The identity matrix shown in the panel is sliced into horizontal blocks as indicated, each of which is associated with its own unique CGC space [not shown] as derived from the Lie algebra of the symmetry under consideration. Each of these slices then directly enters as a reduced multiplet space A_v in a separate row in the QSpace as in Eq. (5).

For simplicity, in the absence of truncation and without any further unitary rotation, the tensor-product on the multiplet level can be represented as an identity A -tensor with a clear one-to-one correspondence of input to output multiplets. This is depicted in Fig. 2(b) in terms of an identity matrix in the reduced multiplet space. The identity matrix in panel (b) then is sliced horizontally into blocks for each (q, q') that contributes to q'' . In the presence of outer multiplicity, the state space for q'' needs to be *enlarged* to accommodate the additional multiplets. The slicing (horizontal solid lines) then also proceeds for every output multiplet resulting from outer multiplicity, as indicated in panel (b). As a result, $M_{q''}^{[q, q']}$ slices are associated with exactly the same $Q \equiv \{q, q', q''\}$, distinguishable only through their Clebsch–Gordan coefficients. These slices directly enter as A_v in separate rows in a QSpace as in Eq. (5).

In summary, outer multiplicity requires an adaptation of the multiplet space, which is naturally incorporated into a QSpace by allowing multiplet entries with the same $\{Q\}_v$ labels yet with clearly distinguishable CGC spaces. That is, specific records are also considered to refer to *different* state spaces if their CGC spaces are not exact copies (up to a global factor that can be incorporated into the multiplet data) but rather orthogonal to each other [see Eq. (A.39)]. In practice, this is checked within a small numerical threshold ($\sim 10^{-12}$) accounting for numerical double precision noise. The great advantage of this prescription is that then multiplicities fall completely in line with the rest of the MPS algorithm without any specific further treatment.

Finally, it is important to notice that the same concept of relaxing the uniqueness of the $\{Q\}_v$ labels actually also can become relevant for symmetries that *do not* have intrinsic outer multiplicity in its actual sense. Yet, in fact, through contractions *intermediate objects* can arise of rank larger than three [e.g. see the QSpaces indicated by the dashed boxes marked by X in Fig. 4], where records in a QSpace with the same $\{Q\}_v$ labels can also have *incompatible* CGC spaces, in the sense that they are *not* the same up to overall factors. In this case, also the uniqueness of the $\{Q\}_v$ must be relaxed temporarily. For simplicity, this will also be referred to as outer multiplicity.

2.4. Contractions

The contraction of QSpaces will be introduced in the following in terms of a simple example, namely the orthonormalization condition on the combined state space in a tensor-product space. Putting symmetry labels aside for the sake of the argument, the A -tensor $A_{ij}^{[\sigma]} \equiv \langle i\sigma | j \rangle$ in Eq. (9) combines the state spaces $|i\sigma\rangle$ into a combined (possibly truncated) orthonormal state space $|j\rangle$. This directly leads to the standard orthogonality relation for an A -tensor,

$$\sum_{i\sigma} A_{ij}^{[\sigma]*} A_{ij'}^{[\sigma]} = \delta_{jj'}, \quad (11)$$

which is a simple example for the simultaneous contraction of two tensors *w.r.t.* to two common indices, here i and σ . By construction, it is completely analogous in structure to the orthogonality condition of CGCs as in App. Sec. (A.39). Including symmetries, the contraction in Eq. (11) is depicted in terms of QSpaces in Fig. 3. Overall, indices are represented by lines, and lines connecting two blocks such as the indices i and σ are summed over, *i.e.* contracted. In practice, contraction of QSpaces as defined in Eq. (5) happens at several levels, since state indices are labeled by composite indices that refer to a symmetry basis of the type $|qn; q_z\rangle$. This implies for a contraction $\sum_{i=i'}$ of two QSpace objects with respect to some common state space i and i' , that (i) the q -labels q_i and $q_{i'}$ of the QSpaces as in Eq. (5) must be matched for the indices i and i' , respectively. For a given specific match of rows v and v' then, this is followed (ii) by the contraction of the corresponding reduced multiplet spaces, and (iii) by exactly the same contraction of the CGC spaces, one for each symmetry. This procedure derives from Eq. (8), since the contraction of two tensors $B^{(1)}$ and $B^{(2)}$ for a given match v and v' , can be simply decomposed as the *sequential* contraction of its constituents, *i.e.* the reduced multiplet space and the corresponding CGC spaces,

$$\left[B_v^{(1)} \otimes \left(\bigotimes_{s=1}^{n_s} C_{s;v}^{(1)} \right) \right] \cdot \left[B_{v'}^{(2)} \otimes \left(\bigotimes_{s=1}^{n_s} C_{s;v'}^{(2)} \right) \right] = \left[B_v^{(1)} \cdot B_{v'}^{(2)} \right] \otimes \left(\bigotimes_{s=1}^{n_s} \left[C_{s;v}^{(1)} \cdot C_{s;v'}^{(2)} \right] \right). \quad (12)$$

Here the multiplication “ \cdot ” is interpreted as contraction *w.r.t.* to a certain subset of shared dimensions between the tensors $B^{(1)}$ and $B^{(2)}$. Note that the rank of a QSpace and its index order are always shared by the multiplet space and CGC spaces for consistency. Hence the overall contraction of the QSpaces is directly reflected in the elementary contraction of the plain numerical tensors A_v and $\{C\}_v$. That is, the *contraction pattern* depicted schematically in Fig. 3, drawn in terms of boxes with connecting lines, is exactly the same on all levels of the contraction. By collecting the remaining *non-contracted* q -labels, this forms a new entry v'' in the resulting QSpace, with the (tensor) index order of the resulting tensor dimensions again being the same for all $\{Q\}_{v''}$, $A_{v''}$, and $\{C\}_{v''}$ for consistency.

Finally, the resulting QSpace is made unique in the $\{Q\}_{v''}$ labels as far as outer multiplicity permits. Records can only be combined, *i.e.* summed over, *iff* the CGC spaces for given records are all the same up to global factors which can be absorbed into the multiplet data, instead (see Section 2.3). Outer multiplicity plays no special role with contractions otherwise. Note that independent of whether or not outer multiplicity is present, when specifying a *subset* of tensor dimensions within $\{Q\}_v$ for contraction, the resulting QSpace will, in general, always have *many* contributions to the same $\{Q\}_{v''}$. For comparison, consider the completely analogous case of regular square matrices of dimension $D > 1$: a matrix element $(M)_{ij}$ is uniquely identified in the overall index (i, j) , while for example, the index i by itself is not sufficient, of course, as it refers to an entire row of matrix elements. When two matrices M_1 and M_2 are multiplied together,

$$(B)_{jj'} = (M_1 M_2)_{jj'} = \sum_{i=i'} (M_1)_{ji} (M_2)_{i'j'}, \quad (13)$$

the common index space (second index of M_1 and first index of M_2) is summed over, *i.e.* contracted. Every match $i = i'$ results in a contribution. In particular, for some given j and j' , all D matches $i = i'$ contribute and are summed up to the same output space (j, j') . In the case of QSpaces the situation

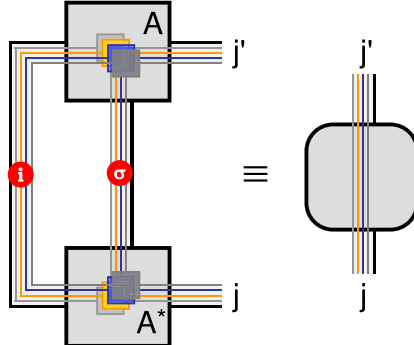


Fig. 3. (Color online) Contraction of (i) an A -tensor or (ii) an irreducible operator into a scalar. All indices specified are composite indices of the type $|qn; q_z\rangle$. An A -tensor describes a (truncated) basis transformation of the product-space of the new local space $|\sigma\rangle$ with an effective previously constructed basis $|i\rangle$, resulting in the combined state space $|j'\rangle \equiv \sum_{i'\sigma} A_{ij'}^{(\sigma)} |\sigma'\rangle |i'\rangle$, with the corresponding bra-space $\langle j| \equiv \sum_{i\sigma} A_{ij}^{(\sigma)*} \langle i| \langle \sigma|$ depicted in the lower part of the figure. The result is the scalar identity operator, reflecting the orthonormality condition equation (11). An entirely different interpretation of the same contraction pattern can be given when the A -tensor is replaced by an IROP F^q . The contraction then describes Eq. (14b) and yields a scalar operator, with its generic QSpace representation schematically depicted to the right.

is *exactly* analogous. All matches $i = i'$ in the q -labels q_i and $q_{i'}$ for the contracted index must be included. The only real consequence of outer multiplicity is that in the resulting QSpace B in Eq. (13) not necessarily all records with the same $\{Q\}_v$ labels can be merged by adding them together. In the specific case of the contraction in Eq. (11), however, the resulting QSpace is simply the identity, and as such a scalar operator with unique $\{Q\}_v$.

2.5. Scalar operators

Given the definition of an A -tensor in Eq. (9), the contraction of the two QSpaces A and A^* in Fig. 3 leads to the identity operator $\hat{\mathbf{1}}^{(C)} \equiv \sum_j |j\rangle \langle j|$ in the possibly truncated combined space C [cf. Eq. (11)]. Clearly, this also provides a strong check on the numerical implementation of the symmetries. In particular, $\hat{\mathbf{1}}^{(C)}$ represents a (trivial) example of a scalar operator, that can be described as rank-2 QSpace. The CGC spaces are all identity matrices (up to overall factors that can be associated with the multiplet space), and therefore the lines, that usually connect to the CGC spaces within a QSpace, can be directly connected through from j to j' on the r.h.s. of Fig. 3, with the CGC spaces themselves no longer shown. In the given case, due to the orthonormality condition in Eq. (11), also the reduced multiplet space is given by identity matrices. This actually also would allow to connect through the thick black line on the r.h.s. of Fig. 3, and thus also to skip the large remaining block on the r.h.s. for the reduced multiplet space altogether.

Fig. 3, however, allows yet an entirely different interpretation. Remember that an irreducible operator set \hat{F}^q has a completely analogous structure and interpretation in terms of its internal CGC spaces when compared to an A -tensor (cf. Fig. 1). Therefore it must hold that the scalar-product-like contraction,

$$\hat{F}^2 \equiv \hat{F} \cdot \hat{F}^\dagger \equiv \sum_{q_z} \hat{F}_{q_z}^q (\hat{F}_{q_z}^q)^\dagger \quad (14a)$$

also results in a scalar operator (note that through the Wigner–Eckart theorem, by convention, the state space associated with the *right* index of the operator \hat{F}^q is combined with the multiplet space q ; cf. Appendix A.7). With $\sigma \equiv (q_1; q_z)$ and the further sum through the operator (matrix) multiplication, Eq. (14a) shares exactly the same contraction pattern as discussed in Fig. 3 in the context of the orthonormality of A -tensors earlier. Here the resulting scalar operator, however, can have arbitrary positive hermitian matrices in its multiplet space still, represented by the large gray

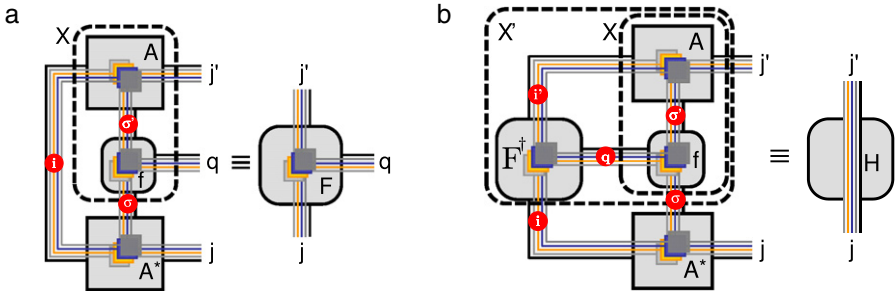


Fig. 4. (Color online) Typical evaluation of matrix elements given an A -tensor. The nested dashed boxes $X^{(i)}$ indicate the sequential order of contractions prior to the final contraction. In panel (a), the local IROP set \hat{f}^q acts within the state space $|\sigma\rangle$ of a given site. Its local matrix elements, $\langle\sigma|\hat{f}^q|\sigma'\rangle$, are assumed to be known and described in terms of the local rank-3 QSpace f . The local IROP set is mapped into the larger effective space linked through the A -tensor, $|j\rangle = \sum_{i\sigma} A_{ij}^{[\sigma]} |\sigma\rangle |i\rangle$. The overall result is the rank-3 QSpace F on the r.h.s., i.e. the desired matrix elements $F_{jj'}^{[q]} \equiv \langle j|\hat{f}^q|j'\rangle$. Panel (b) depicts a typical scalar nearest-neighbor contribution to a Hamiltonian $\hat{H} \equiv [\hat{f}^q]_k^\dagger \cdot [\hat{f}^q]_{k+1}$ of two consecutive sites, say k and $k+1$ using their respective A -tensors. This contraction already uses an effective description of the local operator \hat{f}_k^\dagger at site k in terms of the QSpace F^\dagger , obtained from the A -tensor $A_{(k)}$ at site k as in panel (a) from the prior iteration. Using the A -tensor $A_{(k+1)}$ of site $k+1$, the overall contraction can be completed as indicated.

box on the r.h.s. of Fig. 3. The reduction of Eq. (14a) to a scalar operator is also intuitively clear, given that the Hamiltonian itself is typically constructed in terms of scalar operators of exactly this type [see, for example, Eq. (A.48) or Eq. (A.60) given the Hamiltonian in Eq. (A.46)]. The notation in Eq. (14a) emphasizes that in the scalar product the *same* irreducible operator set \hat{F}^q must be taken, considering that the IROP \hat{F}^q is *different* from the IROP $(\hat{F}^\dagger)^q$. Nevertheless, since $(\hat{F}_{qz}^q)^\dagger \sim (\hat{F}^\dagger)_{-qz}^q$, up to possible signs originating from the definition of the CGC algebra [e.g. compare the QSpaces (C.3) in Table C.1 and discussion], these signs are irrelevant in the scalar contraction. Hence it follows that also

$$\tilde{F}^2 \equiv \hat{F}^\dagger \cdot \hat{F} \equiv \sum_{qz} (\hat{F}_{qz}^q)^\dagger \hat{F}_{qz}^q \quad (14b)$$

is a scalar operator, yet different from Eq. (14a), as indicated by the tilde on \tilde{F}^2 . Similarly, note that if the A -tensor had been contracted on the right instead of the left index in Fig. 3, this also would have yielded a scalar operator, namely a reduced density matrix up to normalization (e.g. Fig. 5 below using $\rho_k \equiv \mathbf{1}$).

2.6. Operator matrix elements

The typical calculation of matrix elements of operators for iterative methods such as NRG or DMRG is depicted schematically in Fig. 4. While the complex many body states are generated iteratively and described by A -tensors [cf. Eq. (9)], an elementary irreducible operator set \hat{f}^q , on the other hand, usually operates locally within the state space $|\sigma\rangle$ of a specific site. Therefore, the operator is described initially in terms of the matrix elements $f_{\sigma\sigma'}^{[q]} \equiv \langle\sigma|\hat{f}^q|\sigma'\rangle$. The link to the many body states is given through the A -tensor that connects given site to a generated effective state space $|i\rangle$, $|j\rangle = \sum_{i\sigma} A_{ij}^{[\sigma]} |\sigma\rangle |i\rangle$. The matrix elements of an IROP in the combined space $|j\rangle$ then become,

$$F_{jj'}^{[q]} \equiv \langle j|\hat{f}^q|j'\rangle = \sum_{i\sigma, i'\sigma'} A_{ij}^{[\sigma]*} A_{i'j'}^{[\sigma']} \underbrace{\langle i|\langle\sigma|\hat{f}^q|\sigma'\rangle|i'\rangle}_{\equiv \delta_{ii'} f_{\sigma\sigma'}^{[q]}} = \left[\sum_{\sigma} A^{[\sigma]\dagger} \left(\sum_{\sigma'} f_{\sigma\sigma'}^{[q]} A^{[\sigma']} \right) \right]_{jj'}. \quad (15)$$

It is exactly this procedure that is depicted in Fig. 4(a). The matrix elements are calculated in a two-stage process. The sum in the round brackets of Eq. (15) (contraction of σ') is carried out first, leading

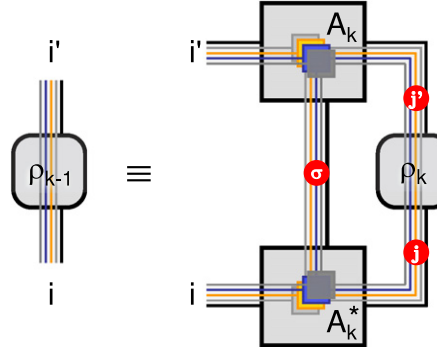


Fig. 5. (Color online) Backward update of density matrix ρ_k given in the effective basis $|j\rangle$ of a system up to and including site k (right index) by tracing out the local state space $|\sigma_k\rangle$ (middle index) given the basis transformation A_k that introduced site k . The result is the reduced density matrix ρ_{k-1} in the effective basis $|i\rangle$ of the system up to and including site $k - 1$.

to the temporary rank-4 tensor with open indices (i, j', σ, q) [box X in Fig. 4(a)]. This rank-4 tensor then is contracted simultaneously in the indices i and σ with the A^* tensor, providing the final result shown on the r.h.s. of Fig. 4(a). Quite generally, for contractions including several blocks as in Fig. 4, these are always done sequentially, adding one block at a time. This is explicitly indicated in Fig. 4 by the (nested) dashed boxes, with the final contraction connecting the remaining tensor to the outermost dashed box. Every individual contraction then follows the multi-stage process over composite indices as described earlier in Section 2.4.

The so obtained effective description $F_k^{[q]}$ of an operator \hat{f}^q acting on site k using A_k can be used then to describe, for example, the typical scalar nearest-neighbor contribution $[\hat{f}^q]_k^\dagger \cdot [\hat{f}^q]_{k+1}$ to the Hamiltonian including site $k + 1$. This operation is shown in Fig. 4(b). In particular, one may use the identity A -tensor A_{k+1}^{id} for site $k + 1$, such that the resulting Hamiltonian is constructed in the full tensor-product space $|\sigma\rangle_{k+1}|i\rangle_k$ of the system up to and including site $k + 1$. Here $|i\rangle_k$ describes the effective space up to and including site k , whereas $|\sigma\rangle_{k+1}$ describes the new local state space of site $k + 1$. This exactly corresponds the two-stage prescription used within the NRG (and similarly also for the DMRG) to build the Hamiltonian for the next iteration: (i) the tensor-product space including the newly added site must be mapped into proper symmetry spaces. This is taken care of by the construction of the identity A -tensor A_{k+1}^{id} . (ii) The new Hamiltonian is built using this identity A -tensor through contractions as shown in Fig. 4(b) [note that while the presence of outer multiplicity in QSpace f is typically inherited by QSpace F through the basis transformation as in Fig. 4(a), the internal contraction over the IROP set index q in Fig. 4(b) eventually leads to a scalar contribution to the Hamiltonian, as discussed with Eq. (14b)]. After diagonalization and state space truncation in the combined state space, the part of the resulting unitary matrix describing the kept states can be contracted onto A_{k+1}^{id} , yielding the actual final A_{k+1} .

2.7. Density matrix and backward update

Consider the density matrix $\hat{\rho}_k \equiv \sum_{jj'}(\rho_k)_{jj'}|j\rangle\langle j'|$ given in the basis $|j\rangle_{(k)}$, which is assumed to include all sites of a system up to and including site k . With the local state space of the last site k described by $|\sigma_k\rangle$, tracing out this last site from the density matrix ρ_k corresponds to contracting the A_k -tensor that connected site k to the system's MPS,

$$\hat{\rho}_{k-1} \equiv \text{tr}_{\sigma_k}(\hat{\rho}_k) = \sum_{ij,i'j',\sigma} A_{ij}^{[\sigma_k]*} A_{i'j'}^{[\sigma_k]} (\rho_k)_{jj'}|i\rangle\langle i'| = \sum_{ii'} (A^{[\sigma_k]\dagger} \rho_k A^{[\sigma_k]})_{ii'} |i\rangle\langle i'|. \quad (16)$$

Eq. (16) leads to a density matrix $\hat{\rho}_{k-1}$, which now is written in the many-body basis $|i\rangle_{(k-1)}$ which includes all sites up to and including site $k - 1$. This *backward update* is a well-known operation within the NRG [23,31,40,41]. Its graphical depiction is given in Fig. 5 [note that the sum over i and i' in Eq.

(16) connects to state spaces that are not yet contracted; hence these correspond to open indices in Fig. 5].

The backward update of the density matrix in Eq. (16) preserves its properties as a density matrix and as a scalar operator. The former directly follows from the realization that the orthonormality condition equation (11) with the A-tensor in the last line of Eq. (16) is exactly equivalent to a complete positive map. Moreover, by tracing out part of a system such as a site that has been added through a tensor product space and that itself can be fully categorized using the symmetries present, this *isotropic averaging* by itself cannot break symmetries. This is to say, that the partial trace in Eq. (16) preserves the property of a scalar operator. However, the trace over CGC spaces adds important weight factors to the reduced multiplet spaces, which are crucial, for example, to preserve the overall trace of the density matrix during back-propagation. While the contraction in Fig. 5 can be easily performed, in practice, without the explicit knowledge of these weights, their determination is straightforward and instructive, nevertheless, as will be shown in the following.

The contraction in Fig. 5 clearly also holds for the CGC spaces of every symmetry individually. Therefore it is sufficient to focus on one specific symmetry. Let i contain several multiplets q_i , and consider, for simplicity, the special case where the local state space σ contains one specific multiplet q_σ only. In addition, also the reduced density matrix $\hat{\rho}_k$ is chosen such that it only picks one very specific multiplet q_j . Focusing on the Clebsch–Gordan coefficients $C_{q_{iz} q_{jz}}^{[q_{\sigma z}]} \equiv \langle q_i q_{iz}; q_\sigma q_{\sigma z} | q_j q_{jz} \rangle$ for chosen symmetry then, which properly combine the irreducible multiplets q_i and q_σ into the multiplet q_j , the contraction in Eq. (16) with respect to the fixed q_j is given by

$$\begin{aligned} & \sum_{q_{\sigma z} q_{jz} q_{j'z}} \langle q_{i'} q_{i'z}; q_\sigma q_{\sigma z} | q_j q_{j'z} \rangle \langle q_i q_{iz}; q_\sigma q_{\sigma z} | q_j q_{jz} \rangle^* \cdot \delta_{q_{jz} q_{j'z}} \\ &= \sum_{q_{\sigma z}} \langle q_{i'} q_{i'z}; q_\sigma q_{\sigma z} | \left(\sum_{q_{jz}} |q_j q_{jz}\rangle \langle q_j q_{jz}| \right) |q_i q_{iz}; q_\sigma q_{\sigma z} \rangle \\ &= f_{q_i q_j} \cdot \delta_{q_i q_{i'}} \delta_{q_{iz} q_{i'z}}, \end{aligned} \quad (17)$$

where the $\delta_{q_{jz} q_{j'z}}$ in the first line comes from the assumption that the initial $\hat{\rho}_k$ is a scalar. The last identity follows from the fact that also $\hat{\rho}_{k-1}$ shall be a scalar operator. Alternatively, the last equality can also be understood as a general intrinsic completeness property of Clebsch–Gordan coefficients. Either way, the remaining factor $f_{q_i q_j}$ in the last line must be independent of the z-labels. The factor $f_{q_i q_j}$ then, in a sense, reflects the weight of how the IREP q_i together with the traced over IREPs q_σ contributes to the final total q_j . If, for example, for fixed q_i and the known set of q_σ some final total q_j cannot be reached, then it holds $f_{q_i q_j} = 0$ for this case.

From the scalar property of $\hat{\rho}_{k-1}$, Eq. (17) can be further constrained to some specific $q_i = q_{i'}$. Also summing over $q_{iz} = q_{i'z}$ then, the second line in Eq. (17) becomes equal to $\text{tr}(\sum_{q_{jz}} |q_j q_{jz}\rangle \langle q_j q_{jz}|) = d_{q_j}$, i.e. the internal multiplet dimension of the IREP q_j . Together with the last line in Eq. (17), it follows,

$$f_{q_i q_j} = \frac{d_{q_j}}{d_{q_i}} \quad (18)$$

as demonstrated, for example, for SU(2) in Ref. [23]. Note that Eq. (18) holds in general for arbitrary symmetries, and also in the presence of outer multiplicity. This follows by recalling that one of the main assumptions that entered Eq. (17) was to pick one specific multiplet q_j . This single IREP, however, may equally well also have been any of the multiplets resulting from outer multiplicity, say multiplet $q_j \rightarrow q_{j,\alpha}$, which nevertheless again leads to Eq. (18).

3. Implications for DMRG and beyond

This section sketches strategies for using non-abelian symmetries in the traditional DMRG [2,20] with generalizations to more general tensor networks. While the suggested procedures eventually may be further optimized still, nevertheless, they demonstrate the versatility of the presented QSpace framework. A particularly useful object in this context is the identity A-tensor that was already introduced in Section 2.2.

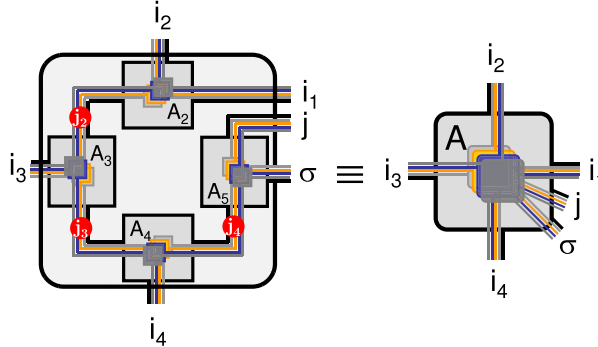


Fig. 6. (Color online) Generalized A -tensor that combines multiple state spaces, *i.e.* four effective state spaces $|i_1\rangle, \dots, |i_4\rangle$ together with one local degree of freedom $|\sigma\rangle$. Here it is assumed that all input state spaces describe proper orthonormal state spaces that act in different spaces, such that they can be combined into a simple product space. The index j , finally, represents the common global state space. In particular, it can be used to truncate the global Hilbert space to the state space of interest (within the DMRG, this may simply be the ground state, where the index j , being a singleton dimension, simply may be skipped then). While the general Clebsch–Gordan coefficients for the entire object may not be easily available (object to the right), the overall A -tensor can be built iteratively by adding one state space at a time (object to the left), starting, say, from A_1 which links the two state spaces i_1 and i_2 into the combined state space j_2 and hence allows to employ Clebsch–Gordan coefficients in the usual manner. The state space j_2 can then be combined with state spaces i_3 , and so forth. Contraction of the intermediate indices j_2, \dots, j_4 , finally, leads to the generalized A -tensor to the right.

3.1. Generalized A -tensor for tensor networks

The prototypical A -tensor as defined in Eq. (9) combines two physically distinct state spaces in terms of their tensor-product space. One may be interested, however, in the case where three or more state spaces need to be combined in the description of a single combined state space, while nevertheless also respecting symmetries. This situation, for example, occurs regularly in the context of tree [42,43] or tensor network states [8,12–14,18]. Let m be the number of states spaces to be combined. Then this requires the generalized Clebsch–Gordan coefficients $\langle q_1 q_{1z}; \dots; q_m q_{mz} | q_z \rangle$. Once known, in principle they can be combined compactly into a generalized A -tensor of rank $m + 1$. The question is, how to obtain such a generalized A -tensor in a simple manner, in practice.

For this, the QSpace structure introduced in this paper proves very useful. In particular, a generalized A -tensor can be obtained based on the *iterative pairwise addition* of individual state spaces, which is a well-established procedure at every step. The situation is depicted schematically in Fig. 6. To be specific, Fig. 6 considers four effective state spaces $|i_\alpha\rangle \equiv |q_\alpha q_{\alpha z}\rangle$ with $\alpha = 1, \dots, 4$, together with a local state space $|\sigma\rangle \equiv |q_5 q_{5z}\rangle$, thus having $m = 5$. This specific setting may correspond, for example, to the situation in a tensor network state that describes a two-dimensional system which, from the point of view of a specific site with state space σ , has four effective states spaces to the top, bottom, left, and right, respectively. Note, however, that here at least in principle the state spaces $|i_\alpha\rangle$ with $\alpha = 1, \dots, m$ are assumed to be *physically different, orthonormal* state spaces, such that their tensor-product space is a well-defined meaningful Hilbert space. Starting with state spaces $|i_1\rangle$ and $|i_2\rangle$ in Fig. 6, their state space can be combined in terms of and identity A -tensor A_2^{id} in the usual fashion using standard Clebsch–Gordan coefficients. The resulting state space $|j_2\rangle$ then can be combined with state space $|i_3\rangle$ using another identity A -tensor A_3^{id} , thus obtaining $|j_3\rangle$. The procedure is repeated, for example, until at the last step the local state space $|\sigma\rangle$ is added, resulting in the full combined state space $|j\rangle$, properly categorized in terms of symmetries. The iteratively generated $m - 1$ identity A -tensors A_k^{id} , on the other hand, can be contracted into a single tensor of rank $m + 1$ by contracting the intermediate indices j_2, \dots, j_{m-1} . This then results in the desired generalized A -tensor, shown at the *r.h.s.* of Fig. 6. Furthermore, in the context of DMRG or tensor network states, one is typically interested in a single state, such as the ground state of the system. In this case, the full combined state space $|j\rangle$ is truncated to a single state. Thus the index $|j\rangle$ becomes a singleton and as such can be dropped, for simplicity. In general, by explicitly including the CGC spaces in the QSpace in Eq. (5), generalized

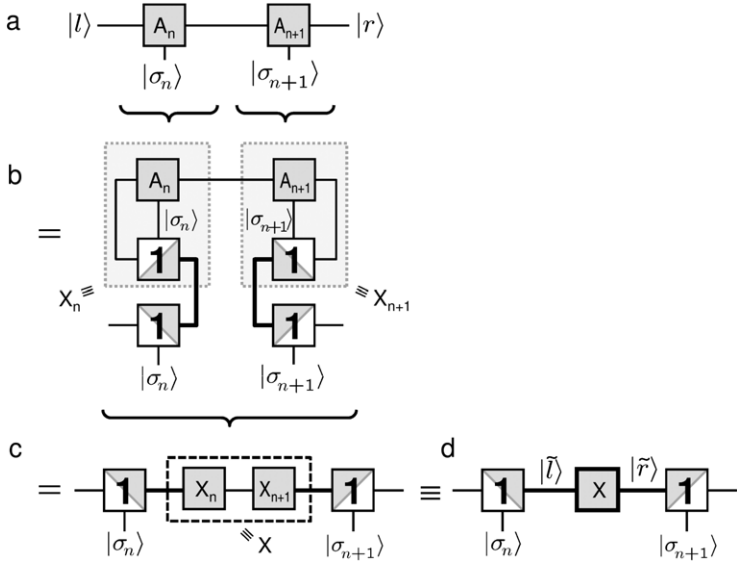


Fig. 7. DMRG treatment of a two-site setup using identity A -tensors. The internal CGC structure [cf. Fig. 1] is hidden in given case, for simplicity. Panel (a) Generic setup with orthonormalized state spaces for the left and the right block of the system (open indices left and right), while explicitly considering the pair of intermediate sites n and $n + 1$. Panel (b) Insertion of an identity, i.e. twice the unitary identity A -tensor, for site n and the left block (for site $n + 1$ and the right block) allows to fuse the local state spaces with their respective environments. Contracting the QSpaces X_n and X_{n+1} into $X \equiv X_n \cdot X_{n+1}$ (panel c), the setup in panel (d) is obtained. Overall, this allows to treat the more complex rank-4 two-site setup in panel (a) in terms of an intermediate rank-2 QSpace X in panel (d) which is connected to two enlarged (fused) effective orthonormal state spaces \tilde{l} and \tilde{r} (indicated by thick lines).

Clebsch–Gordan coefficients can be easily obtained in terms of a generalized A -tensor, which itself is constructed through a transparent iterative procedure.

3.2. Two-site treatment

A strategy for the treatment of a two-site setup common to the DMRG is sketched in Fig. 7. For this, consider the generic setup of two adjacent sites n and $n + 1$ within an MPS setup with local state spaces $|\sigma_n\rangle$ and $|\sigma_{n+1}\rangle$, respectively (panel a). The state spaces $|l\rangle$ to the left ($n' < n$) and $|r\rangle$ to the right ($n' > n + 1$) are assumed to be orthonormal and written in terms of proper multiplet spaces. Using symmetries, this two-site configuration is considered inefficient, however, since the local description of the Hamiltonian fractures into many contributions. Therefore from a practical point of view, it turns out advantageous even already on the level of plain abelian symmetries, to transform the rank-4 two-site setup [cf. Fig. 7(b)] to an intermediate rank-2 bond-configuration [cf. Fig. 7(d)]. Using identity A -tensors, this can be done exactly even in the presence of complex non-abelian symmetries.

In order to simplify the description of the two site setup, the left state space and the local state space $|\sigma_n\rangle$ are linked through an identity tensor into the combined *non-truncated* multiplet spaces $|s_n\rangle$. This mapping which respects symmetries, corresponds to a unitary transformation U . Therefore inserting $UU^\dagger = 1$, the identity A -tensor needs to be inserted twice, as indicated to the left of Fig. 7(b). Here the identity A -tensor is drawn such that the two input spaces connect to the white triangle, while the gray triangle solely links to the output space. This specific depiction serves to emphasize the underlying *unitary* mapping in terms of CGCs from one basis to another. Nevertheless, for simplicity, on the level of reduced matrix elements, i.e. the multiplet space, an identity matrix is maintained (cf. Section 2.2). The original tensor A_n can be contracted now with the upper identity A -tensor in Fig. 7(b), leading to the rank-2 QSpace X_n . Exactly the same treatment can be repeated for the right

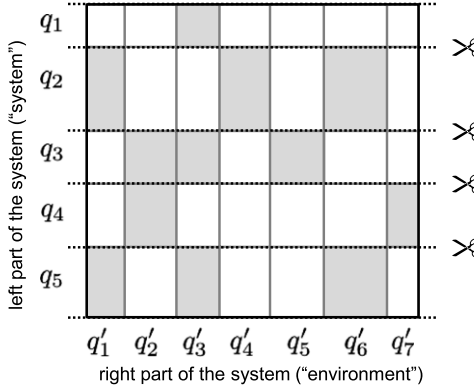


Fig. 8. State space truncation given the coefficient matrix X in Eq. (19) [cf. Fig. 10(d)]. Here X is schematically depicted in multiplet space in terms of groups (blocks) of multiplets for both, the effective state space $|l\rangle$ for the left part (rows), as well as the effective state space $|r\rangle$ for the right part (columns) of the physical system analyzed. Blocks shaded in gray are considered non-zero, whereas white blocks are considered all-zero. For the purpose of truncation, it is sufficient to group the multiplets q_i for the left part of the system, while arranging (q'_i, q_ψ) as columns in multiplet space, and perform SVD for each block of rows for a specific q_i in multiplet space only.

part of the system: site $n + 1$ is combined with the state space $|r\rangle$ for the sites ($n' > n + 1$) through their own identity A -tensor. The latter is again inserted twice, and after contraction this leads to QSpace X_{n+1} . The two QSpaces X_n and X_{n+1} , finally, are contracted into $X \equiv X_n \cdot X_{n+1}$ (panel c).

As seen in panel (d), the configuration resulting from this transformation is such that sites n and $n + 1$ are now fully fused without truncation through identity A -tensors with the left and the right part of the system, respectively. The original wave function, on the other hand, is exactly encoded in the intermediate rank-2 QSpace X . The enlarged tensor-product state-spaces [indicated by thick lines in panels (b-d)] eventually connects to QSpace X in panel (d). The wave-function encoded in QSpace X can be updated then in the usual DMRG spirit, after rewriting all operators relevant for the Hamiltonian within this local bond-configuration. The resulting improved \tilde{X} can be truncated then, followed by an exact shift of the focus from sites n and $n + 1$ to the next pair of sites, e.g. $n + 1$ and $n + 2$. The last two steps are explained in some more detail next.

3.3. State space truncation

Consider a wave function $|\psi\rangle$ written in the effective local configuration of Fig. 7(d),

$$|\psi\rangle = \sum_{l,r} X_{lr}|l\rangle|r\rangle, \quad (19)$$

having skipped the tildes, i.e. $|\tilde{l}\rangle \rightarrow |l\rangle$, and suppressing symmetry labels, for simplicity. Assume this wave function $|\psi\rangle$ has a well defined global symmetry described by the set of labels q_ψ . Now, both state spaces, $|l\rangle$ as well as $|r\rangle$, represent multiplet spaces that are grouped into blocks of states that belong to the same symmetry multiplets. This is depicted schematically in Fig. 8 for the matrix X in multiplet space. There white blocks are considered all-zero, while blocks shaded in gray are considered non-zero. For a shaded block therefore, by definition, its product space of the symmetries q_i in $|l\rangle$ (rows) and q'_i in $|r\rangle$ (columns) must allow q_ψ as a valid global multiplet. Given the labeling in terms of multiplet labels q_ψ , moreover, it is convenient to consider a full single multiplet $|\psi\rangle$, rather than picking a specific state from the internal space of multiplet q_ψ . Consequently, while the coefficient space X corresponds to a matrix, i.e. a rank-2 object in the multiplets l and r as depicted in Fig. 8, overall it is natural to consider the QSpace X to have rank-3. For a single multiplet q_ψ , this only affects the CGCs, while the multiplet space acquires a singleton dimension.

One may trace out the right part of the system (together with the third index regarding the CGC space of $|\psi\rangle$), equivalent to calculating $X \cdot X^\dagger$ in terms of QSpaces. Given a well defined global symmetry for $|\psi\rangle$, the resulting reduced density matrix, is a scalar operator, i.e. block-diagonal in the multiplet spaces q_i , corresponding to the blocks of rows in Fig. 8. From this, it follows that the eigenvalues and eigenvectors of the reduced density matrix can be computed *independently and thus separately* for each block of rows to the same label q_i . When calculating the reduced density matrix above, on the level of CGCs, this corresponds to the situation already discussed in Section 2.7 in that the CGC spaces contract to identities. Note, however, that the labels of the indices (state spaces) in Fig. 5 acquire a somewhat altered interpretation here, i.e. $(i, \sigma) \rightarrow j$ becomes $(l, r) \rightarrow \psi$. It follows from Eq. (18) then, that the corresponding weight factors for the reduced density matrix, that originate from the CGC spaces, are *completely independent* of the internal dimensionality $d_{q'_i}$ of the multiplets q'_i that represent the multiplet space $|r\rangle$. Therefore for the purpose of truncation, instead of explicitly calculating the reduced density matrix, it is equally sufficient to use standard SVD decomposition on the non-zero blocks in a row for a specific q_i in Fig. 8. That is, truncation can be performed fully on the level of multiplets only, temporarily putting aside the CGC spaces. Consequently, SVD allows to rewrite the QSpace $X = U \cdot (SV^\dagger)$, where U is a “scalar operator”. That is, all CGC spaces of U are identities, and the newly generated intermediate index inherits the symmetry labels of the multiplets l , i.e. is block-diagonal in q_i . In order to proceed to the next DMRG iteration then, say sites $n + 1$ and $n + 2$, the resulting truncated QSpace \tilde{R} from $\tilde{X} = U \cdot (\tilde{S}\tilde{V}^\dagger) \equiv U\tilde{R}$ can simply be contracted onto A_{n+1} , whereas U is contracted onto A_n . Overall, this allows to truncate within properly orthonormalized state spaces in the presence of arbitrary non-abelian symmetries, which thus again reduces the dimension on the bond between sites n and $n + 1$.

Note furthermore, that the constraint to a single wave function with well-defined multiplet label q_ψ can be significantly relaxed. It was already argued above, that it is convenient to consider the QSpace X of rank-3, which thus keeps all states that constitute the single multiplet q_ψ . However, this directly opens the door towards the *simultaneous* simulation of several multiplets $\{\psi_k\}$ with possibly different multiplet spaces $\{q_{\psi_k}\}$. Clearly, if each individual state ψ_k belongs to a well-defined overall symmetry multiplet, then the reduced density matrix built from the scalar operator $\rho = \sum_k |\psi_k\rangle\langle\psi_k|$ will still be block-diagonal in the symmetry spaces. Therefore SVD can still be performed for every individual block of rows q_i , while fusing the multiplet spaces for ψ with the multiplet spaces for the right part of the system, i.e. $q'_i \rightarrow (q'_i, q_\psi)$.

3.4. Wave function prediction

Following the two-site update depicted in Fig. 7 above together with subsequent truncation on the multiplet level, the local description of the wave function ψ can be carried over exactly to the next bond: using the respective identity A -tensors for sites $n + 1$ towards the left and $n + 2$ towards the right part of the system, this then allows to switch to the bond-configuration between sites $n + 1$ and $n + 2$, exactly as already discussed in Section 3.2.

4. Correlation functions

Correlation functions are usually calculated with respect to operators whose transformation under given symmetries is known. This is specifically so, as these operators often naturally derive from the same fundamental building blocks, that also enter the Hamiltonian. In the presence of non-abelian symmetries, a single specific operator then that is not a scalar operator, is usually part of a larger irreducible operator set. In practice, thus also its correlation function is calculated w.r.t. the *full* IROP, for simplicity, as will be explained in the following.

Consider, for example, the retarded Green's function

$$G_\sigma(\omega) \equiv \langle d_\sigma | d_\sigma^\dagger \rangle_\omega \quad (20)$$

that, in the time domain, creates a particle of preserved flavor σ , and destroys it some time later. Clearly, a particle with the same flavor must be destroyed later, otherwise the Green's function is zero,

i.e. the Green's function is diagonal with respect to symmetries. Now in the presence of symmetries, it must be possible to write the operators d_σ^\dagger as part of an irreducible operator set, e.g. some spinor (IROP) $\hat{\psi}^q$ that transforms according to IREP q with internal dimension d_q (in the case of plain abelian symmetries, it typically holds $d_q = 1$, i.e. the operator d_σ^\dagger is the only member of the IROP). Thus the calculation of the very specific correlation function with respect to specific elements d_σ and d_σ^\dagger above can be replaced by the Green's function

$$G_{\psi^q}(\omega) \equiv \langle (\hat{\psi}^q)^\dagger \|\hat{\psi}^q \rangle_\omega. \quad (21)$$

To be clear, if $d_q > 1$, this includes the scalar product of the spinor components, and thus one is actually calculating the same Green's functions as in Eq. (20) d_q times,

$$\begin{aligned} G_{\psi^q}(\omega) &= \sum_{q_z=1}^{d_q} \langle (\hat{\psi}_{q_z}^q)^\dagger \|\hat{\psi}_{q_z}^q \rangle_\omega = d_q \cdot \langle d_{(\sigma)} \| d_{(\sigma)}^\dagger \rangle_\omega \\ \Rightarrow G_{(\sigma)}(\omega) &= \frac{1}{d_q} G_{\psi^q}(\omega) \end{aligned} \quad (22)$$

with $G_{(\sigma)}$ independent of σ within its multiplet, as implied by the round brackets. This apparent overhead, however, only affects the CGC space, so this is negligible numerical overhead, yet makes the calculation conceptually simple. Specifically, when calculating matrix elements and their contribution to the Green's function, eventually all indices can be fully contracted, so there is no need for a special treatment of a specific z -label that represents a peculiar d_σ^\dagger . Moreover, given the discussion of scalar operators in Section 2.5 earlier, one realizes that the scalar product $\hat{\psi}^\dagger \cdot \hat{\psi}$ of the IROP $\hat{\psi}^q$ yields a scalar operator.

In the following, two explicit prototypical examples for correlation functions are given that are used explicitly for the numerical results presented in this paper. The first example is the spin–spin correlation function or magnetic susceptibility $\chi_d(\omega)$ defined at some site d . In the presence of spin SU(2) symmetry,

$$\begin{aligned} \chi_d(\omega) &= \langle S_{x,d} \| S_{x,d} \rangle_\omega = \langle S_{y,d} \| S_{y,d} \rangle_\omega = \langle S_{z,d} \| S_{z,d} \rangle_\omega \\ &\equiv \frac{1}{3} \langle \hat{\mathbf{S}}_d \| \hat{\mathbf{S}}_d \rangle_\omega. \end{aligned} \quad (23)$$

Clearly, the local operator $\hat{S}_d^2 \equiv \hat{\mathbf{S}}_d \cdot \hat{\mathbf{S}}_d$ is a scalar operator, with the corresponding spinor $\hat{\mathbf{S}}_{(d)}$ given by [cf. Eq. (A.11)]

$$\hat{\mathbf{S}} \equiv \begin{pmatrix} -\frac{1}{\sqrt{2}} \hat{S}_+ \\ \hat{S}_z \\ +\frac{1}{\sqrt{2}} \hat{S}_- \end{pmatrix}.$$

The second example is the spectral function for a single spinful channel in the presence of spin and particle–hole SU(2) symmetry. The spinor is given by [cf. Eq. (A.59)],

$$\hat{\psi} \equiv \begin{pmatrix} s \hat{c}_\uparrow^\dagger \\ \hat{c}_\downarrow \\ s \hat{c}_\downarrow^\dagger \\ -\hat{c}_\uparrow \end{pmatrix}.$$

In the evaluation of the correlation function,

$$\langle \hat{\psi}^\dagger \|\hat{\psi} \rangle_\omega = \sum_{q_z=1}^{d_q=4} \langle \hat{\psi}_{q_z}^\dagger \|\hat{\psi}_{q_z} \rangle_\omega = \langle \hat{c}_\uparrow \| \hat{c}_\uparrow^\dagger \rangle_\omega + \langle \hat{c}_\downarrow^\dagger \| \hat{c}_\downarrow \rangle_\omega + \langle \hat{c}_\downarrow \| \hat{c}_\downarrow^\dagger \rangle_\omega + \langle \hat{c}_\uparrow^\dagger \| \hat{c}_\uparrow \rangle_\omega$$

the signs, including $s \equiv \pm 1$, of the individual components are irrelevant. Given the spin symmetry and the fact, that in the presence of particle–hole symmetry spectral functions are symmetric with respect to $\omega = 0$, and in general $G_{B,B^\dagger}(\omega) \equiv \langle B \| B^\dagger \rangle_\omega = G_{B^\dagger,B}(-\omega)$, it follows that all four contributions above describe exactly the same function, indeed, and therefore

$$G_\sigma(\omega) \equiv \langle \hat{c}_\sigma \| \hat{c}_\sigma^\dagger \rangle_\omega = \frac{1}{4} \langle \hat{\psi}^\dagger \|\hat{\psi} \rangle_\omega.$$

5. The numerical renormalization group

The non-abelian setup described above is straightforwardly applicable to the NRG [3,44]. Before doing so in detail, here a brief reminder of the essentials of NRG is given, followed by the introduction of the model Hamiltonian to be analyzed. By construction, the NRG deals with so-called quantum impurity models – an arbitrary small quantum system (the *impurity*) that is in contact with a macroscopic non-interacting typically fermionic bath. Each part is simple to solve exactly on its own. The combination of both, specifically in presence of interactions at the location of the impurity, however, gives rise to strongly-correlated quantum-many-body effects.

The systematic approach introduced by Wilson [3] was a logarithmic discretization in energy space of the continuum of the bath (coarse graining), followed by an exact mapping onto a semi-infinite so-called Wilson-chain, with the intact impurity space coupled only to the very first site of this chain. Given the half-bandwidth $W := 1$ of the bath, the discretization parameter $\Lambda > 1$, typically $\Lambda \gtrsim 1.7$, defines the logarithmic discretization in terms of the intervals $\pm[\Lambda^{-m}, \Lambda^{-(m+1)}]$ with $m \geq 0$ an integer, and energies taken relative to the Fermi energy $\varepsilon_f \equiv 0$. Each of these intervals is then described by a single effective fermionic state, with its coupling and exact energy position chosen consistently w.r.t. the hybridization of the original continuum model [45,46]. The resulting discretized model is then mapped onto the semi-infinite Wilson-chain (Lanczos tridiagonalization) [47]. Hereby, the logarithmic discretization of the non-interacting bath translates to an effective tight-binding chain, with the hopping $t_k \sim \Lambda^{-k/2}$ between sites k and $k + 1$, decaying exponentially in the discretization parameter Λ . The latter then justifies the essential renormalization group ansatz of the NRG in terms of *energy scale separation* – large energies are considered first, with approximate eigenstates at large energies *discarded* and considered unimportant for the description of the still following lower energy scales. Thus each site of the Wilson chain corresponds to an energy shell with a characteristic energy scale $\omega_k \equiv \frac{a}{2}(\Lambda + 1)\Lambda^{-k/2}$. Here the constant a of order 1 is chosen such, $t_k/\omega_{k+1} \rightarrow 1$ for large k [41].

In practice, when considering the system up to site k , the Hamiltonian of the rest of the system is ignored, equivalent to assuming degeneracy in the state space of the remainder of the system. With \hat{H}_k the full Hamiltonian \hat{H} including the Wilson chain up to site k , its eigenstates $|s\rangle_k, \hat{H}_k|s\rangle_k = E_s^k|s\rangle_k$, and with $|e\rangle_k$ an arbitrary state of the rest of the system following site k , then the essential spirit of NRG after coarse graining of the bath can be condensed in the following approximation [48],

$$H|se\rangle_k \simeq E_s^k|se\rangle_k, \quad (24)$$

expressing energy scale separation, with $|se\rangle_k \equiv |s\rangle_k \otimes |e\rangle_k$. The energies E_s^k are usually taken relative to the ground state energy E_0^k of iteration k , and rescaled by the energy scale ω_k . All of this will be referred to as rescaled energies, and has the advantage that independent of the Wilson shell k , energies are always of order 1.

In this paper, the state space truncation at a given NRG iteration is energy-based, i.e. all states with $E_s^k \leq E_K$ are kept, typically with $E_K \simeq 5 \dots 7$ in rescaled energies. The number of kept states N_K thus changes dynamically [41,44,46].

5.1. Full density matrix

Within the NRG [3], a complete many-body basis set can be formulated from the state space discarded at every iteration [48]. Initially introduced for explicit time-dependence of quantum quenches, they actually can also be used to improve on existing calculations for thermodynamical quantities and expectation values [49], with a clean extension to arbitrary temperatures using the full density matrix (FDM) [31]. The density matrix $\hat{\rho} \equiv e^{-\beta\hat{H}}/Z$ with $\beta = 1/k_B T$, k_B the Boltzmann constant and T the temperature, obviously commutes with the Hamiltonian and is a scalar operator in itself. Within the FDM-NRG approach [31], the density matrix

$$\hat{\rho} = \frac{1}{Z} \sum_{k; qn; qz; e} e^{-\beta E_{qn}^k} |qn; qz; e\rangle_k \langle qn; qz; e|, \quad (25)$$

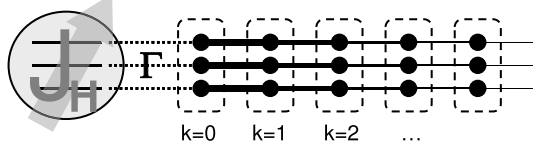


Fig. 9. Schematic depiction of the fully screened Kondo-Anderson hybrid model [Eq. (27)] with $m = 3$ in the NRG setup of a Wilson chain. Three d-levels with onsite Hund's interaction of strength J_H couple uniformly to their respective channel with hybridization Γ . The semi-infinite Wilson chain for each channel represents a tight-binding chain with exponentially decaying couplings, that interacts with the other channels through the impurity only. For a given NRG iteration, all terms in the Hamiltonian of the same energy scale must be included simultaneously, leading to an extended Wilson site [dashed boxes] of three spinful fermionic levels with a state space of $3^4 = 64$ states each.

can be constructed straightforwardly in terms of a QSpace for every Wilson shell k . Here $s \equiv (qn)$ stands for the multiplet label for a given shell k . Note that the symmetry of the states e is irrelevant here, as this space is fully traced over. Given the usual practice of NRG to rescale and shift energies at every iteration, all of this, of course, must be undone before entering Eq. (25) [given a general thermal density matrix, of course, *all* energies in Eq. (25) must be (i) at the same energy scale, *i.e.* non-rescaled, and (ii) specified with respect to a *common* energy reference, *e.g.* the overall ground state energy of the Wilson chain] [31].

By construction, all eigenenergies E_{qn}^k are degenerate, *i.e.* do not depend on the z -labels. With the reduced density matrix being a scalar operator, therefore the CGC spaces in the QSpaces describing Eq. (25) are all proportional to identity matrices, leading to the overall normalization

$$Z = \sum_{q;qn} d_q d_w^{N-k} e^{-\beta E_{qn}^k}, \quad (26)$$

where d_q is the internal dimension of multiplet q , and d_s^{N-k} reflects the degeneracy *w.r.t.* the rest of the Wilson chain of final length N , with d_w the state space dimension of a Wilson site [31].

5.2. Model: symmetric three-channel system

The historically first physical system where Kondo physics was observed was that of Fe impurities in Au [28,29]. The effective microscopic model for this material, however, is far from trivial. It was argued only very recently in an extended study [27] that the physics of the five d-orbitals of substitutional Fe in Ag or Au is dominated by 3-fold degenerate triplet space t_{2g} , with the doublet space e_g split-off by crystal fields and thus playing a minor role. Together with the effective spin 3/2 of the iron impurity, this then results in an SU(3) symmetric fully screened 3-channel Kondo model.

The actual model analyzed [27] is depicted schematically in Fig. 9. It consists of $m = 3$ spinful d-levels comprising the impurity, that are interacting through the Hund's coupling of strength J_H . Each of these impurity levels is coupled to its own spinful bath channel with uniform hybridization Γ . This leads to the Kondo-Anderson hybrid Hamiltonian,

$$\hat{H} \equiv \hat{H}_d + \sum_{i=1}^{m=3} \sum_{p\sigma} \left[\sqrt{\frac{2\Gamma}{\pi}} (\hat{d}_{i\sigma}^\dagger \hat{c}_{ip\sigma} + \text{H.c.}) + \varepsilon_p \hat{c}_{ip\sigma}^\dagger \hat{c}_{ip\sigma} \right], \quad (27a)$$

where all energies will be given in context in units of the half-bandwidth $W := 1$. The impurity is described by

$$\hat{H}_d \equiv -J_H \hat{\mathbf{S}} \cdot \hat{\mathbf{S}}, \quad (27b)$$

with the impurity spin

$$\hat{\mathbf{S}}_\alpha \equiv \sum_i^m \hat{\mathbf{S}}_{i,\alpha} \equiv \sum_{i=1}^m \sum_{\sigma\sigma'} \left(\frac{1}{2} \tau_\alpha \right)_{\sigma\sigma'} \hat{d}_{i\sigma}^\dagger \hat{d}_{i\sigma'} \quad (27c)$$

given in terms of the Pauli matrices τ_α with $\alpha \in \{x, y, z\}$. Here $\hat{d}_{i\sigma}^\dagger$ [$\hat{c}_{ip\sigma}^\dagger$] creates a particle with spin $\sigma \in \{\uparrow, \downarrow\}$ on d-level i at energy $\varepsilon_d = 0$ [in bath channel i at energy ε_p], respectively. For $J_H \gtrsim \Gamma$, an effective spin-3/2 forms at the impurity, leading to a symmetric fully-screened spin-3/2 system. The resulting Kondo temperature T_K decays exponentially with J_H/Γ , with T_K quickly becoming the smallest energy scale in the system. In practice, choosing $J_H = 2\Gamma/(m + \frac{1}{2})$ leads to comparable Kondo temperatures T_K for different m . Compared to the standard Kondo Hamiltonian with $\mathbf{S} \cdot \mathbf{s}$ coupling of the dot spin \mathbf{S} with the lead spin \mathbf{s} , the Hamiltonian in Eq. (27) in terms of Γ and J_H also allows for charge-fluctuations, while the model maintains particle-hole symmetry.

In particular, the Anderson-like model in Eq. (27) has the advantage that the impurity self-energy $\Sigma(\omega)$ can be evaluated within the NRG in a simple fashion. From a more technical point of view, this allows the straightforward calculation of an improved spectral function from the self-energy [50]. The impurity Green's function [cf. Eq. (22)]

$$\begin{aligned} G_{(i\sigma)}(\omega) &\equiv \langle \hat{d}_{(i\sigma)} \| \hat{d}_{(i\sigma)}^\dagger \rangle_\omega \\ &\equiv G'_{(i\sigma)}(\omega) - i\pi G''_{(i\sigma)}(\omega), \end{aligned} \quad (28)$$

consisting of real and imaginary part, respectively, is constructed within the NRG framework, as usual, from the spectral function $A_{(i\sigma)}(\omega) \equiv -\frac{1}{\pi} \text{Im}G_{(i\sigma)}(\omega) \equiv G''_{(i\sigma)}(\omega)$. Subsequently, the real part $G'_{(i\sigma)}(\omega)$ is obtained through the Kramers-Kronig transform of $A_{(i\sigma)}(\omega)$ [44]. The calculation of the additional correlation function $F_{(i\sigma)}(\omega)$ then,

$$F_{(i\sigma)}(\omega) \equiv \langle [\hat{d}_{(i\sigma)}, \hat{H}_d] \| \hat{d}_{(i\sigma)}^\dagger \rangle_\omega, \quad (29)$$

obtained similarly from its spectral part $F''_{(i\sigma)}(\omega) \equiv -\frac{1}{\pi} \text{Im}F(\omega)$, allows to evaluate the self-energy $\Sigma(\omega)$ at the impurity [50]

$$\Sigma_{(i\sigma)J_H} \equiv \frac{F_{(i\sigma)}}{G_{(i\sigma)}}, \quad (30)$$

Note that, the commutator of the IROP $\hat{d}_{(i\sigma)}$ with the scalar Hamiltonian in Eq. (29) again leads to an IROP w.r.t. the same IREP q . Moreover, by symmetry, both $G_{(i\sigma)}$ and $F_{(i\sigma)}$ are independent of $(i\sigma)$, as indicated by the subscript bracket, and hence will be skipped altogether in the following, for simplicity.

5.2.1. Kondo limit from numerical perspective

While the procedure to obtain the self-energy is straightforward for an Anderson-like model, there is no simple way to do so for the plain Kondo-like model with $\mathbf{S} \cdot \mathbf{s}$ interaction [50]. However, from the NRG point of view, the transition from one to the other is straightforward. That is, knowing that the Kondo temperature T_K decays exponentially with J_H/Γ , both, J_H as well as Γ can be taken *much* larger than the bandwidth $W := 1$ of the model, while keeping their ratio constant,

$$J_H, \Gamma \gg 1, \quad \frac{J_H}{\Gamma} \simeq \text{const.} \quad (31)$$

This is a well-known procedure in the analytical Schrieffer-Wolff transformation for the Anderson model into a Kondo model [51]. But, of course, exactly the same strategy can also be pursued here within the NRG [see Fig. 10 later]. For the local density of states at the impurity this leads to a well-separated nearly discrete contribution to the spectral function at $|\omega| \gg 1$ far outside the bandwidth. For the spectral range within the bandwidth, the actual spectral function for the Kondo-model emerges. In particular, this procedure allows to fully eliminate the free-orbital (FO) regime with strong charge-fluctuations in the Anderson-like model right within the first truncation step. From a numerical point of view, this is desirable as the FO regime is typically the most expensive one. For example, for the model discussed here using the symmetries below, using energy-based truncation indicates that about a factor of 5...10 more multiplets are required for the FO regime as compared to the local moment (LM) or strong coupling (SC) regime at later NRG iterations [cf. Fig. 11]. Nevertheless, by maintaining an Anderson-like description, the impurity self-energy remains easily accessible numerically within the NRG, even though essentially the correlation functions for the Kondo model are calculated.

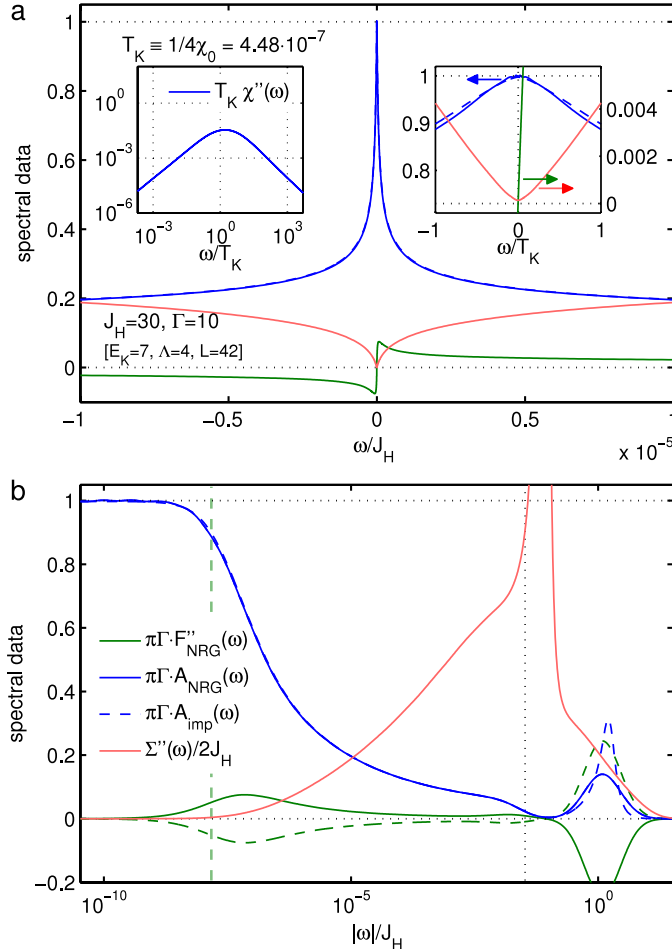


Fig. 10. (Color online) $SU(2)_{\text{spin}} \otimes U(1)_{\text{charge}} \otimes SU(3)_{\text{channel}}$ analysis of the symmetric three-channel Anderson model [Eq. (27)] with model parameters specified in the lower left of panel (a); the same data as in panel (a) is shown vs. $\log(|\omega|)$ in panel (b) to zoom into the Kondo peak at small frequencies with the legend for both panels shown in panel (b). The spectral data A_{NRG} and the auxiliary F''_{NRG} are shown together with the derived self-energy $\Sigma''(\omega)$ and the improved spectral function A_{imp} (see text). A zoom around $\omega = 0$ is show in the right inset of panel (a), with the left (right) axis belonging to $A(\omega)$ [$\Sigma''(\omega)$ and $F''(\omega)$], respectively. The spectral data for $A(\omega)$ and $\Sigma''(\omega)$ is symmetric around $\omega = 0$ and strictly positive, while $F''(\omega)$ is antisymmetric. In panel (b) therefore the $\omega < 0$ branch of $F''(\omega)$ has been plotted in dashed lines, same color otherwise. The left inset to panel (a) shows the spin-spin spectral data $\chi''(\omega)$, with the resulting $T_K \equiv 1/4\chi_0$ indicated in panel (b) and the left insets of both panels by the vertical dashed line.

6. NRG results

The model in Eq. (27) is a true three-channel system, in that it is not possible to simply decouple a certain unitary superposition of bath channels. Furthermore, within an NRG iteration, a site from each channel must be included as they have the same coupling strength, i.e. energy scale, as schematically depicted in Fig. 9 [dashed boxes].

The non-abelian symmetries present in the system are,

- total spin symmetry: $SU(2)_{\text{spin}}$,
- particle-hole symmetry in each of the three channels: $SU(2)_{\text{charge}}^{\otimes 3}$, and
- channel symmetry: $SU(3)_{\text{channel}}$.

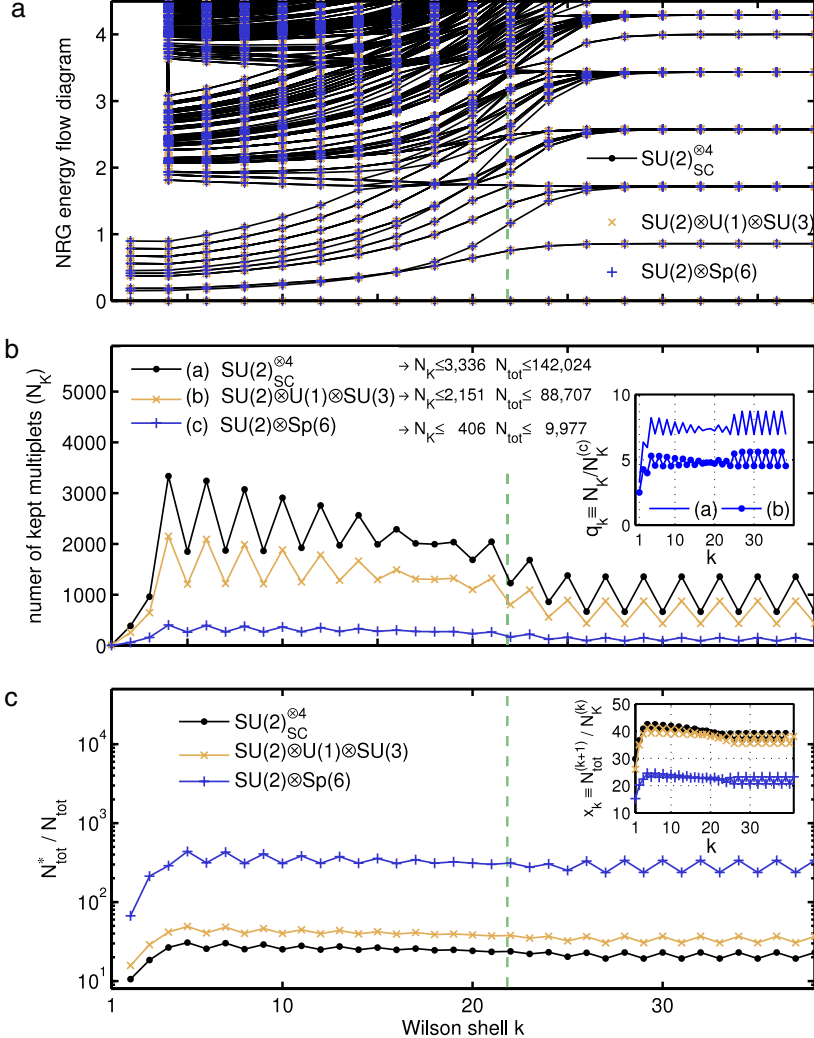


Fig. 11. (Color online) Comparison of the efficiency of the symmetry settings as outlined in Eq. (32) for the calculation of the spectral data in Fig. 10 for the 3-channel model in Eq. (27). For a fair comparison, all calculations were performed using the same energy-based truncation with $E_K = 7$ for the same discretization $\Lambda = 4$ as in Fig. 10. The vertical dashed lines in all panels indicates the energy scale of T_K . Panel (a) compares the energy flow diagrams resulting for even iterations from the individual NRG runs, indicating perfect consistency for all symmetry settings. Panel (b) shows the number of kept multiplets for each iteration. For each symmetry setting, at the top of the panel the maximum dimension in the multiplet space over the entire NRG run is specified for kept (N_k) and total (N_{tot}), i.e. kept and discarded space, respectively. The inset shows the ratio $q_k \equiv N_k/N_k^{(c)}$ of the multiplets that needed to be kept for the symmetry settings in Eq. (32a) and Eq. (32b) relative to the case when the full $Sp(6)$ is included [Eq. (32c)]. Panel (c) shows the ratio N_{tot}^*/N_{tot} of the actual Hilbert-space dimension (N_{tot}^*) at a given iteration, which includes the internal multiplet dimensions, relative to the dimension of the multiplet space (N_{tot}). The inset shows the ratio x_k that describes the increase in the number of multiplets when adding a new site prior to truncation.

The latter symmetry $SU(3)_{\text{channel}}$, however, *does not* commute with particle–hole symmetry, while it does commute with the total charge $U(1)_{\text{charge}}$, i.e. the abelian subalgebra of particle–hole symmetry [cf. Eq. (A.72), and subsequent discussion]. Having non-commutative symmetries, however, directly suggests a larger enveloping symmetry, which in the present case is the symplectic symmetry $Sp(6)$ [30] [i.e. $Sp(2m)$ with $m = 3$, cf. Appendix A.10].

This allows us to consider the following symmetry settings,

$$\text{SU}(2)_{\text{spin}} \otimes \text{SU}(2)_{\text{charge}}^{\otimes 3} \equiv \text{SU}(2)_{\text{SC}}^{\otimes 4}, \quad (32a)$$

$$\text{SU}(2)_{\text{spin}} \otimes \text{U}(1)_{\text{charge}} \otimes \text{SU}(3)_{\text{channel}}, \text{ and} \quad (32b)$$

$$\text{SU}(2)_{\text{spin}} \otimes \text{Sp}(6). \quad (32c)$$

All of these symmetry settings have been implemented, in practice, and applied within the NRG framework, with results presented in the following. The first setting in (32a) represents a more traditional NRG scenario based on a set of plain SU(2) symmetries. The second setting (32b) includes SU(3)_{channel} together with the simple abelian symmetry U(1)_{charge} for total charge, while the last setting (32c) represents the actual full symmetry of the model.

Even though the second setting in (32b) actually includes an abelian component in terms of charge, it nevertheless represents a stronger symmetry as compared to the first setting (32a). Since SU(3)_{channel} is a rank-2 symmetry with two commuting z-operators, *i.e.* generators of the Cartan subalgebra, it possesses a two-dimensional multiplet representation. This results in much larger multiplets for setting (32b), with the bare SU(3) multiplet dimensions easily reaching up to 100 (*e.g.* $d_q \leq 125$ for the NRG run underlying Fig. C.14, *cf.* Appendix C.3). As a consequence, this allows, on average, smaller multiplet spaces and thus better numerical performance.

The first two symmetry settings in (32) emphasize different symmetry aspects, yet allow to break certain symmetries which, nevertheless, are present in the model Hamiltonian in Eq. (27). The first symmetry setup (32a) strongly emphasizes particle-hole symmetry, while it does not use the symmetric coupling of the levels to their respective channels. The channel symmetry can thus be broken without reducing the symmetry setting (32a). The second symmetry setting (32b), on the other hand, emphasizes the channel symmetry (uniform Γ), while it allows to break the particle-hole symmetry. Hence, in principle, a uniform level-shift could be applied to the d-levels within this setting. Only the third symmetry (32c) captures the full symmetry of the model, as it combines channel symmetry with particle-hole symmetry into the enveloping symmetry Sp(6). This is a rank-3 symmetry with multiplet dimensions now easily reaching up to a several thousands (*e.g.* see Table C.8 for actual multiplets generated in a full NRG run). A more detailed general discussion and comparison of all of above symmetry setups in terms of their overall multiplet structure and representation of a site with three spinful levels (*i.e.* a Wilson site) is given in Appendix C.3.

6.1. Spectral functions

The spinor $\hat{\psi}^q$ to be used for fermionic hopping term as well as for the calculation of spectral functions can be represented for all symmetry settings by IROPs with a well-defined multiplet label q [*cf.* Eq. (22)]. For the first symmetry setting in (32), $\text{SU}(2)_{\text{SC}}^{\otimes 4}$, the IROP for the calculation of spectral functions involves three 4-component spinors, $\hat{\psi}_i^{[4]}$ for short, one for every channel $i = 1, \dots, (m = 3)$. The corresponding IROP labels are $q_1 = (\frac{1}{2}, \frac{1}{2}, 0, 0)$, $q_2 = (\frac{1}{2}, 0, \frac{1}{2}, 0)$, and $q_3 = (\frac{1}{2}, 0, 0, \frac{1}{2})$, respectively. The number of components in the spinor derives from the two participating SU(2) multiplets (S, C) = $\frac{1}{2}$ for spin and one specific channel, thus having $2 \times 2 = 4$ operators in one specific IROP $\hat{\psi}_i^{[4]}$, indeed. With this, the hopping in the Hamiltonian, for example, is given by $\hat{h}_{k,k+1} = \sum_{i=1}^m \hat{\psi}_{k,i}^{[4]\dagger} \cdot \hat{\psi}_{k+1,i}^{[4]}$. Note that this excludes the hermitian conjugate part, as this is already fully incorporated through the particle-hole symmetry [see Eq. (A.73b)]. Furthermore, note that particle-hole symmetry gives rise to intrinsic even-odd alternations for the spinors along a chain [see Appendix A.9.2 for a detailed discussion].

In contrast, the second symmetry setting in (32), $\text{SU}(2)_{\text{spin}} \otimes \text{U}(1)_{\text{charge}} \otimes \text{SU}(3)_{\text{channel}}$, leads to a single 6-component spinor, $\hat{\psi}^{[6]}$ for short. Its IROP multiplet label is given by $q = (\frac{1}{2}, -\frac{1}{2}, 0, 1)$. This combines a 2-dimensional SU(2)_{spin} multiplet $S = \frac{1}{2}$ and an abelian 1-dimensional multiplet $C_z = -\frac{1}{2}$ with the 3-dimensional SU(3)_{channel} multiplet $T = (0, 1)$, resulting in the $2 \times 1 \times 3 = 6$ operators in the multiplet. For comparison, here the hopping term in the Hamiltonian in Eq. (27) is reduced to a total of two terms, $\hat{h}_{k,k+1} = (\hat{\psi}_k^{[6]\dagger} \cdot \hat{\psi}_{k+1}^{[6]} + \text{H.c.})$ [see Eq. (A.73a)].

Finally, for the third symmetry setting in (32), $SU(2)_{\text{spin}} \otimes Sp(6)$, again a single spinor $\hat{\psi}^q$ is obtained, but now with 12 components, written as $\hat{\psi}^{[12]}$ for short. Its IROP label is given by $q = (\frac{1}{2}, 1\ 0\ 0)$, which combines the 2-dimensional $SU(2)_{\text{spin}}$ multiplet $S = \frac{1}{2}$ with the 6-dimensional $Sp(6)$ multiplet $(1\ 0\ 0)$, i.e. defining representation of $Sp(6)$. Overall, this again recovers the $2 \times 6 = 12$ components of the spinor, indeed. For comparison, now the hopping term in the Hamiltonian in Eq. (27) is reduced to the single term $\hat{h}_{k,k+1} = (\hat{\psi}_k^{[12]\dagger} \cdot \hat{\psi}_{k+1}^{[12]})$. The scalar contraction of the spinor $\hat{\psi}^{[12]}$ with itself recovers the original 12 terms in the fermionic hopping structure between two sites in the Hamiltonian in Eq. (27). Since particle-hole symmetry is part of $Sp(6)$, this again implies that (i) the hermitian conjugate is already taken care of in the hopping term, and (ii) that $Sp(6)$ again gives rise to the same intrinsic even-odd alternations for the spinors along a chain, exactly analogous to what has already been encountered for standard particle-hole symmetry.

The correlation functions calculated for the model in Eq. (27) are presented in Fig. 10, with the model parameters indicated at the bottom left of panel (a). Panel (a) shows the spectral data on a linear scale, while panel (b) shows the same data vs. $\log(\omega)$ which therefore allows a logarithmic zoom into the low energy regime. The legend shown with panel (b) also applies to panel (a). The data in Fig. 10 was obtained using the symmetry setting in (32b) including $SU(3)_{\text{channel}}$. Note that having chosen an energy-based NRG truncation with $E_K = 7$, the spectral data for the other two symmetry settings is identical, hence not shown. While the calculation is somewhat more involved for the more traditional setup (32a), it becomes significantly more compact still when finally including $Sp(6)$ as in (32c). Their individual numerical efficiency will be discussed with Fig. 11 below.

In Fig. 10, the spectral function obtained from the NRG is plotted as $A_{\text{NRG}}(\omega) \equiv G''_{\text{NRG}}(\omega)$. The spectral data satisfies the Friedel sum-rule to an excellent approximation, in that $\lim_{\omega \rightarrow 0} (\pi \Gamma A_{\text{NRG}}(\omega)) = 1$ [see right inset to panel (a) for a zoom around $\omega = 0$]. The self-energy $\Sigma(\omega)$ was obtained by calculating the additional correlation function $F_{\text{NRG}}(\omega)$ [Eq. (29), to be used in Eq. (30)]. The imaginary part $\Sigma''(\omega) \equiv -\frac{1}{\pi} \text{Im} \Sigma(\omega)$, plotted in Fig. 10, clearly approaches zero in a smooth parabolic fashion at the Fermi energy, i.e. $\lim_{\omega \rightarrow 0} \Sigma(\omega) = \lim_{\omega \rightarrow 0} \frac{d}{d\omega} \Sigma(\omega) = 0$, as expected for a system whose low-energy behavior corresponds to that of a Fermi liquid. This is seen more clearly still in the zoom around $\omega = 0$ in right inset of Fig. 10(a), with the self-energy data associated with the right axis. The self-energy $\Sigma(\omega)/J_H$ sharply drops within $|\omega| \lesssim T_K$ from order 1 accurately down to about 10^{-4} which is considered the NRG resolution limit.

The improved spectral function $A_{\text{imp}}(\omega)$ derived from the self-energy [50] is also shown in Fig. 10 [dashed red (black) line]. Within the Kondo regime, the result closely follows the original $A_{\text{NRG}}(\omega)$, as demonstrated in the zoom in the right inset of Fig. 10(a) or also in panel (b). As expected from the self-energy treatment [50], the improved spectral function $A_{\text{imp}}(\omega)$ allows clearly sharper resolution for structures at finite frequencies, specifically so for larger A . This can be observed, for example, for the hybridization side peaks in Fig. 10(b) at the energy of the Hund's coupling J_H . Having chosen J_H much larger than the bandwidth [with the bandwidth indicated by the vertical dotted line in panel (b)], these hybridization side peaks essentially correspond to very narrow, nearly discrete peaks that are much overbroadened through the standard log-Gauss broadening of the NRG [31,44]. In principle, these side peaks could be narrowed significantly further by an adaptive broadening scheme [52]. For the purposes of this paper, however, this was irrelevant.

The dynamically generated exponentially small Kondo temperature T_K for the system can be determined by taking the full-width-at-half-maximum (FWHM) of the Kondo peak in the spectral function. However, with NRG somewhat sensitive to broadening of the underlying discrete data [44] (see also supplementary material in Ref. [31]), T_K is simply determined therefore through the static magnetic susceptibility $\chi_0 =: 1/4T_K$ [50], where χ_0 is obtained from the impurity spin-spin correlation function $\chi(\omega) \equiv \langle S_{(z),d} \| S_{(z),d} \rangle_\omega \equiv \chi'(\omega) - i\pi \chi''(\omega)$ evaluated at $\omega = 0$, with $S_{(z),d}$ the total spin at the impurity [cf. Eq. (23)]. The resulting spin-spin spectral function $\chi''(\omega)$ is shown in the left inset to Fig. 10(a), together with the resulting $T_K = 4.4 \cdot 10^{-7}$ (in units of bandwidth). As expected, $\chi''(\omega)$ shows a pronounced maximum around T_K . The value for T_K is also indicated by the vertical dashed line in panel (b).

The NRG data presented in Fig. 10 clearly suggests converged data, even without necessarily having to resort to self-energy to get the low energy physics correct [27]. The convergence is also

supported by the analysis of the *discarded weight* [41] which, inspired by DMRG, analyzes the decay of the eigenspectrum of site-specific reduced density matrices built from the ground state space a few iterations later. For given NRG run, the discarded weight is estimated as $\varepsilon_{\chi=5\%}^D = 3 \cdot 10^{-11}$. This suggests good convergence, in agreement with Ref. [41]. If, for example, an energy truncation of $E_K = 5, \dots, 6$ had been used, instead, NRG intrinsic parameter dependent deviations of up to ten percents can still be seen *w.r.t.* to the Friedel sum-rule or the agreement of $A_{\text{NRG}}(\omega)$ with $A_{\text{imp}}(\omega)$.

6.2. Detailed comparison of symmetry settings

An NRG specific technical comparison of the symmetry settings in Eq. (32) for the calculation in Fig. 10 is presented in Fig. 11. The underlying truncation had been energy-based in all calculations ($E_K = 7$), thus leading to a fair comparison in terms of accuracy. With this, the physical properties, and in particular the energy flow diagram [3,50] in Fig. 11(a), show perfect agreement using either symmetry setting. Having sufficiently many states implies that for symmetries, that are not explicitly and thus exactly included in the QSpace setup, their unintended breaking due to numerical double precision noise does not play role.

Fig. 11(b) shows the number of kept multiplets for each iteration k . Having chosen J_H and Γ much larger than the bandwidth [cf. Fig. 10(a)], the free-orbital regime is absent, with the transition from the local moment to the strong coupling regime given by the energy scale of T_K [vertical dashed line at $k \simeq 22$]. As expected from physical grounds, also the local moment regime ($k < 22$) requires a larger state space (multiplet) dimension still for the same accuracy, *i.e.* the same E_K , as compared to the strong coupling regime ($k > 22$).

With the state space truncation based on the energy cutoff $E_K = 7$, the actual Hilbert state space dimension, *i.e.* when including the internal CGC space dimensions, is exactly the same for all symmetry settings. In particular, the maximum total Hilbert state space dimension per iteration that was diagonalized exactly for either symmetry setting was $N_{\text{tot}}^* \leq 4369,024$ or $N_K^* \leq 68,266$ *w.r.t.* kept space only. These state spaces could be strongly reduced to the effective and manageable multiplet dimension as indicated at the top of Fig. 11(b), with Wilson shell specific multiplet dimensions plotted in the panel.

Fig. 11(c) analyzes the actual reduction in multiplet space due to presence of the CGC spaces in terms of the ratio of the actual Hilbert space dimension N_{tot}^* relative to the total multiplet dimension N_{tot} for each site along the Wilson chain. Depending on the symmetry setting, on average, the treatment of non-abelian symmetries allows to reduce the Hilbert space dimension by at least a factor of 16, 20, or 300 for the symmetries in (32), respectively. This demonstrates an enormous numerical gain, considering that the numerical cost of NRG roughly scales like $\mathcal{O}(N_{\text{tot}}^3)$. Note that it is exactly through the dimensional reduction to multiplet spaces, that above NRG calculations had been feasible in practice, and this within a few hours of runtime. In contrast, the plain abelian setting simply would not have been able to deal with the underlying Hilbert state space dimension using state of the art workstations [cf. App. Table C.6].

Within the kept space, the multiplet dimension of the first two settings in (32a) and (32b) relative the setting including the $\text{Sp}(6)$ are shown in the inset to Fig. 11(b) [(a) and (b), respectively]. This clearly demonstrates a further reduction by a factor of about 5...8 when including the full $\text{Sp}(6)$ symmetry. From the same inset, it is also clear that the symmetry setting in Eq. (32b) including $\text{SU}(3)_{\text{channel}}$ allows, on average, a 40% further reduction of the number of multiplets in the simulation as compared to the $\text{SU}(2)_{\text{SC}}^{\otimes 4}$ setting.

Furthermore, the inset to Fig. 11(c) shows the ratio $x_k \equiv N_{\text{tot}}^{(k+1)} / N_K^{(k)}$ which indicates the increase in the total number of multiplets when adding a new site *prior* to truncation. While this factor shows a clear reduction from the actual dimension of the local Hilbert space of a Wilson site of $4^3 = 64$ states, the ratio x_k is somewhat larger than what one may naively expect, considering that, depending on the symmetry, a Wilson site reduces to a total number of 4, 10 or 13 multiplets [see App. Tables C.5, C.4 and C.3, respectively]. On the other hand, given non-abelian symmetries, the combination of two multiplets typically leads to clearly *more* than just one overall multiplet. In this sense, the major gain of using non-abelian symmetries is given by the state space reduction demonstrated in Fig. 11(b). For

the first two symmetry settings in (32), the multiplet space increase by adding a new site in terms of a product space reduces the original abelian factor of 64 only modestly down to about 38. Only when using of the full $\text{Sp}(6)$, this leads to a significant further reduction of the ratio x_k down to about 20, which thus becomes nearly comparable in numerical cost to a two-channel calculation with abelian symmetries, where a Wilson sites adds $4^2 = 16$ states to the system.

The $\text{SU}(3)$ representations that are explicitly generated in the calculation of Fig. 10 using $\text{SU}(2)_{\text{spin}} \otimes \text{U}(1)_{\text{charge}} \otimes \text{SU}(3)_{\text{channel}}$ are listed in Fig. C.14 [Appendix C.3]. The largest Clebsch–Gordan space that is split off with respect to the $\text{SU}(3)$ sector only is the $(4, 4)$ representation with an internal multiplet dimension of 125. In other words, by explicitly accounting for $\text{SU}(3)$ symmetries, in the present case, a 125-fold degeneracy in the Hamiltonian had been reduced to a *single* multiplet, with the $\text{SU}(3)$ symmetry space taken care of separately with minor computational overhead. Nevertheless, the eigenstates in the $\text{SU}(3)$ setting still show significant degeneracies. These can be entirely removed only by using the full $\text{Sp}(6)$ symmetry, which allows to remove *original degeneracies in the Hamiltonian of several thousands*. Note that on top of above symmetries, the spin $\text{SU}(2)$ multiplets present yet another independent multiplet space that enters as a tensor product, thus enlarging the overall symmetry space still further.

In terms of overall runtime on a state-of-the-art 8-core workstation, this translated to about 6 h of runtime for the $\text{SU}(2)_{\text{SC}}^{\otimes 4}$ symmetries, as compared to about 4.5 h of runtime when including $\text{SU}(3)_{\text{channel}}$. Using the full symmetry as in (32c), on the other hand, took about 24 h. While significantly more efficient in terms of storage requirements [cf. App. Table C.7] thus facilitating calculations on standard workstations, the huge CGC spaces in the last setting must be dealt with carefully. As can be seen from Fig. 11(b), the total number of kept multiplets hardly reaches 400, while the $\text{Sp}(6)$ multiplets are fully comparable in terms of dimensionality, with some multiplets even much larger internally than the actual number of multiplets considered [cf. App. Table C.8]. While the sparse algebra had been optimized by ourselves to also make use of the parallel shared memory capacity [cf. Appendix C.3.2], in contrast, the full multiplet spaces had access to the highly optimized shared BLAS libraries. The latter benefitted the first two symmetry settings (32a) and (32b) in terms of overall runtime. However, there is clearly room for further improvement in dealing with the sparse algebra for larger rank symmetries as in (32c).

7. Summary and outlook

A generic and transparent framework has been presented for the implementation of non-abelian symmetries in tensor-networks in terms of QSpaces. For this, it was assumed that all participating state spaces are strictly orthonormal and can be assigned proper well-defined symmetry labels. Therefore the presented framework is straightforwardly applicable to the traditional DMRG as well as to the NRG. The latter was demonstrated in detail in this paper for an $\text{SU}(3)$ symmetric 3-channel problem, which in the presence of particle–hole symmetry can be further enlarged still to the symplectic symmetry $\text{Sp}(6)$. By reducing the actual state space to the reduced multiplet space, while factorizing the Clebsch–Gordan coefficient space, this allows an efficient description of all relevant tensors. While the explicit Clebsch–Gordan algebra bears little overhead for combinations of lower rank symmetries, the average internal multiplet dimensions grow quickly with increasing rank r of a symmetry. In practice, one may roughly estimate that the typical internal multiplet dimension grows like $\mathcal{O}(10^r)$, for example, having $r = 0, 1, 2, 3$ for abelian, $\text{SU}(2)$, $\text{SU}(3)$, and $\text{Sp}(6)$, respectively. Starting with $r = 3$, an efficient sparse scheme on all CGC spaces becomes crucial. For symmetries with rank larger than three, finally, it appears desirable to develop general strategies and sum rules for the contraction of extended complex networks of CGC spaces based on $6n$ - j symbols.

A detailed self-contained general introduction to non-abelian symmetries is given in Appendix A, followed by many explicit examples that arise in practice (Appendix C). Several further highlights explained in detail in Appendix B are: (i) a straightforward numerical recipe for the general calculation of Clebsch–Gordan coefficients based on explicit product space decomposition in the presence of multiplicity, (ii) a generic recipe for the determination of irreducible operator sets, and last but not least, (iii) also a general algorithm to get the framework for several symmetries initialized from plain Fock space. The latter does not require any initial detailed knowledge of specific symmetry labels other

than the general action of the underlying generators. These are known in second-quantized form and thus also easily defined in Fock space.

While the work presented here is limited to situations where effective state spaces are orthonormal and thus can be simply categorized using well-defined symmetry labels, this eventually may be relaxed to some extent. For example, orthonormal state spaces are not straightforwardly applicable to two-dimensional systems with two-dimensional tensor networks due to the presence of loops. Nevertheless, the indices that connect tensors may be given a more physical interpretation in terms of actual auxiliary physical state spaces [53,54]. This had been at the very basis of the original AKLT construction [37,55] which subsequently was generalized to two-dimensional (i)PEPS networks [56,57]. With parity symmetry [58–60] and simple abelian symmetries such as Z_n [61] successfully employed for two-dimensional fermionic systems, iTEBD based algorithms [62,63] may open the grounds to also use the non-abelian tensor framework as described in this work in a widened context.

Finally, it is emphasized that also superoperators permit full treatment in terms of symmetries using Clebsch–Gordan coefficient spaces [64,65]. Note, for example, that the reduced density matrices considered in this work are all block-diagonal w.r.t. symmetries. As such they correspond to vectors in superoperator space with well-defined symmetry label, in that the *difference* of its quantum labels in regular operator space is zero throughout. In general, this may also open the door to using the QSpace framework presented here to the simulation of Liouvillian superoperators such as they occur, for example, in the Lindblad equation for driven systems.

Acknowledgments

I want to thank Jan von Delft, Arne Alex, and Alan Huckleberry for fruitful discussions on $SU(N)$ representation theory, and also G. Zarand and I. Weymann for helpful discussions on the implementation of non-abelian symmetries in context of conventional NRG calculations. In addition, I want to thank the people above and also Markus Hanl for their critical reading of the manuscript. This work received support from the DFG (SFB-631, De-730/3-2, De-730/4-2, SFB-TR12, WE4819/1-1).

Appendix A. Non-abelian symmetries 101

The general more pedagogical introduction of non-abelian groups in this appendix emerges from a practical numerical background of treating quantum many-body phenomena. It does not claim to cover non-abelian symmetries in every theoretical detail, yet requires certain elementary concepts which will be reviewed briefly. The main focus of this appendix then is on practical applications in quantum lattice models. Specifically, this targets the numerical renormalization group (NRG) [3,44], density matrix renormalization group (DMRG) [2,36,37] or more generally tensor networks [8,25], yet also exact diagonalization, which itself may be formulated in a matrix product state language. This appendix offers a general treatment of continuous non-abelian symmetries, with modifications towards abelian, point-groups, or discrete non-abelian symmetries straightforward. Overall, this appendix should be self-contained, sufficient and hopefully helpful to deal with general abelian and non-abelian symmetries in numerical simulations.

The non-abelian symmetries of concern in this paper are continuous symmetries. An element \hat{G} of the corresponding Lie group $\hat{\mathcal{G}}$ can be parameterized by a set of g continuous, independent, and real parameters a_σ [38,66,67],

$$\hat{G}(a_1, \dots, a_g) = \exp\left(i \sum_{\sigma=1}^g a_\sigma \hat{S}_\sigma\right), \quad (\text{A.1})$$

with g the dimension of the symmetry group. Infinitesimal operations with $a_\sigma \ll 1$ then define the set of g generators $\{\hat{S}_\sigma\}$, the number of which thus also reflects the dimension of the group (note that the identity operator is a trivial operation which therefore is never part of the set of generators). For unitary symmetries, as considered throughout in this paper, the generators in Eq. (A.1) are hermitian. Furthermore, when dealing with exponentially large yet finite-dimensional quantum-many-body

Hilbert spaces, the non-abelian symmetries necessarily also have finite-dimensional, *i.e.* compact Lie algebras.

The commutator relations of the generators in Eq. (A.1),

$$[\hat{S}_\sigma, \hat{S}_\mu] = \sum_v f_{\sigma\mu v} \hat{S}_v, \quad (\text{A.2})$$

determine the tensor of the *structure constants* $f_{\sigma\mu v}$, which itself fully defines the underlying *Lie algebra*. The tensor $f_{\sigma\mu v}$ is antisymmetric in that by construction $f_{\sigma\mu v} = -f_{\mu\sigma v}$, yet not necessarily fully antisymmetric also w.r.t. to the last index v [in principle, it can be made fully antisymmetric using the *Cartan–Killing metric*, while distinguishes between co- and contravariant indices in Eq. (A.2) [66,67]; for simplicity, however, this distinction is not made in this paper]. All generators are assumed to be connected to each other through above commutator relations. That is, if a subgroup of generators fully decouples in that it commutes with the rest of the generators, then this subgroup forms a symmetry of its own. In this sense the group of generators for a specific *simple* symmetry is irreducible.

A set of matrices $\{R_\sigma\}$, that obeys exactly the same commutator relations as the generators (operators) $\{\hat{S}_\sigma\}$ in Eq. (A.2), allows a one-to-one correspondence between the matrices $\{R_\sigma\}$ and the generators of the symmetry. It is called a *matrix representation* of the Lie algebra. If the *carrier space*, *i.e.* the vector space within which the matrix representation is defined, is fully explored through repeated application of the individual matrices of the representation, then this is called an *irreducible* matrix representation, to be denoted as $\{I_\sigma\}$ henceforth. It is unique up to an overall similarity transformation. Together with its carrier space it refers to an irreducible representation (IREP), specified by a unique label q . If, on the other hand, part of the carrier space of a matrix representation decouples, the representation is called *reducible*. This will be discussed in significantly more detail later in the context of state space decomposition in Appendices A.5 and A.6.

Consider an irreducible matrix representation $\{I_\sigma^q\}$ for IREP q of dimension d_q . Its carrier space is spanned by the *multiplet* $|q\rangle \equiv \{|qq_z\rangle\}$, where q_z references the individual states within the multiplet q (consider, for example, spin multiplets, where $|qq_z\rangle \equiv |S, S_z\rangle$). The states $|qq_z\rangle$ forms an irreducible space w.r.t. the action of the generators, in that for an arbitrary symmetry operation \hat{G} as in Eq. (A.1),

$$\hat{G}|qq_z\rangle = \sum_{q'_z} G_{q_z, q'_z}^q |qq'_z\rangle, \quad (\text{A.3a})$$

some linear superposition within the same multiplet space arises. The coefficients G_{q_z, q'_z}^q form a $d_q \times d_q$ dimensional matrix, which represents the symmetry operation \hat{G} within multiplet q , and is given by $G^q \equiv \exp(i \sum_\sigma a_\sigma I_\sigma^q)$ for some arbitrary but fixed values a_σ .

Similar to the multiplet space $|qq_z\rangle$ of dimension d_q , an *irreducible operator* (IROP) set $\hat{F}^q \equiv \{\hat{F}_{q_z}^q\}$ can be defined in a completely analogous manner. While it is not constrained to a specific carrier space, the IROP \hat{F}^q consists of a set of d_q operators that are associated with multiplet q . As such, it can be written as a vector of operators, *i.e.* a generalized spinor. For a given symmetry operation \hat{G} then, the IROP transforms analogously to Eq. (A.3a), which for an operator implies

$$\hat{G}\hat{F}_{q_z}^q \hat{G}^{-1} = \sum_{q'_z} G_{q_z, q'_z}^q \hat{F}_{q'_z}^q. \quad (\text{A.3b})$$

On the level of infinitesimal operations, $|a_\sigma| \ll 1$, in contrast to the plain action of generators on a ket-state as in Eq. (A.3a), Eq. (A.3b) shows that the transformation of an IROP directly translates to *commutator relations* [*l.h.s.* of Eq. (A.3b)] with the generators of the symmetry, instead.

The practical relevance of above general statements will be discussed in much detail in what follows, together with many examples relevant in actual numerical calculations.

A.1. Simple example: rotational symmetry

A simple and well-known example of a non-abelian symmetry is the rotational group SO(3) in real space in three dimensions. An arbitrary rotation can be written as $G = e^{iS}$ with S an arbitrary

hermitian, yet fully complex three-dimensional *matrix* (hence no hats). The latter is required for G to be real. Consequently, this leaves three real parameters (a_x, a_y, a_z), with $S = a_x S_x + a_y S_y + a_z S_z$. The generators [38]

$$S_x = \begin{pmatrix} 0 & 0 & 0 \\ 0 & 0 & -i \\ 0 & i & 0 \end{pmatrix}, \quad S_y = \begin{pmatrix} 0 & 0 & i \\ 0 & 0 & 0 \\ -i & 0 & 0 \end{pmatrix}, \quad S_z = \begin{pmatrix} 0 & -i & 0 \\ i & 0 & 0 \\ 0 & 0 & 0 \end{pmatrix} \quad (\text{A.4})$$

represent infinitesimal rotations around the x , y , and z -axis, respectively. The $\text{SO}(3)$ symmetry therefore has dimension $g = 3$, and its Lie algebra is defined by,

$$[\hat{S}_\sigma, \hat{S}_\mu] = i \sum_v \varepsilon_{\sigma\mu\nu} \hat{S}_v, \quad (\text{A.5})$$

with $\sigma, \mu, \nu \in \{x, y, z\}$ and $\varepsilon_{\sigma\mu\nu}$ the Levi-Civita tensor, having switched to general operator notation [operator \hat{S} (with hat) rather than matrix S]. Being generators of $\text{SO}(3)$, the matrix representation in Eq. (A.4) already represents a 3-dimensional IREP. As it is the simplest non-trivial IREP for the Lie algebra of $\text{SO}(3)$, it is also called its *defining representation*. By combining state spaces that share this symmetry then, many other IREPs can be generated, including, for example, the (trivial) scalar representation of dimension one.

With respect to continuous functions $f(x, y, z)$ in three-dimensional space, the generators of infinitesimal rotations are given by the differential operator described by the angular momentum operator $\hat{\mathbf{L}} = \hat{\mathbf{r}} \times \hat{\mathbf{p}}$ with $\hat{\mathbf{p}} \sim \nabla_{\mathbf{r}}$. By construction, its three components \hat{L}_i also obey exactly the same Lie algebra as the generators in Eq. (A.5). The same also holds for the spin algebra $\text{SU}(2)$ in complex space, which describes the symmetry for spinful particles such as electrons if rotational spin symmetry is not broken, *i.e.* in the absence of an external magnetic field. Hence the rotational group $\text{SO}(3)$ is isomorphic to the spin $\text{SU}(2)$. In contrast to $\text{SO}(3)$, however, the defining representation of $\text{SU}(2)$ is two-dimensional [cf. Eq. (A.6)], and hence also allows half-integer spin multiplets, which are entirely absent in $\text{SO}(3)$. Having essentially twice as many multiplets in $\text{SU}(2)$ as compared to $\text{SO}(3)$, $\text{SU}(2)$ is thus called a double cover or 2:1 cover of $\text{SO}(3)$.

A.2. $\text{SU}(2)$ spin algebra

In this paper, the setup and notation for non-abelian symmetries is generalized from $\text{SU}(2)$. Therefore the symmetry $\text{SU}(2)$ will be recapitulated in some more detail, introducing the semantics used for the general treatment of non-abelian symmetries later. In this sense, the semantics used in this paper is somewhat more inclined towards the physics background, rather than strictly adhering to the mathematical language of Lie algebras. The latter, nevertheless, will be indicated in context.

Similar to the $\text{SO}(3)$ symmetry, an arbitrary unitary transformation in two-dimensional complex space is given by $G = e^{iS}$ with S an arbitrary two-dimensional hermitian matrix. This again has three independent real parameters (a_x, a_y, a_z), such that $S = a_x S_x + a_y S_y + a_z S_z$. Here $S_\sigma = \frac{1}{2} \tau_\sigma$, with $\sigma \in \{x, y, z\}$, is given by the standard Pauli spin matrices τ_σ ,

$$\tau_x = \begin{pmatrix} 0 & 1 \\ 1 & 0 \end{pmatrix}, \quad \tau_y = \begin{pmatrix} 0 & -i \\ i & 0 \end{pmatrix}, \quad \tau_z = \begin{pmatrix} 1 & 0 \\ 0 & -1 \end{pmatrix}. \quad (\text{A.6})$$

For $\text{SU}(2)$, this represents the smallest non-trivial matrix representation, therefore this also becomes its defining representation. The commutator relations of the matrices τ_σ are *exactly* the same as for $\text{SO}(3)$ in Eq. (A.5), since $\text{SU}(2)$ also refers to the same rotational symmetry. Therefore, the generators for $\text{SU}(2)$ will again also be denoted by the operators $\{\hat{S}_\sigma\}$ with $\sigma \in \{x, y, z\}$ in what follows.

For a general irreducible representations of $\text{SU}(2)$, *e.g.* a spin multiplet, the usual choice of basis is such that the z -component of the spin operator, \hat{S}_z , becomes diagonal in its matrix representation S_z , while the other two operators \hat{S}_x and \hat{S}_y remain non-diagonal (due to their non-commuting properties, only one spin component can be fully diagonalized, given the freedom of a similarity transformation for the whole representation). Using the notation $|qq_z\rangle \equiv |S, S_z\rangle$ for general spin multiplets, the

multiplet label q (q -label) then can take the values $q = 0, \frac{1}{2}, 1, \frac{3}{2}, 2, \dots$ with the internal multiplet label (z -label) spanning the $2q + 1$ values $q_z \in \{-q, -q + 1, \dots, +q\}$. The raising and lowering operators (RLOs) are defined as [32]

$$\hat{S}_\pm \equiv \hat{S}_x \pm i\hat{S}_y, \quad (\text{A.7})$$

such that $\hat{S}_- \equiv (\hat{S}_+)^{\dagger}$, with the commutator relations

$$[\hat{S}_z, \hat{S}_\pm] = \pm \hat{S}_\pm \quad (\text{A.8a})$$

$$[\hat{S}_+, \hat{S}_-] \equiv [\hat{S}_+, \hat{S}_+^\dagger] = 2\hat{S}_z. \quad (\text{A.8b})$$

For spin multiplets $|qq_z\rangle$ then, it holds [32]

$$\begin{aligned} \hat{S}_z |qq_z\rangle &= q_z |qq_z\rangle \\ \hat{S}_\pm |qq_z\rangle &= \sqrt{q(q+1) - q_z(q_z \pm 1)} |q, q_z \pm 1\rangle. \end{aligned} \quad (\text{A.9})$$

While the operator set $\{\hat{S}_x, \hat{S}_y, \hat{S}_z\}$ generates the SU(2) symmetry group, this set itself *does not* yet represent an irreducible operator (IROP), in that it does not yet transform according to a specific symmetry multiplet. For this, a specific linear superposition of the original operators as in Eq. (A.8b) is required. In particular, the transformation of an IROP set under given symmetry is completely analogous to the transformation of the symmetry eigenstates in Eq. (A.9). As indicated with Eq. (A.3b), the major difference is that the action of a generator \hat{S}_σ applied onto a state is simply replaced by the *commutator* of the generator with an operator. For example, for an IROP \hat{F}^q given in terms of the set of operators $\{\hat{F}_{q_z}^q\}$ which transform like the (state) multiplet q , it follows for consistency with Eq. (A.9),

$$[\hat{S}_z, \hat{F}_{q_z}^q] = q_z \hat{F}_{q_z}^q \quad (\text{A.10a})$$

$$[\hat{S}_\pm, \hat{F}_{q_z}^q] = \sqrt{q(q+1) - q_z(q_z \pm 1)} \cdot \hat{F}_{q_z \pm 1}^q. \quad (\text{A.10b})$$

This allows, for example, to complete the operator \hat{S}_z into an *irreducible* spin operator set as follows. Clearly, $[\hat{S}_z, \hat{S}_z] = 0 \cdot \hat{S}_z$, which implies that the operator \hat{S}_z has z -label $q_z = 0$, i.e. $\hat{S}_0^q \equiv \hat{S}_z$ with q still unknown. Applying the RLOs yields the operators corresponding to $q_z = \pm 1$,

$$\underbrace{[\hat{S}_\pm, \hat{S}_0^q]}_{=[\hat{S}_\pm, \hat{S}_z]=\mp \hat{S}_\pm} = \sqrt{q(q+1) + 0} \cdot \hat{S}_{\pm 1}^q.$$

With the further application of RLOs yielding zero, i.e. $[\hat{S}_+, \hat{S}_+] = [\hat{S}_-, \hat{S}_-] = 0$, the operator space is thus exhausted. The *irreducible* spin operator set therefore has three members $q_z \in \{-1, 0, +1\}$, and thus transforms like a spin multiplet $q = \max(q_z) = 1$,

$$\hat{S}^1 \equiv \{\hat{S}_{q_z}^1\} \equiv \begin{pmatrix} \hat{S}_{1,+1} \\ \hat{S}_{1,0} \\ \hat{S}_{1,-1} \end{pmatrix} = \begin{pmatrix} -\frac{1}{\sqrt{2}} \hat{S}_+ \\ \hat{S}_z \\ +\frac{1}{\sqrt{2}} \hat{S}_- \end{pmatrix}. \quad (\text{A.11})$$

Note that the signs and prefactors are crucial for consistency with the Wigner–Eckart theorem later.

In above derivation, the z -operator in Eq. (A.10a) allowed to directly determine the z -label q_z . The RLOs in Eq. (A.10b), on the other hand, served to explore the multiplet space, in that they generated the remaining operators $\hat{F}_{q_z}^q$ with proper well-defined prefactors. In the given case of spin SU(2), these factors are known [*cfr. r.h.s. of Eq. (A.10b)*]. In situations, where they may not be known right away, they can nevertheless be determined in a straightforward manner. For simplicity, in the absence of inner multiplicity for a given multiplet, for canonical raising or lowering operator S_\pm (see Appendix A.3.2) the combined application of \hat{S}_\pm followed by \hat{S}_\pm^\dagger onto an operator of given multiplet q results in the same operator, *i.e.*

$$[\hat{S}_\pm^\dagger, [\hat{S}_\pm, \hat{F}_{q_z}^q]] = a_{\pm}^2 \hat{F}_{q_z}^q,$$

from which the prefactor a_{\pm}^2 can be easily determined. The analogous situation for a state space multiplet $|qq_z\rangle$ is $\hat{S}_{\pm}^\dagger \hat{S}_{\pm} |qq_z\rangle = a_{\pm}^2 |qq_z\rangle$, with $a_{\pm}^2 \geq 0$ since $\hat{S}_{\pm}^\dagger \hat{S}_{\pm}$ is a positive operator; in the case of spin SU(2), this exactly reflects the prefactor on the r.h.s. of Eq. (A.10b), i.e. $a_{\pm}^2 = q(q+1) - q_z(q_z \pm 1) \geq 0$. Therefore if the application of \hat{S}_{\pm} results in a new operator component in the multiplet, i.e. $a_{\pm}^2 > 0$, then this operator is exactly given by

$$\hat{F}_{q_z}^q = \frac{1}{\sqrt{a_{\pm}^2}} [\hat{S}_{\pm}, \hat{F}_{q_z}^q]. \quad (\text{A.12})$$

This already contains the correct normalization and sign, with the latter strictly determined by the outcome of the commutator. The z -label q_z can be derived directly from the structure constants of the underlying Lie algebra, i.e. Eq. (A.10a). For a more general discussion on IROPs and their general decomposition also in the presence of inner multiplicity for the IROP multiplet q , see Appendix A.7.

A.3. Generators and symmetry labels

Within a quantum mechanical framework, symmetries \mathcal{S} are described by a set of generators \hat{S}_{σ} that leave the Hamiltonian \hat{H} of the system invariant. Therefore it must hold for all generators of the symmetries considered that

$$[\hat{S}_{\sigma}, \hat{H}] = 0. \quad (\text{A.13})$$

Thus by definition, the Hamiltonian is a *scalar* operator. The generators of independent symmetries \mathcal{S} and \mathcal{S}' commute trivially, by definition, as they operate in independent symmetry sectors. Therefore, for simplicity, a single specific non-abelian symmetry \mathcal{S} is considered in the following, also referred to as *simple* non-abelian symmetry, a prototypical example being SU(N).

Therefore let \mathcal{S} be a simple non-abelian symmetry. By construction then, its set of generators $\{\hat{S}_{\sigma}\}$ is fully connected via the structure constants in Eq. (A.2), i.e. is irreducible but not necessarily an IROP yet [e.g. see previous discussion for SU(2)]. With the symmetry reflected in the unitary transformation $\hat{G} = e^{i\varepsilon \hat{S}_{\sigma}}$ with hermitian \hat{S}_{σ} [cf. Eq. (A.1)], it follows that for infinitesimal $\varepsilon \ll 1$, the invariance of the Hamiltonian under this unitary transformation, i.e. $\hat{U}\hat{H}\hat{U}^\dagger = \hat{H}$, is trivially equivalent to Eq. (A.13).

In order to ensure maximally independent generators, all operators in $\{\hat{S}_{\sigma}\}$ can be taken orthogonal with respect to each other and specifically also with respect to the identity matrix (which is always excluded from the set of generators $\{\hat{S}_{\sigma}\}$). This requires a scalar or inner product for matrices, which is provided by

$$\langle A, B \rangle \equiv \text{tr}(A^\dagger B), \quad (\text{A.14})$$

together with the resulting Frobenius norm $\|A\|^2 = \langle A, A \rangle = \text{tr}(A^\dagger A)$. For the generators of the symmetry, thus one requires

$$\text{tr}(S_{\sigma}^\dagger S_{\sigma'}) = a_{\sigma} \delta_{\sigma\sigma'} \quad (\text{A.15a})$$

$$\text{tr}(S_{\sigma}) = \text{tr}(\mathbf{1}^\dagger S_{\sigma}) = 0, \quad (\text{A.15b})$$

The generators in Eq. (A.15b) are understood as finite-dimensional matrix representations of the operators \hat{S}_{σ} in some specific carrier space, here the defining representation. Moreover, the orthogonality w.r.t. to the identity in the last equation implies that all generators S_{σ} are traceless. Note that if $\mathbf{1}$ had been amongst the generators, it would form a subgroup of its own, and hence can be split off as a U(1) factor. This is exactly, for example, what distinguishes the unitary group U(N) from the special unitary group SU(N).

A.3.1. Z-operators (Cartan subalgebra)

For a given simple non-abelian symmetries, it is always possible to identify a maximal set of mutually commuting hermitian generators which form the so-called *Cartan subalgebra* of

the symmetry's Lie algebra. These can be fully diagonalized simultaneously (together with the Hamiltonian), and hence can be considered diagonal. They shall be referred to as the *z-operators* [as they generalize the concept of the operator S_z for $SU(2)$],

$$[\hat{S}_z, \hat{S}_{z'}] = 0 \quad (\text{z-operators}). \quad (\text{A.16})$$

For a given Hamiltonian \hat{H} then, this implies that every eigenstate $\hat{H}|n\rangle = E_n|n\rangle$, in addition, can also be labeled with its respective set of symmetry labels $|n\rangle \rightarrow |qn; q_z\rangle$, leading to

$$\hat{H}|qn; q_z\rangle = E_{qn}|qn; q_z\rangle. \quad (\text{A.17})$$

Here q identifies the multiplet, *i.e.* a set of states q_z that are connected in an irreducible manner through all of the generators of the symmetry. While the index n originally identified all states in given Hilbert space, it is now sufficient that it labels the multiplet within the space of multiplets that share the same q . The composite index (qn) then is referred to as the *multiplet index*. Similarly, also the eigenenergies E_{qn} in Eq. (A.17) acquire symmetry labels. These, however, are independent of q_z since, by construction, the states within a symmetry multiplet are degenerate in energy. More generally, with q_z entirely determined by symmetry for a given multiplet q , they can easily be generated and thus omitted where convenient.

Given a specific multiplet qn , the labels q_z are equal to the eigenvalues of the z-operators,

$$\hat{S}_z|qn; q_z\rangle = q_z|qn; q_z\rangle \quad (\text{z-labels}), \quad (\text{A.18})$$

which will be referred to as *z-labels*. If more than one z-operator is associated with given symmetry δ , say a total of r z-operators, where r thus defines to the *rank* of the symmetry, then the z-label structure associated with a multiplet also consist of a collective set of r z-labels (note that r needs to be differentiated here from the rank r of a tensor or QSpace as used in the main text). For example, the symmetry group $SU(N)$ has rank $r = N - 1$. Therefore the rank of $SU(2)$ is 1, *e.g.* a single label q suffices to identify a state within an $SU(2)$ spin multiplet. $SU(3)$, on the other hand, already acquires a two-dimensional label structure for q_z , and thus also for q .

Note that the z-labels in Eq. (A.18) for the states of a specific multiplet q may not necessarily be unique, in that the *same* q_z may occur multiple times. Let m_z describe how often a specific z-label occurs within given multiplet q . Then the presence of $m_z > 1$ for at least one z-label is called *inner multiplicity*. It is then necessary to introduce an extra label α that uniquely identifies the state within this degeneracy,

$$|qn; q_z\rangle \rightarrow |qn; q_z\alpha_z\rangle, \quad (\text{inner multiplicity}) \quad (\text{A.19})$$

with $\alpha_z \in \{1, \dots, m_z\}$. While inner multiplicity is absent for $SU(N \leq 2)$, it occurs on a regular basis for $SU(N \geq 3)$. The situation for *outer* multiplicity is analogous (see Appendix A.5).

The label for the entire multiplet q (to be referred to collectively as *q-labels*) is in principle arbitrary, yet must be unique to identify the multiplet. Since for a continuous symmetry infinitely many IREPs exist, it is natural that the *q-labels* inherit the r -dimensional label structure of the z-labels. In particular, it is possible to construct a set of r scalar operators, called Casimir operators, that define a unique set of r constants for each multiplet. In practice, however, the *q-labels* are derived from $q \equiv \max\{q_z\}$, *i.e.* by the z-labels corresponding to the *maximum weight state* (see Appendix A.3.3) which in principle can be related to the constants derived from the Casimir operators [38].

A.3.2. Raising and lowering operators (roots)

While for an arbitrary unitary element \hat{G} of the symmetry hermitian $\{\hat{S}_\sigma\}$ are required, on the level of generators, in principle, arbitrary linearly-independent linear superpositions within the space of generators \hat{S}_σ can be taken. Using such a reorganized set of generators, instead, this still preserves Eq. (A.13), yet alters the structure constants $f_{\sigma\mu\nu}$ for given symmetry δ . This freedom is used in the following to define canonical raising and lowering operators, which are non-hermitian, in general.

Consider the action of a generator \hat{S}_σ onto a symmetry eigenstate $|qn; q_z\rangle$. The z-operators are special, in that they are diagonal and hence return the same state, yet weighted by the eigenvalue q_z .

The remaining generators, however, are non-diagonal, hence change the state and thus explore the multiplet space. In general, these generators can be reorganized such that all of them represent proper raising or lowering operators (RLOs), with the canonical commutator relations,

$$[\hat{S}_z, \hat{S}_\sigma] = f_{z\sigma\sigma} \hat{S}_\sigma \equiv f_{z\sigma} \hat{S}_\sigma, \quad (\text{A.20})$$

with no summation over σ . The action of these canonical RLOs in z -label space, in the literature also referred to as *root space*, then defines the canonical form. By definition, the canonical RLOs $\{\hat{S}_\pm\}$ of a specific Lie algebra are expected to have the property that their application onto a symmetry eigenstate in the multiplet with well-defined z -labels will generate another eigenstate of the z -operators, yet with raised or lowered, *i.e.* *well-defined different* z -labels. This is exactly what is expressed through the commutator relations in Eq. (A.20). In particular, the structure constants take the simple form, where a non-zero contribution can only arise if the last two indices in $f_{z\sigma\sigma'}$ are identical, hence the shortcut notation $f_{z\sigma}$ in the last term in Eq. (A.20). By construction, $f_{z\sigma}$ is fully antisymmetric. Note that Eq. (A.20) also can be interpreted as an eigenvalue equation for the generators of the group. Since the z -operators \hat{S}_z are symmetric, the resulting eigenvalue problem is always well-defined with real eigenvalues $f_{z\sigma}$.

As a specific example, Eq. (A.20) was already encountered for SU(2) in Eq. (A.8a). Here it states more generally that the commutator of an arbitrary generator \hat{S}_σ with a z -operator yields the very same operator \hat{S}_σ up to the scalar structure factor $f_{z\sigma}$. This factor can be zero, *e.g.* when \hat{S}_σ refers to another z -operator as in Eq. (A.16), therefore $f_{zz'} = 0$. For every z -operator, however, there must exist at least one RLO \hat{S}_σ with $f_{z\sigma} \neq 0$, since otherwise the group of generators would be reducible.

With Eq. (A.20), the application of a generator \hat{S}_σ onto a symmetry eigenstate $|qn; q_z\rangle$ yields

$$\begin{aligned} \hat{S}_z \cdot \hat{S}_\sigma |qn; q_z\rangle &= \underbrace{[\hat{S}_z, \hat{S}_\sigma]}_{\stackrel{(A.20)}{=} f_{z\sigma} \hat{S}_\sigma} |qn; q_z\rangle + \hat{S}_\sigma \cdot \underbrace{\hat{S}_z}_{=q_z |qn; q_z\rangle} |qn; q_z\rangle \\ &= (q_z + f_{z\sigma}) \hat{S}_\sigma |qn; q_z\rangle. \end{aligned} \quad (\text{A.21})$$

If \hat{S}_σ is an RLO with $f_{z\sigma} \neq 0$, the state $\hat{S}_\sigma |qn; q_z\rangle$ is again a symmetry eigenstate, yet with a uniform shift in the z -labels,

$$q_z \rightarrow q_{z'} \equiv q_z + f_{z\sigma}. \quad (\text{A.22})$$

Therefore the action of an RLO \hat{S}_σ in root space is generic, *i.e.* independent of the specific multiplet q or the state q_z under consideration. Nevertheless, the RLO may annihilate the state, *i.e.* $\hat{S}_\sigma |qn; q_z\rangle = 0$, which is essential to obtain a finite-dimensional multiplet space. Furthermore, Eq. (A.22) allows to pair up raising and lowering operators. That is, if \hat{S}_σ is a raising operator, then with

$$[\hat{S}_z, (\hat{S}_\sigma)^\dagger] = -[\hat{S}_z, \hat{S}_\sigma]^\dagger = -f_{z\sigma} (\hat{S}_\sigma)^\dagger, \quad (\text{A.23})$$

the operator $(\hat{S}_\sigma)^\dagger$ changes the z -labels exactly in the opposite direction as \hat{S}_σ in Eq. (A.22). In this sense, $(\hat{S}_\sigma)^\dagger \equiv \hat{S}_{-\sigma}$ represents the corresponding lowering operator. The actual definition of what is a raising or lowering operator is not entirely unique, as it depends on the specific underlying sorting scheme of the z -labels adopted in root space. This does not matter, however, as long as the sorting is done consistently throughout [66,67].

In the presence of inner multiplicity a few complications arise. Most importantly, an RLO usually will generate a superposition in the $m_{z'}$ -fold degenerate state space in the resulting $q_{z'}$,

$$\hat{S}_\sigma |qn; q_z \alpha_z\rangle = \sum_{\alpha_{z'}=1}^{m_{z'}} s_{q_z \alpha_z; q_{z'} \alpha_{z'}}^{[q\sigma]} |qn; q_{z'} \alpha_{z'}\rangle \quad (\text{A.24})$$

with some coefficients $s_{q_z \alpha_z; q_{z'} \alpha_{z'}}^{[q\sigma]}$. As a consequence, the application of a raising operator \hat{S}_σ followed by its complimentary lowering operator \hat{S}_σ^\dagger onto a symmetry eigenstate,

$$\hat{S}_\sigma^\dagger \hat{S}_\sigma |qn; q_z \alpha_z\rangle = \sum_{\alpha_{z'}=1}^{m_z} s_{q_z; \alpha_z \alpha_{z'}}^{[q\sigma]} |qn; q_z \alpha_{z'}\rangle \quad (\text{A.25})$$

with some other coefficients $s_{q_z; \alpha_z \alpha_{z'}}^{[q\sigma]}$, does return to the same symmetry labels q_z , yet *not necessarily to the same state*. If the resulting state in Eq. (A.25) does not replicate the initial state $|qn; q_z \alpha_z\rangle$ up to an overall factor, then this allows to explore the other states in the degenerate subspace at q_z . This is relevant for the decomposition of state spaces, where the resulting state as in Eq. (A.25) needs to be orthonormalized in a consistent fashion with respect to the already explored states of the multiplet including the state $|qn; q_z \alpha_z\rangle$ (see Appendix B.1, for more details on the numerical implementation).

While all z -operators are required, e.g. for the definition of the z -labels, it is usually not required to explicitly construct all of the RLOs, as some of these operators can be generated through a product of a smaller set of RLOs. As will be seen below in the case of $SU(N)$ or $Sp(2n)$, the number of actually required RLOs can always be reduced to the rank of the symmetry, i.e. the number of z -operators. This minimal set of RLOs will be referred to as *simple* RLOs, consistent with their general notation in the literature as *simple roots* of the symmetry. In a sense, these simple RLOs are the ones that induce the smallest shifts in the z -labels [66,67]. Again, their definition is not entirely unique, depending on conventions such as normalization of generators or what specific sorting scheme is applied to the z -labels. The simple RLOs still fully generate and connect the state spaces of any IREP. The underlying intuitive reason is that an r -dimensional z -label structure only requires r linearly independent vectors to explore its space (for a rigorous proof, see for example Refs. [66,67]). Therefore given r z -operators $\{Z_1, \dots, Z_r\}$, it is sufficient to choose a specific subset of r raising operators $\{S_{1+}, \dots, S_{r+}\}$, with the corresponding lowering operators $S_{i-} \equiv (S_{i+})^\dagger$. This reduction to simple RLOs is very useful in practice, yet does not restrict the non-abelian treatment in any way.

A.3.3. Maximum-weight state

Consider some multiplet q of internal dimension d_q for a given non-abelian symmetry group \mathcal{S} of rank r . Then each of the d_q states carries a set of r z -labels. When depicted graphically as points in r -dimensional space, this is called the *weight diagram* for the multiplet [for $SU(3)$, for example, a collection of weight diagrams generated in an actual NRG run is shown in Fig. C.14]. Since the z -operators are traceless, the values of the z -labels are naturally centered around the origin, i.e. $q_z = 0$. Inner multiplicity, if present, decreases as a function of distance $|q_z|$ to the origin, such that the outermost points in a weight diagram always refer to unique states without any remaining multiplicity. By choosing a *lexicographic* ordering in the r z -labels [38], the *maximum weight* (MW) is defined by

$$q_{\text{MW}} \equiv \max\{q_z\}. \quad (\text{A.26})$$

The state with $q_z = q_{\text{MW}}$ is called the maximum-weight state. This state is guaranteed to be unique to the multiplet for non-abelian symmetries [38,66,67], hence can be used as label for the entire multiplet, i.e. $q = q_{\text{MW}}$. While the state space $|q_z| = \max(|q_z|)$ will not be unique, in general, since it refers to several states at the circumference of the weight diagram, $\max\{q_z\}$ does provide a unique set of z -labels. This underlines the importance of lexicographic ordering.

As an example, consider the well-known spin $SU(2)$. The states within the multiplet q are labeled by $|qq_z\rangle$ where $q_z = -q, \dots, +q$ identifies each state within the multiplet. This results in a one-dimensional weight diagram, with the multiplet itself labeled by the maximum weight states, $q = \max(q_z)$, indeed.

Clearly, the q -labels for a multiplet themselves are also not entirely unique and hence depend on convention. In particular, if the rank of a symmetry group \mathcal{S} is $r > 1$, the order of the z -operators themselves is a priori arbitrary. Hence there is a certain freedom in the order of the z -labels, which in return affects the definition of the maximum weight state. Given a certain order in the z -operators

then, the lexicographic sorting of sets of z -labels is typically done in reverse order, *i.e.* starting with the *last* of the r label for a given q_z . Moreover, having identified q_{MW} , this still leaves the freedom to use a linearly independent transform of q_{MW} as a label for the entire multiplet for consistency with the literature. For example, for SU(3) [Sp(6)] this is discussed with Eq. (A.34) [Eq. (A.91a)], respectively.

A.4. Example SU(N)

A.4.1. Defining representation

The symmetry SU(N) is defined as the unitary symmetry of an N -dimensional space. The defining representation, *i.e.* the IREP with smallest non-trivial dimension, is therefore given by $N \times N$ dimensional matrices. Since according to Eq. (A.15b) all generators are traceless, only $N - 1$ diagonal z -operators exist, the diagonals of which form an N -dimensional orthogonal vector space that is also orthogonal to the diagonal of the identity matrix. The raising (lowering) operators are chosen as $N \times N$ matrices with a single entry of 1 anywhere in the upper (lower) triangular space, respectively, away from the diagonal. For this, let

$$|e_i\rangle \equiv (0, \dots, 0, 1_{(i)}, 0, \dots, 0)^T, \quad (\text{A.27a})$$

with $i \in \{1, \dots, N\}$ be the N -dimensional cartesian column basis vectors, and

$$E_{ij} \equiv |e_i\rangle\langle e_j|, \quad (\text{A.27b})$$

the matrices of the related operator basis, which also contain just a single entry of 1 in their $N \times N$ dimensional matrix space, *i.e.* $(E_{ij})_{i'j'} = \delta_{ii'}\delta_{jj'}$. Then the generators can be written as follows,

$$S_{i \neq j}^{\text{SU}(N)} = E_{ij} = \begin{cases} \text{raising operator for } i < j \\ \text{lowering operator for } i > j \end{cases} \quad (\text{A.28a})$$

$$S_{z,k < N}^{\text{SU}(N)} = \left(\sum_{i=1}^k E_{ii} \right) - kE_{k+1,k+1}. \quad (\text{A.28b})$$

These matrices are orthogonal as in Eq. (A.15), while the (arbitrary) normalization was chosen such that, for convenience, all entries are integers. The choice of generators for SU(N) in Eq. (A.28) guarantees canonical RLOs, and thus simplifies the group's commutator relations *w.r.t.* z -operators exactly the way as indicated in Eq. (A.20). This can be easily seen by observing that for a diagonal operator of the type $(\hat{Z})_{ij} = z_i\delta_{ij}$, the matrix elements of the commutator with an arbitrary operator $(\hat{S})_{ij} = s_{ij}$ is given by

$$[\hat{Z}, \hat{S}]_{ij} = s_{ij}(z_i - z_j),$$

that is, existing non-zero matrix elements in \hat{S} are weighted by differences in diagonal elements of \hat{Z} , while there cannot arise any new matrix elements unequal to zero in $[\hat{Z}, \hat{S}]$ as compared to \hat{S} . Clearly, if \hat{S}_\pm only has a single non-zero entry as for the operators in Eq. (A.28a), it follows $[\hat{Z}, \hat{S}_\pm] = \text{const} \cdot \hat{S}_\pm$, in agreement with Eq. (A.20).

From Eq. (A.28a) above, a total of $\frac{1}{2}N(N - 1)$ different raising operators arise. However, not all of these are required to fully explore the multiplet space. Consider, for example, the subset of $r = N - 1$ raising operators

$$\{S_+^{\text{SU}(N)}\}_r \equiv \{\hat{S}_{12}^{\text{SU}(N)}, \hat{S}_{23}^{\text{SU}(N)}, \dots, \hat{S}_{N-1,N}^{\text{SU}(N)}\}, \quad (\text{A.29})$$

which thus matches the rank r of the symmetry group SU(N) and thus also the number of z -operators. From repeated application of these operators, it is easily seen that the remaining raising operators not contained in Eq. (A.29) can be generated. For example, $\hat{S}_{13}^{\text{SU}(N)}$ is generated by $\hat{S}_{12}^{\text{SU}(N)} \cdot \hat{S}_{23}^{\text{SU}(N)}$. Therefore, above minimal set of r raising operators with their hermitian conjugate set of lowering operators is sufficient, indeed, to explore all multiplet spaces.

A.4.2. The symmetry $SU(3)$

The defining representation for $SU(3)$ is chosen as in Eq. (A.28), with the z -operators given by,

$$Z_1 \equiv \begin{pmatrix} 1 & 0 & 0 \\ 0 & -1 & 0 \\ 0 & 0 & 0 \end{pmatrix}, \quad Z_2 \equiv \begin{pmatrix} 1 & 0 & 0 \\ 0 & 1 & 0 \\ 0 & 0 & -2 \end{pmatrix}. \quad (\text{A.30})$$

Their diagonals can be collected as rows into a matrix,

$$z = \begin{pmatrix} 1 & -1 & 0 \\ 1 & 1 & -2 \end{pmatrix}, \quad (\text{A.31})$$

the columns of which give the z -labels (z_1, z_2) for the three states in the defining representation (see large black dots in Fig. A.12). This represents the weight diagram for the defining representation.

The canonical commutator relations as in Eq. (A.20) yield the structure constants (f) _{z,σ} $\equiv f_{z\sigma}$ for $z \in \{1, 2\}$ and $\sigma \in \{12, 23, 31\}$,

$$f = \begin{pmatrix} 2 & -1 & -1 \\ 0 & 3 & -3 \end{pmatrix}. \quad (\text{A.32})$$

The columns in Eq. (A.32) thus define the roots, *i.e.* the shift in z -labels when applying either S_{12} , S_{23} , or S_{31} , respectively. These vectors (roots) are depicted in Fig. A.12 by large thick arrows. Clearly, the three points in the weight diagram of the defining representation can be connected by these roots, equivalent to (repeatedly) applying raising or lowering operators.

With the convention, that z -labels are lexicographically sorted starting with the last z -label, *i.e.* sorting *w.r.t.* z_2 first and then z_1 , the three states in the defining representation are already properly sorted from largest to smallest [left to right in Eq. (A.30)]. Furthermore, Eq. (A.32) shows that S_{12} and S_{23} correspond to positive roots, since $(2, 0) > (0, 0)$ and also $(-1, 3) > (0, 0)$. As their application makes z -labels *larger*, they represent raising operators, indeed, while S_{31} is a lowering operator, all in agreement with Eq. (A.28a). The third raising operator thus would be S_{13} with root $(1, 3)$ which, however, is not a simple root and hence can be dropped.

Finally, $SU(3)$ still contains well-known $SU(2)$ subalgebras. That is, for example, by using S_{12} as a raising operator for the (x, y) subspace together with its corresponding z -operator $[S_{12}, S_{12}^\dagger] =: 2S_z^{(12)} = Z_1$ while keeping the y component abelian, this shows that every *line of points* in the (z_1, z_2) plane in Fig. A.12 parallel to S_{12} must correspond to a proper $SU(2)$ multiplet. The same also holds for the two remaining permutations of (x, y, z) using S_{23} or S_{31} for the $SU(2)$ subspace, instead. These $SU(2)$ subalgebras clearly obey the standard commutator relations for $SU(2)$.

A.4.3. Symmetry labels for $SU(3)$

The q -labels for a given IREP within $SU(3)$ are derived from its maximum-weight labels $q_{\text{MW}} \equiv \max\{(z_1, z_2)\}$. With the z -labels additive through tensor products (see Appendix A.6 below), the z -labels of arbitrary multiplets must be integer multiples of the z -labels of the defining representation. This immediately excludes the z -labels (points) in Fig. A.12 that are crossed out. In particular, with the columns of Eq. (A.31) being linearly dependent, one may therefore use the columns of

$$\tilde{z} = \begin{pmatrix} 1 & 0 \\ 1 & 2 \end{pmatrix}, \quad (\text{A.33})$$

as basis for the maximum weight labels, for consistency with literature [38,68]. Given q_{MW} , the actual label of the multiplet then is determined by

$$q \equiv (q_1, q_2) \equiv \tilde{z}^{-1} \cdot q_{\text{MW}} = \begin{pmatrix} 1 & 0 \\ -\frac{1}{2} & \frac{1}{2} \end{pmatrix} q_{\text{MW}}. \quad (\text{A.34})$$

This prescription makes the q -labels independent of the specific normalization conventions chosen for the z -operators. Furthermore, with $\tilde{z} = z \cdot (1, 0, -1)^T$ and the vectors in the columns in Eq. (A.33)

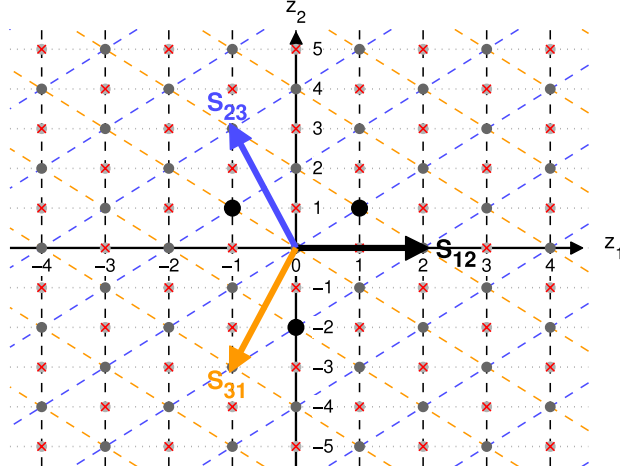


Fig. A.12. (Color online) Root space (z_1, z_2) for $SU(3)$. The three large black dots depict the weight diagram of the three-dimensional defining representation of $SU(3)$. Large arrows indicate the shifts in z -labels due to the action of the raising operators S_{12}, S_{23} , and the lowering operator S_{31} , while dashed lines close to orthogonal to these arrows indicate lines of constant S_{12}, S_{23} , and S_{31} (color match with corresponding arrows). Dark symbols indicate accessible z -labels, while light crossed-out symbols are not accessible within $SU(3)$ (see text).

being positive by the adopted sorting scheme, this guarantees plain positive integers for the multiplet labels q . These labels also lie dense, in the sense that any (q_1, q_2) with $q_i \geq 0$ results in a valid multiplet.

The defining representation with $q_{MW} = (1, 1)$ has the q -label $(1, 0)$. Its weight diagram together with many further examples for multiplets, as generated, in practice, from an actual NRG run using $SU(3)$, are presented in Fig. C.14. Note, however, that weight diagrams are mainly a matter of presentation of multiplets, while in practice a listing of z -labels suffices to describe the multiplet space.

A.5. Decomposition into irreducible representations

The generators of a specific symmetry group \mathcal{S} represent an irreducible finite set of operators $\{\hat{S}_\sigma\}$, assumed to act in the full Hilbert space of a given physical system. Within (small) subspaces of the system, finite dimensional matrix representations can be constructed that obey exactly the same commutator relations as the generators in terms of their structure constants in Eq. (A.2). As such, a given matrix representation $\{R_\sigma\}$ inherits all the properties of the generators. In particular, the matrix representation has the same number of operators as $\{\hat{S}_\sigma\}$ with a one-to-one correspondence in the symmetry label σ . Therefore the z -operators as well as the RLOs share exactly the same interpretation within the D -dimensional carrier space of $\{R_\sigma\}$.

Consider some arbitrary matrix representation $\{R_\sigma\}$ that may have emerged, for example, from a tensor product space. As it operates in a D -dimensional carrier space, all of its matrices share the same dimension $D \times D$. Assume a well-defined symmetry eigenstate within this space is available, to be called seed state, with a typically easy example being a maximum weight state. Then repeated application of RLOs from the set $\{R_\sigma\}$ generates a (sub)space which eventually describes a full symmetry multiplet, i.e. an IREP. By construction this subspace already diagonalizes the z -operators. Thus the z -labels are known, which also provides the q -labels for the multiplet, e.g. by simply taking the maximum weight labels, $q_1 = q_{MW}$.

If this multiplet q_1 with d_{q_1} symmetry eigenstates spans the entire D -dimensional carrier space, then the matrix representation $\{R_\sigma\}$ is already irreducible. If only a subspace of the D -dimensional carrier space was generated, i.e. $d_{q_1} < D$, the matrix representation $\{R_\sigma\}$ is reducible. Multiplet q_1 then defines a fully separated space, given the symmetry operations in $\{R_\sigma\}$. Combining the orthonormal state space of multiplet q_1 as columns into a matrix V_1 , the matrix representation $\{R_\sigma\}$ can be cast

into the space of multiplet q_1 , $R_\sigma \rightarrow I^{[q_1]} \equiv V_1^\dagger R_\sigma V_1$, which thus constructs the irreducible matrix representation $I^{[q_1]}$ for IREP q_1 .

In case the D -dimensional vector space is not exhausted yet, above procedure can be repeated with another seed state within the remainder of the vector space, generating further irreducible multiplets q_2, q_3, \dots , until the D -dimensional vector space is fully exhausted. By combining the state spaces of the multiplets thus generated, the resulting unitary matrix $V \equiv [V_1, V_2, \dots]$ allows to block-decompose the original matrix representation $\{R_\sigma\}$ in terms of its irreducible representations,

$$V^\dagger R_\sigma V = \bigoplus_q M_q I_\sigma^{[q]} \quad (\text{A.35})$$

where q runs through all IREPs $I^{[q]}$. Note that a given IREP may be generated multiple times in the decomposition, which is indicated by the *outer multiplicity* $M_q \in [0, 1, 2, \dots]$. The presence of outer multiplicity therefore refers to the situation that $M_q > 1$ for at least one q in the decomposition. In this case, also inner multiplicity may occur, which refers to non-uniqueness of z -labels within an irreducible multiplet [cf. Eq. (A.19)], both of which are specifically relevant, for example, for $SU(N > 2)$ or $Sp(2n > 2)$.

As seen from above construction, the matrix representation $I^{[q]}$ of IREP q is tightly connected to the symmetry multiplet q . In general, $I^{[q]}$ is unique only up to a global similarity transformation, as this does not affect commutator relations. By using its related multiplet state space, however, this space (i) can be chosen such that it diagonalizes all z -operators, and (ii) can put into a well-defined order as provided, for example, by the lexicographic ordering in the z -labels used to define the maximum weight state. Based on this basis, the matrix representation $I^{[q]}$ can be determined uniquely. This procedure on obtaining unique irreducible matrix representations will be adopted throughout.

The decomposition in Eq. (A.35), finally, can be done fully numerically along the same lines as already sketched above. Particular attention, however, must be paid to issues related to inner and outer multiplicities for overall consistency. This will be discussed in more detail in Appendix B.1.

A.6. Tensor product spaces

Consider two irreducible matrix representations $I^{[q_1]}$ and $I^{[q_2]}$ of some non-abelian symmetry group δ , with their matrix elements written in the basis of the symmetry eigenstates $|q_1 q_{1z}\rangle$ and $|q_2 q_{2z}\rangle$ of the two IREPs q_1 and q_2 , respectively. The two multiplets are assumed to live in different spaces, so they can be joined through a tensor product, i.e. $|q_1 q_{1z}\rangle |q_2 q_{2z}\rangle \equiv |q_1 q_{1z}; q_2 q_{2z}\rangle$. Then the generators of the symmetry in the combined space are defined in an *additive* fashion, which derives from the origin of the generators in infinitesimal symmetry operations, cf. Eq. (A.1),

$$R_\sigma^{\text{tot}} \equiv I_\sigma^{[q_1]} \otimes \mathbf{1}^{[q_2]} + \mathbf{1}^{[q_1]} \otimes I_\sigma^{[q_2]}. \quad (\text{A.36})$$

Note that the additivity of the symmetry generators *directly* also implies the additivity of z -labels for non-abelian symmetries in general. And even if the non-abelian part of the $SU(N)$ symmetry is broken, e.g. reduced to an abelian symmetry with quantum labels q_z , these are, of course, still additive.

By construction, the tensor product representation $\{R_\sigma^{\text{tot}}\}$ in Eq. (A.36) is also a representation of the symmetry, as it obeys the same commutator relations within the combined system as the IREPs $I_\sigma^{[q_i]}$ within their individual space,

$$\begin{aligned} [R_\sigma^{\text{tot}}, R_{\sigma'}^{\text{tot}}] &= [\underbrace{R_\sigma^{[q_1]}, R_{\sigma'}^{[q_1]}}_{=\sum_\mu f_{\sigma\sigma'\mu} R_\mu^{[q_1]}} \otimes \mathbf{1}^{[q_2]} + \mathbf{1}^{[q_1]} \otimes [\underbrace{R_\sigma^{[q_2]}, R_{\sigma'}^{[q_2]}}_{=\sum_\mu f_{\sigma\sigma'\mu} R_\mu^{[q_2]}}] \\ &= \sum_\mu f_{\sigma\sigma'\mu} R_\mu^{\text{tot}}. \end{aligned} \quad (\text{A.37})$$

The product representation $\{R_\sigma^{\text{tot}}\}$, however, is typically reducible. The resulting decomposition into IREPs is done exactly the same way as in Eq. (A.35).

The unitary transformation that rotates the product space $|q_1 q_{1z}; q_2 q_{2z}\rangle$ into its combined symmetry multiplets $|qq_z; (\alpha)\rangle$ is given by the Clebsch–Gordan coefficients (CGCs),

$$|qq_z; (\alpha)\rangle = \sum_{q_{1z}, q_{2z}} |q_1 q_{1z}; q_2 q_{2z}\rangle \underbrace{\langle q_1 q_{1z}; q_2 q_{2z}|qq_z; (\alpha)\rangle}_{\equiv C_{q_{1z}q_{2z};(\alpha)}^{[q_{2z}]}} \quad (\text{A.38})$$

with the shorthand notation $C_{q_{1z}q_{2z};(\alpha)}^{[q_{2z}]}$ for CGCs, consistent with the MPS tensors in the main body of the paper [cf. Eq. (10)]. Note that the CGCs implicitly also carry the multiplet labels q_1 , q_2 , and q . The index α has been added to account for possible outer-multiplicity [cf. Eq. (A.35)], in that for input multiplets q_1 and q_2 the same output multiplet q can appear $M_q^{[q_1, q_2]}$ times, therefore $\alpha = 1, \dots, M_q^{[q_1, q_2]}$ for a given q . If outer multiplicity is absent, the index α can be omitted, hence the round brackets around α in Eq. (A.38) or Eq. (A.39).

As outer multiplicity also refers to *different* multiplets and hence state spaces, the Clebsch–Gordan coefficients, reflecting a unitary transformation, obey the general orthogonality condition,

$$\sum_{q_{1z}q_{2z}} C_{q_{1z}q_{2z};(\alpha)}^{[q_{2z}]} C_{q_{1z}q_{2z};(\alpha')}^{[q_{2z}]} = \delta_{q_z, q'_z} \cdot (\delta_{\alpha, \alpha'}). \quad (\text{A.39})$$

This holds within the same output multiplet q , whereas the overlap between different output multiplets is strictly zero. While outer multiplicity is intrinsically connected to the underlying symmetry and hence to CGCs, in addition, this also affects the output multiplet space which must accommodate the additional multiplets [e.g. see QSpace discussion in the main text; note also that Eq. (A.39) is completely analogous in structure to the orthogonality relation of A -tensors as in Eq. (11)].

A.7. Irreducible operator sets and Wigner–Eckart theorem

Consider a set of generators $\{\hat{S}_\sigma\}$ of some symmetry group \mathcal{S} that a Hamiltonian \hat{H} commutes with. Then all energy eigenstates of the Hamiltonian can be categorized with well-defined quantum-labels, as indicated in Eq. (A.17). In order to maintain an effective book keeping of the quantum labels when calculating matrix elements of operators, it must be possible to similarly categorize the operators themselves. Typically, the operators of interest are closely related to the Hamiltonian, i.e. consist of operators that also appear in the Hamiltonian or are composites thereof, such as creation, annihilation, occupation, spin operators, etc. Since the Hamiltonian can be properly constructed within the given symmetry, so can be its constituents.

An *irreducible operator set* is constructed in a completely analogous fashion as an irreducible state space, with an explicit example already derived for the spin operator in Eq. (A.11) using Eq. (A.10). Consider the generic setup of a set of generators $\{\hat{S}_\sigma\}$ including RLOs. Then irreducible state multiplets can be generated through iterative application of these operators,

$$\hat{S}_\sigma |qq_z\rangle = s_{q_z q'_z}^{[q_\sigma]} |qq'_z\rangle, \quad (\text{A.40})$$

as in Eq. (A.24), while ignoring inner multiplicity for the sake of the argument and having dropped the energy multiplet index n for simplicity. Given an operator \hat{F} , on the other hand, its transformation according to a symmetry is fully reflected in its *commutator relations* with the generators of the symmetry. This is easily motivated through infinitesimal symmetry operations as in Eq. (A.3b). The commutator relations, on the other hand, also emerge naturally when analyzing the effect of a generator of the symmetry acting onto a symmetry state $|qq_z\rangle$ that already also has the operator \hat{F} applied to it,

$$\hat{S}_\sigma \cdot \hat{F} |qq_z'\rangle = [\hat{S}_\sigma, \hat{F}] |qq_z'\rangle + \hat{F} \cdot \hat{S}_\sigma |qq_z'\rangle. \quad (\text{A.41})$$

The second term on *r.h.s.* clearly describes the symmetry properties of the state $|qq_z\rangle$, while the first term yields the transformation properties of the operator \hat{F} which are independent of the carrier space. This is similar to what has already been seen in Eq. (A.21) for the combined action of two generators.

Now iff an operator set $\hat{F}^q \equiv \{\hat{F}_{q_z}^q\}$ transforms exactly the same way as the state space of IREP q in Eq. (A.40), that is

$$[\hat{S}_\sigma, \hat{F}_{q_z}^q] = s_{q_z q_z}^{[q_\sigma]} \hat{F}_{q_z'}^q, \quad (\text{A.42})$$

then the operator set \hat{F}^q is called an *irreducible operator* (IROP) set that transforms like the multiplet q . It carries the symmetry labels (q, q_z) the same way as an irreducible state multiplet does.

A.7.1. IROP decomposition

In the case that a specific member of the IROP set is already known, then Eq. (A.42) allows to generate the full IROP set exactly the same way as a state multiplet can be generated. Again, the maximum weight label determined the multiplet q that the IROP represents. This was exactly the procedure adopted, for example, to obtain the spin operator in Eq. (A.11). Furthermore, Eq. (A.11) also serves as a simple demonstration that the space of generators itself clearly also can be cast into a single IROP. The corresponding multiplet is called the *regular representation* then.

More generally, it is instructive to realize that irreducible operator sets (IROPs) and symmetry multiplets (IREPs) can be treated on a nearly equal footing. In particular, the notion of proper orthonormalization of state spaces can be directly applied also to IROP sets, up to a global normalization factor. This is motivated by the observation, that given a scalar multiplet $|0\rangle$ for which $|F_{q_z'}^q\rangle \equiv F_{q_z'}^q |0\rangle \neq 0$, i.e. does not vanish, then $|F_{q_z}^q\rangle$ represents the multiplet *vector space* for IREP q . With proper overall normalization of the IROP F^q , it follows

$$\delta_{q_z, q_z'} = \langle F_{q_z}^q | F_{q_z'}^q \rangle = \langle 0 | F_{q_z}^{q\dagger} F_{q_z'}^q | 0 \rangle.$$

The last equation also holds, if the scalar multiplet $|0\rangle$ is replaced by an arbitrary other symmetry eigenstate $|qq_z\rangle$. For matrix representations of IROPs and operators more generally, this motivates the scalar or inner product for two matrices as in Eq. (A.14). Thus equipped with scalar product and norm for matrices, an IROP decomposition can be done *exactly* the same way as the multiplet decompositions for symmetry multiplets starting from a specific symmetry eigenstate (IROP component). This is important, in particular, in the presence of inner multiplicity in the multiplet of an IROP for consistency with the Wigner–Eckart theorem.

A.7.2. Wigner–Eckart theorem

It follows from Eqs. (A.41) and (A.42), that the states resulting from the IROP $\{\hat{F}_{q_{1z}}^{q_1}\}$ applied to a multiplet $|q_2 q_{2z}\rangle$,

$$\begin{aligned} \hat{S}_\sigma \cdot \hat{F}_{q_{1z}}^{q_1} |q_2 q_{2z}\rangle &= \underbrace{[\hat{S}_\sigma, \hat{F}_{q_{1z}}^{q_1}]}_{=s_{q_{1z} q_{1z}'}^{[q_1 \sigma]} \hat{F}_{q_{1z}'}^{q_1}} |q_2 q_{2z}\rangle + \hat{F}_{q_{1z}}^{q_1} \cdot \underbrace{\hat{S}_\sigma}_{=s_{q_{2z} q_{2z}'}^{[q_2 \sigma]} |q_2 q_{2z}'\rangle} |q_2 q_{2z}\rangle, \end{aligned}$$

transforms exactly the same way under given symmetry as a tensor product of two state multiplets,

$$\begin{aligned} \hat{S}_\sigma \cdot |qq_z\rangle_1 |qq_z\rangle_2 &= \underbrace{\hat{S}_{1\sigma} |qq_z\rangle_1}_{=s_{q_{1z} q_{1z}'}^{[q_1 \sigma]} |qq_z'\rangle_1} \otimes |qq_z\rangle_2 + |qq_z\rangle_1 \otimes \underbrace{\hat{S}_{2\sigma} |qq_z\rangle_2}_{=s_{q_{2z} q_{2z}'}^{[q_2 \sigma]} |qq_z'\rangle_2}, \end{aligned}$$

using Eqs. (A.36) and (A.40). Therefore the action of an IROP \hat{F}^{q_1} onto the state space of an IREP q_2 shares exactly the same algebraic structure in terms of symmetries like the product space of the two multiplets q_1 and q_2 .

This motivates the Wigner–Eckart theorem. With the definition of the Clebsch–Gordan coefficients in Eq. (A.38), it is thus clear that up to scalar factors depending on the normalization of the operator set, the *same* CGCs also apply for the state space decomposition arising out of $\hat{F}_{q_{1z}}^{q_1} |q_2 q_{2z}\rangle$. In particular, it follows for the matrix elements of the operator w.r.t. a given state space,

$$\begin{aligned} \langle qq_z; (\alpha) | \hat{F}_{q_{1z}}^{q_1} |q_2 q_{2z}\rangle &\equiv \langle qq_z; (\alpha) | \cdot (\hat{F}_{q_{1z}}^{q_1} |q_2 q_{2z}\rangle) \\ &= \langle q; (\alpha) | \hat{F}^{q_1} |q_2\rangle \cdot C_{q_{1z} q_z; (\alpha)}^{[q_2 z]}, \end{aligned} \quad (\text{A.43})$$

where, again, α accounts for possible outer multiplicity. $\langle q; (\alpha) || \hat{A}_{q_1} || q_2 \rangle$ is called the *reduced matrix element*. It is entirely independent of the z -labels, i.e. the internal structure of the IREPs q_1 , q_2 , and q .

The first line in Eq. (A.43) specifies the adopted convention for matrix elements given the Wigner–Eckart theorem: the operator is acting to the *right* ket-state, the symmetry labels of which are combined. The resulting object is contracted with the bra-states. This is important for consistency, since the IROP \hat{F}^q is subtly different from the IROP $(\hat{F}^\dagger)^q$. Therefore one *must* be careful with expressing a matrix element through $\langle qq_z \hat{F} | q_2 q_{2z} \rangle = \langle q_2 q_{2z} \hat{F}^\dagger | qq_z \rangle^*$. Even though usually $(F_{q_z}^q)^\dagger \sim (\hat{F}^\dagger)_{-q_z}^q$, further signs may be needed to ensure for consistency within the Clebsch–Gordan coefficients [e.g. see discussion around Eq. (A.49) later].

A.8. Several independent symmetries

A physical system often exhibits several symmetries. Each of the $\lambda = 1, \dots, n_s$ symmetries \mathcal{S}^λ is completely described by its own set of generators $\{\hat{S}_\sigma^\lambda\}$. As these symmetries act independently of each other, this implies that their generators must commute,

$$[\hat{S}_\sigma^\lambda, \hat{S}_{\sigma'}^{\lambda'}] = 0 \quad \text{for } \lambda \neq \lambda'. \quad (\text{A.44})$$

This allows to assign independent quantum labels $(q^\lambda q_z^\lambda)$ with respect to each individual symmetry [cf. discussion following Eq. (1) in the main paper]. On the multiplet level, the symmetries are given compactly by the combined *q-labels*, $q \equiv (q^1, q^2, \dots, q^{n_s})$, while similarly their *z-labels* are given by $q_z \equiv (q_z^1, q_z^2, \dots, q_z^{n_s})$. Here the elementary multiplet labels q^λ and q_z^λ can already consist of a set of labels themselves, the number of which is determined by the rank r of the respective symmetry \mathcal{S}^λ [cf. Eq. (A.18)].

When a non-abelian symmetry is broken, it is reduced to simpler subalgebras. In particular, it may be reduced to its abelian core of *z*-operators (Cartan subalgebra). For example, consider the rotational spin SU(2) symmetry. This symmetry can be broken by applying a magnetic field. The system still maintains, however, a continuous rotational symmetry around the axis of the magnetic field, leaving the q_z symmetry intact, while the multiplet label q becomes irrelevant. Similarly, if particle–hole symmetry (see later) is broken, only the abelian quantum number of total charge [i.e. the *z*-label] remains.

Abelian symmetries therefore fit seamlessly into the general non-abelian framework outlined in this paper. With the multiplet label q irrelevant, the q_z are promoted to the status of a *q-label*, instead, with no *z*-labels remaining [with all multiplets being one-dimensional, the *z*-labels are no longer required, i.e. can be set to zero, for simplicity]. This then allows to write the abelian symmetry in terms of trivial scalar Clebsch–Gordan coefficients. The latter, nevertheless, are important as they account for the proper addition rules *w.r.t.* the abelian *z*-labels,

$$\langle q_{1(z)} q_{2(z)} | q_{(z)} \rangle = \delta_{q_{(z)}, q_{1(z)} + q_{2(z)}}. \quad (\text{A.45})$$

A.9. Symmetries in physical systems

In the following, several examples of symmetries in simple physical systems will be given, with the associated spinors and irreducible operator sets explained in detail. In particular, this concerns fermionic systems with spin or particle–hole symmetry.

For the model Hamiltonians in strongly correlated electron systems, correlation through interaction plays an important role, while the terms describing interaction typically preserve certain underlying global symmetries. Since the arguments of demonstrating symmetries of a specific Hamiltonian, however, are rather similar, in general, it suffices to consider a simple non-interacting Hamiltonian. Simple issues related to interactions are discussed with Eq. (A.58) below.

For simplicity, therefore much of the following discussion will be exemplified in terms of the Hamiltonian of a plain spinful fermionic tight-binding chain,

$$\hat{H} = \sum_k t_k \underbrace{\sum_\sigma (\hat{c}_{k\sigma}^\dagger \hat{c}_{k+1,\sigma} + \text{H.c.})}_{\equiv \hat{h}_{k,k+1}}, \quad (\text{A.46})$$

where $\hat{c}_{k\sigma}^\dagger$ creates a particle at site k with spin $\sigma \in \{\uparrow, \downarrow\}$. The Hamiltonian in Eq. (A.46) has spin-independent hopping amplitudes t_k , hence possesses spin- SU(2) symmetry, $SU(2)_{\text{spin}}$ for short. Furthermore, it is particle-hole symmetric, implying particle-hole SU(2) symmetry, also called charge- SU(2) symmetry, or $SU(2)_{\text{charge}}$ for short.

A.9.1. $SU(2)$ spin symmetry

Using the two-dimensional spinor

$$\hat{\psi}_{S,k} \equiv \begin{pmatrix} \hat{c}_{k\uparrow} \\ \hat{c}_{k\downarrow} \end{pmatrix} \quad (\text{A.47})$$

for each site k , the Hamiltonian in Eq. (A.46) can be rewritten as

$$\hat{H} = \sum_k t_k (\hat{\psi}_{S,k}^\dagger \cdot \hat{\psi}_{S,k+1} + \text{H.c.}), \quad (\text{A.48})$$

where the sum over σ was incorporated in the scalar product of the vector of operators in $\hat{\psi}_{S,k}$. Clearly, the two-dimensional scalar product is invariant under an arbitrary unitary two-dimensional transformation U , i.e. $\psi_k^\dagger \psi_{k+1} = (U\psi_k)^\dagger (U\psi_{k+1})$, thus exhibiting spin- SU(2) symmetry. The spinor in Eq. (A.47) is defined in a site specific manner. When concentrating on a single site, therefore the index k can be dropped for convenience.

The generators of spin- SU(2) symmetry are constructed in terms of the two-dimensional defining representation of $\{S_\sigma\} \equiv \{S_+, S_z, S_-\}$ [cf. Eq. (A.7)]. These can be written as operators (distinguished by the hat) through second quantization in the full Hilbert space,

$$\hat{S}_\sigma = \hat{\psi}_S^\dagger S_\sigma \hat{\psi}_S,$$

which up to prefactors leads to the spin IROP $\hat{S}^1 \equiv \{-\frac{1}{\sqrt{2}}\hat{S}_+; \hat{S}_z; +\frac{1}{\sqrt{2}}\hat{S}_-\}$, already derived in Eq. (A.11). The raising operator, for example, is given by

$$\hat{S}_+ = \hat{\psi}_S^\dagger \begin{pmatrix} 0 & 1 \\ 0 & 0 \end{pmatrix} \hat{\psi}_S = \hat{c}_{\uparrow}^\dagger \hat{c}_{\downarrow},$$

which flips a down-spin to an up-spin for given site. Similarly, the z-operator is given by

$$\hat{S}_z = \hat{\psi}^\dagger \left(\frac{1}{2}\tau_z\right) \hat{\psi} = \frac{1}{2}(\hat{c}_{\uparrow}^\dagger \hat{c}_{\uparrow} - \hat{c}_{\downarrow}^\dagger \hat{c}_{\downarrow}) \equiv \frac{1}{2}(\hat{n}_\uparrow - \hat{n}_\downarrow).$$

Furthermore, $[\hat{S}_+, \hat{c}_{\downarrow}^\dagger] = [\hat{c}_{\uparrow}^\dagger \hat{c}_{\downarrow}, \hat{c}_{\downarrow}^\dagger] = \hat{c}_{\uparrow}^\dagger$ shows that the spinor $\hat{\psi}_S^\dagger$ already represents an IROP for the $q = \frac{1}{2}$ multiplet of $SU(2)_{\text{spin}}$.

$$(\hat{\psi}_S^\dagger)^{[1/2]} = \begin{pmatrix} \hat{c}_{\uparrow}^\dagger \\ \hat{c}_{\downarrow}^\dagger \end{pmatrix}. \quad (\text{A.49a})$$

This is already properly sorted w.r.t. z -labels, in that the second component correspond to the lower $q_z = -\frac{1}{2}$ element of the multiplet, since $[\hat{S}_z, \hat{c}_{\downarrow}^\dagger] = (-\frac{1}{2}) \cdot \hat{c}_{\downarrow}^\dagger$.

In contrast, the IROP for the spinor $\hat{\psi}_S$, i.e. without the dagger, is similar, yet has subtle differences. In particular, with $[\hat{S}_+, \hat{c}_{\uparrow}] = [\hat{c}_{\uparrow}^\dagger c_{\downarrow}, \hat{c}_{\uparrow}] = -\hat{c}_{\downarrow}$, the role of spin within the multiplet is reversed, i.e. $q_z \rightarrow -q_z$, while also an additional sign is acquired,

$$(\hat{\psi}_S)^{[1/2]} = \begin{pmatrix} -\hat{c}_{\downarrow} \\ \hat{c}_{\uparrow} \end{pmatrix}. \quad (\text{A.49b})$$

This extra sign is important in context of the Wigner–Eckart theorem in Eq. (A.43), where the particular order of first applying, i.e. combining an operator with the ket-state is directly related to the order in the Clebsch–Gordan coefficients. This is convention, of course, but consistency is crux.

In terms of the proper IROPs in Eq. (A.49), finally, the Hamiltonian in Eq. (A.46) can be written in either IROP while, however, one must not mix them,

$$\hat{H} = \sum_k t_k \left([(\hat{\psi}_S)^{[1/2]}]^\dagger \cdot (\hat{\psi}_S)^{[1/2]} + \text{H.c.} \right) \quad (\text{A.50a})$$

$$= \sum_k t_k \left((\hat{\psi}_S^\dagger)^{[1/2]} \cdot [(\hat{\psi}_S^{[1/2]})^\dagger + \text{H.c.}] \right). \quad (\text{A.50b})$$

The second line is essentially the same as the spinor expression in Eq. (A.48), yet with the difference, that here the underlying IROP structure has been pointed out explicitly.

A.9.2. SU(2) particle-hole symmetry for spinful system

The particle-hole symmetry $SU(2)_{\text{charge}}$ of the Hamiltonian in Eq. (A.46) can be made apparent in a similar way as for the spin symmetry above. Consider the spinor in the charge sector,

$$\hat{\psi}_{C,k\sigma} \equiv \begin{pmatrix} \hat{c}_{k\sigma} \\ s_k \hat{c}_{k,-\sigma}^\dagger \end{pmatrix}$$

with alternating phases $s_k = (-1)^k$ along the chain in Eq. (A.46). Again, the Hamiltonian can be written as sum over scalar products in the spinors,

$$\begin{aligned} \sum_\sigma \hat{\psi}_{C,k\sigma}^\dagger \cdot \hat{\psi}_{C,k+1,\sigma} &= \sum_\sigma (\hat{c}_{k\sigma}^\dagger \hat{c}_{k+1,\sigma} - \hat{c}_{k,-\sigma}^\dagger \hat{c}_{k+1,-\sigma}^\dagger) \\ &= \hat{h}_{k,k+1}, \end{aligned}$$

suggesting another underlying $SU(2)$ symmetry. Note that the alternating sign s_k is crucial to recover the correct hopping structure in Eq. (A.46). Given the spinor in the charge sector, the raising operator becomes

$$\hat{\psi}_{C,k\sigma}^\dagger \begin{pmatrix} 0 & 1 \\ 0 & 0 \end{pmatrix} \hat{\psi}_{C,k\sigma} = s_k \hat{c}_{k\sigma}^\dagger \hat{c}_{k,-\sigma}^\dagger$$

which, up to a sign, is the same for both spins. It is therefore sufficient in the charge sector to consider a spinor for one specific σ in $\hat{\psi}_{C,k\sigma}$ only. Therefore, again concentrating on a single site and hence dropping the site index k , now with fixed $\sigma = \uparrow$, the spinor in the charge sector is given by,

$$\hat{\psi}_C \equiv \begin{pmatrix} \hat{c}_\uparrow \\ s \hat{c}_\downarrow^\dagger \end{pmatrix}. \quad (\text{A.51})$$

The associated raising operator becomes

$$\hat{C}_+ = s \hat{c}_\uparrow^\dagger \hat{c}_\downarrow^\dagger, \quad (\text{A.52})$$

which now creates a pair of particles with opposite spin, while the z-operator is

$$\begin{aligned} \hat{C}_z &= \hat{\psi}_C^\dagger \left(\frac{1}{2} \tau_z \right) \hat{\psi}_C = \frac{1}{2} (\hat{c}_\uparrow^\dagger \hat{c}_\uparrow - \hat{c}_\downarrow^\dagger \hat{c}_\downarrow) \\ &\equiv \frac{1}{2} (\hat{n}_\uparrow + \hat{n}_\downarrow - 1). \end{aligned} \quad (\text{A.53})$$

With $\hat{n} \equiv \hat{n}_\uparrow + \hat{n}_\downarrow$, the z-operator \hat{C}_z counts the total charge on given fermionic site relative to half-filling. With

$$[\hat{C}_+, \hat{c}_\uparrow] = [s \hat{c}_\uparrow^\dagger \hat{c}_\downarrow^\dagger, \hat{c}_\uparrow] = -s \hat{c}_\downarrow^\dagger \quad (\text{A.54a})$$

$$[\hat{C}_+, \hat{c}_\downarrow] = [s \hat{c}_\uparrow^\dagger \hat{c}_\downarrow^\dagger, \hat{c}_\downarrow] = s \hat{c}_\uparrow^\dagger, \quad (\text{A.54b})$$

this allows to construct the $q = \frac{1}{2}$ IROPs for $SU(2)_{\text{charge}}$,

$$(\hat{\psi}_C)^{[1/2]} = \begin{pmatrix} s\hat{c}_\downarrow^\dagger \\ -\hat{c}_\uparrow \end{pmatrix} \quad (\text{A.55a})$$

$$(\hat{\psi}_C^\dagger)^{[1/2]} = \begin{pmatrix} s\hat{c}_\uparrow^\dagger \\ \hat{c}_\downarrow \end{pmatrix}, \quad (\text{A.55b})$$

again associating the lower component with the $q_z = -\frac{1}{2}$ element of the $q = (1/2)$ multiplet [cf. Eqs. (A.49)]. An irrelevant overall minus sign has been applied to the spinor in Eq. (A.55a) for later convenience. With this, the hopping term in the Hamiltonian in Eq. (A.46) can be rewritten in terms of the scalar products

$$\begin{aligned} \hat{h}_{k,k+1} = & [(\hat{\psi}_{Ck})^{[1/2]}]^\dagger \cdot (\hat{\psi}_{C,k+1})^{[1/2]} \\ & + [(\hat{\psi}_{Ck}^\dagger)^{[1/2]}]^\dagger \cdot (\hat{\psi}_{C,k+1}^\dagger)^{[1/2]}. \end{aligned} \quad (\text{A.56})$$

The spinors in the charge sector do mix spin components, which essentially also requires full spin symmetry [see later discussion of symplectic group $\text{Sp}(2m)$ in Appendix A.10]. More importantly, the construction of the $SU(2)_{\text{charge}}$ symmetry allows it to fully commute with the spin- $SU(2)$ symmetry introduced earlier,

$$\begin{aligned} [\hat{S}_z, \hat{C}_z] &= \frac{1}{4}[\hat{n}_\uparrow - \hat{n}_\downarrow, \hat{n} - 1] = 0 \\ [\hat{S}_z, \hat{C}_+] &= \frac{s}{2} \underbrace{[\hat{c}_\uparrow^\dagger \hat{c}_\uparrow, \hat{c}_\uparrow^\dagger \hat{c}_\downarrow^\dagger]}_{=\hat{c}_\uparrow^\dagger \hat{c}_\downarrow^\dagger} - \frac{s}{2} \underbrace{[\hat{c}_\downarrow^\dagger \hat{c}_\downarrow, \hat{c}_\uparrow^\dagger \hat{c}_\downarrow^\dagger]}_{=\hat{c}_\uparrow^\dagger \hat{c}_\downarrow^\dagger} = 0 \\ [\hat{S}_+, \hat{C}_z] &= \frac{1}{2} \underbrace{[\hat{c}_\uparrow^\dagger \hat{c}_\downarrow, \hat{c}_\uparrow^\dagger \hat{c}_\uparrow]}_{=-\hat{c}_\uparrow^\dagger \hat{c}_\downarrow} + \frac{1}{2} \underbrace{[\hat{c}_\uparrow^\dagger \hat{c}_\downarrow, \hat{c}_\downarrow^\dagger \hat{c}_\downarrow]}_{=\hat{c}_\uparrow^\dagger \hat{c}_\downarrow} = 0 \\ [\hat{S}_+, \hat{C}_+] &= s[\hat{c}_\uparrow^\dagger \hat{c}_\downarrow, \hat{c}_\uparrow^\dagger \hat{c}_\downarrow^\dagger] = sc_\uparrow^\dagger \hat{c}_\uparrow^\dagger = 0. \end{aligned} \quad (\text{A.57})$$

That is, the two symmetries act completely independent of each other and thus can coexist simultaneously, written as the overall symmetry $SU(2)_{\text{spin}} \otimes SU(2)_{\text{charge}}$.

If interactions are present in the system, such as local Coulomb interaction $U\hat{n}_\uparrow\hat{n}_\downarrow$, then the particle-hole symmetric regime requires a specific altered onsite energy relative to the chemical potential. With $\hat{n}_\sigma^2 = \hat{n}_\sigma$, and $\hat{n} \equiv \hat{n}_\uparrow + \hat{n}_\downarrow$, it follows that $\hat{n}_\uparrow\hat{n}_\downarrow = \frac{1}{2}(\hat{n} - 1)^2 + \frac{1}{2}(\hat{n} - 1)$, and therefore

$$\varepsilon_d \hat{n} + U\hat{n}_\uparrow\hat{n}_\downarrow = (\varepsilon_d + \frac{U}{2}) \underbrace{(\hat{n} - 1)}_{=\hat{C}_z} + \frac{U}{2}(\hat{n} - 1)^2 + \text{const.} \quad (\text{A.58})$$

The first term on the r.h.s. is proportional to the \hat{C}_z operator, which thus acts like a magnetic field for $SU(2)_{\text{spin}}$. Therefore for full particle-hole symmetry to hold, this term must be zero, which requires $\varepsilon_d = -\frac{U}{2}$. In particular, in the absence of interaction, this implies $\varepsilon_d = 0$. The actual interaction term, i.e. the second term on the r.h.s. in Eq. (A.58), also resembles \hat{C}_z . Yet it is quadratic, and for this it also holds, $\hat{C}_z^2 = \hat{C}_x^2 = \hat{C}_y^2$. Therefore, this term can actually be written as \hat{C}^2 which itself, like spin \hat{S}^2 for $SU(2)_{\text{spin}}$, represents the Casimir operator for $SU(2)$, and thus is compatible with $SU(2)_{\text{spin}} \otimes SU(2)_{\text{charge}}$.

The actual IROP for particle creation and annihilation given $SU(2)_{\text{SC}}^{\otimes 2} \equiv SU(2)_{\text{spin}} \otimes SU(2)_{\text{charge}}$ symmetry can be generated using above symmetry operations. This generates a four-dimensional spinor. As it turns out, the resulting IROP is the combination of the two IROPs generated in the spin

symmetric case in Eqs. (A.49) as well as in the particle–hole symmetric case in Eqs. (A.55),

$$\hat{\psi}_{\text{CS}}^{\left[\frac{1}{2}, \frac{1}{2}\right]} \equiv \begin{pmatrix} s\hat{c}_\uparrow^\dagger \\ \hat{c}_\downarrow \\ s\hat{c}_\downarrow^\dagger \\ -\hat{c}_\uparrow \end{pmatrix}. \quad (\text{A.59})$$

The multiplet labels $\left[\frac{1}{2}, \frac{1}{2}\right]$ will be derived with Eq. (A.61) below. The signs for the individual components in above IROP have been properly adjusted, considering that the raising operator in the charge sector itself, Eq. (A.52), carries the alternating sign $s_{(k)} = (-1)^k$. For example, commuting \hat{C}_+ onto the fourth component, yields the third component of the spinor $\hat{\psi}_{\text{CS}}$ [cf. Eq. (A.54a)], while commuting \hat{S}_+ onto the third component yields the first component, and so on. Again, keeping track of the alternating sign $s_k = (-1)^k$ is crucial to recover the hopping structure in Eq. (A.46),

$$\begin{aligned} (\hat{\psi}_{\text{CS},k})^\dagger \cdot \hat{\psi}_{\text{CS},k+1} &= -\underbrace{\hat{c}_{k\uparrow}\hat{c}_{k+1,\uparrow}^\dagger}_{=-\hat{c}_{k+1,\uparrow}^\dagger\hat{c}_{k\uparrow}} + \hat{c}_{k\downarrow}^\dagger\hat{c}_{k+1,\downarrow} - \underbrace{\hat{c}_{k\downarrow}\hat{c}_{k+1,\downarrow}^\dagger}_{=-\hat{c}_{k+1,\downarrow}^\dagger\hat{c}_{k\downarrow}} + \hat{c}_{k\uparrow}^\dagger\hat{c}_{k+1,\uparrow} \\ &= \hat{h}_{k,k+1}. \end{aligned} \quad (\text{A.60})$$

The full tight-binding Hamiltonian simply becomes $\hat{H} = \sum_k t_k (\hat{\psi}_{\text{CS},k})^\dagger \hat{\psi}_{\text{CS},k+1}$ where the hermitian conjugate term has been incorporated already in the spinor structure. This also reflects the irrelevance of taking the hermitian conjugate version of the IROP in Eq. (A.59) as this results in essentially the same object after properly reordering its components and taking care of signs.

With Eq. (A.60) being a scalar product in a four-dimensional spinor space, one may be tempted to think that a plain tight binding chain actually has a non-abelian symmetry with a defining representation of dimension 4. This cannot be the symmetry $SU(4)$, however, since $SU(4)$ has rank-3 and thus requires three commuting abelian z-operators. The symmetries discussed here, however, only have two abelian z-operators, namely total spin and total charge. The symmetry that appears compatible with this scenario, at second glance, is the symplectic symmetry $Sp(4)$ [see Appendix A.10 below]. Nevertheless, even the latter can be excluded, since raising and lowering operators are severely constrained by the fact that the creation and annihilation operators appear in pairs for the same fermionic particle in the IROP of Eq. (A.59). Consequently, quadratic operators of the type $(\hat{c}_\sigma)^\dagger\hat{c}_\sigma^\dagger = (\hat{c}_\sigma^\dagger)^\dagger\hat{c}_\sigma = 0$ are immediately excluded. With this, the symmetry of the spinor in Eq. (A.59) has to remain the product of two symmetries, i.e. $SU(2)_{\text{SC}}^{\otimes 2} \equiv SU(2)_{\text{spin}} \otimes SU(2)_{\text{charge}}$.

Having determined the IROP $\hat{\psi}_{\text{CS}}$ in Eq. (A.59) by repeated application of RLOs \hat{S}_\pm and \hat{C}_\pm , the z-labels for each of the four components, on the other hand, can be determined through the z-operators $\hat{C}_z \equiv \frac{1}{2}(\hat{c}_\uparrow^\dagger\hat{c}_\uparrow - \hat{c}_\downarrow^\dagger\hat{c}_\downarrow)$ and $\hat{S}_z \equiv \frac{1}{2}(\hat{c}_\uparrow^\dagger\hat{c}_\uparrow - \hat{c}_\downarrow^\dagger\hat{c}_\downarrow)$, resulting in the z-labels $q_z \equiv (C_z, S_z)$, respectively. The results are summarized in the following table.

[z-operator, IROP component]	(C_z, S_z)
$[\hat{C}_z, s\hat{c}_\uparrow^\dagger] = +\frac{1}{2}(s\hat{c}_\uparrow^\dagger)$ $[\hat{S}_z, s\hat{c}_\uparrow^\dagger] = +\frac{1}{2}(s\hat{c}_\uparrow^\dagger)$	$\left\{ (+\frac{1}{2}, +\frac{1}{2})\right.$
$[\hat{C}_z, \hat{c}_\downarrow] = -\frac{1}{2}(\hat{c}_\downarrow)$ $[\hat{S}_z, \hat{c}_\downarrow] = +\frac{1}{2}(\hat{c}_\downarrow)$	$\left. (-\frac{1}{2}, +\frac{1}{2})\right)$
$[\hat{C}_z, s\hat{c}_\downarrow^\dagger] = +\frac{1}{2}(s\hat{c}_\downarrow^\dagger)$ $[\hat{S}_z, s\hat{c}_\downarrow^\dagger] = -\frac{1}{2}(s\hat{c}_\downarrow^\dagger)$	$(+\frac{1}{2}, -\frac{1}{2})$
$[\hat{C}_z, -\hat{c}_\uparrow] = -\frac{1}{2}(-\hat{c}_\uparrow)$ $[\hat{S}_z, -\hat{c}_\uparrow] = -\frac{1}{2}(-\hat{c}_\uparrow)$	$(-\frac{1}{2}, -\frac{1}{2})$

These z -labels demonstrate that both the charge and spin multiplet contained in $\hat{\psi}_{\text{CS}}$ corresponds to a $q = \frac{1}{2}$ multiplet. The maximum weight state has the z -labels $(\frac{1}{2}, \frac{1}{2})$, which thus labels the spinor, as was already indicated in Eq. (A.59).

Similarly, the local state space of a fermionic site must be organized consistent with the $SU(2)_{\text{spin}} \otimes SU(2)_{\text{charge}}$ symmetry above. The local state space consists of the empty state $|0\rangle$, the singly occupied states $|\uparrow\rangle$ and $|\downarrow\rangle$, and the doubly occupied state $s|\uparrow\downarrow\rangle$. Note that the sign in the last state is crucial, as it is generated by the raising operator \hat{c}_+ acting on the empty state $|0\rangle$. In summary,

State	C	C_z	S	S_z	
$ 0\rangle$	$\frac{1}{2}$	$-\frac{1}{2}$	0	0	
$ \uparrow\rangle \equiv \hat{c}_+^\dagger 0\rangle$	0	0	$\frac{1}{2}$	$+\frac{1}{2}$	
$ \downarrow\rangle \equiv \hat{c}_-^\dagger 0\rangle$	0	0	$\frac{1}{2}$	$-\frac{1}{2}$	
$s \uparrow\downarrow\rangle \equiv s\hat{c}_+^\dagger\hat{c}_-^\dagger 0\rangle$	$\frac{1}{2}$	$+\frac{1}{2}$	0	0	(A.62)

Therefore the local four-dimensional state space of fermionic site is spanned by the two multiplets, $q \equiv (C, S) \in \{(0, \frac{1}{2}), (\frac{1}{2}, 0)\}$. If particle-hole symmetry is broken yet particle number still preserved, then $2C_z$ from the middle column describes the total number of particles relative to half-filling [cf. Eq. (A.53)].

With the ordering convention of state labels being $|C, C_z; S, S_z\rangle$ and $\sigma \in \{\uparrow, \downarrow\} \equiv \{+1, -1\}$, the non-zero matrix elements of the 4-component spinor in Eq. (A.59) can be calculated. For example,

$$\begin{aligned} +s\sigma &= \langle -\sigma | \hat{c}_\sigma \cdot s | \uparrow\downarrow \rangle = s(\uparrow\downarrow | s \cdot \hat{s}\hat{c}_\sigma^\dagger \cdot | -\sigma \rangle^{(*)} \\ &\equiv s(\frac{1}{2}, \frac{+1}{2}; 0, 0 | \hat{\psi}_{(\frac{1}{2}, \frac{+1}{2}; \frac{1}{2}, \frac{\sigma}{2})} | 0, 0; \frac{1}{2}, \frac{-\sigma}{2} \rangle \\ &= s \underbrace{(\frac{1}{2}, \frac{+1}{2}; \frac{1}{2}, \frac{+1}{2}; 0, 0)}_{=1(\text{charge})} \underbrace{\langle 0, 0 | \frac{1}{2}, \frac{\sigma}{2}; \frac{1}{2}, \frac{-\sigma}{2} \rangle}_{=\frac{+\sigma}{\sqrt{2}}(\text{spin})} \langle \frac{1}{2}, 0 | \psi | 0, \frac{1}{2} \rangle \\ &\Rightarrow \langle \frac{1}{2}, 0 | \psi | 0, \frac{1}{2} \rangle = \sqrt{2}. \end{aligned}$$

The order inversion of the matrix element in the first line was used since the spinor $\hat{\psi}_{\text{CS}}$ in Eq. (A.59) contains the creation operator $s\hat{c}_\sigma^\dagger$ and not its hermitian conjugate. The overall complex conjugation $(\cdot)^{(*)}$, however, is irrelevant since all matrix elements are real, hence the notation of putting the asterisk in brackets.

The second non-zero reduced matrix element can be calculated in a similar fashion,

$$\begin{aligned} 1 &= \langle 0 | \hat{c}_\sigma | \sigma \rangle = s \langle \sigma | \cdot s\hat{c}_\sigma^\dagger \cdot | 0 \rangle^{(*)} \\ &\equiv s \langle 0, 0; \frac{1}{2}, \frac{\sigma}{2} | \hat{\psi}_{(\frac{1}{2}, \frac{+1}{2}; \frac{1}{2}, \frac{\sigma}{2})} | \frac{1}{2}, \frac{-1}{2}; 0, 0 \rangle \\ &= s \underbrace{\langle 0, 0 | \frac{1}{2}, \frac{+1}{2}; \frac{1}{2}, \frac{-1}{2}}_{=+\frac{1}{\sqrt{2}}(\text{charge})} \underbrace{\langle \frac{1}{2}, \frac{\sigma}{2}; \frac{1}{2}, \frac{\sigma}{2}; 0, 0 \rangle}_{=1(\text{spin})} \langle 0, \frac{1}{2} | \psi | \frac{1}{2}, 0 \rangle \\ &\Rightarrow \langle 0, \frac{1}{2} | \psi | \frac{1}{2}, 0 \rangle = s\sqrt{2}. \end{aligned}$$

Overall, this leads to the reduced matrix elements in the charge-spin sectors $(C, S) \in \{(0, \frac{1}{2}), (\frac{1}{2}, 0)\}$

$$\psi_{\text{CS}}^{[1/2, 1/2]} = \begin{pmatrix} 0 & s\sqrt{2} \\ \sqrt{2} & 0 \end{pmatrix}. \quad (\text{A.63})$$

Note that although the spinor in Eq. (A.59) has four components, i.e. is of rank-3, on the reduced multiplet level in Eq. (A.63) the spinor becomes a two-dimensional object as expected from an IROP. The further internal structure is entirely taken care of by rank-3 Clebsch-Gordan coefficients, which have been omitted in Eq. (A.63) [for a full description of $\psi_{\text{CS}}^{[1/2, 1/2]}$ including Clebsch-Gordan coefficients, see QSpace (C.5) in the Appendix].

The operator in Eq. (A.63) is non-hermitian. In the context of two-site hopping, however, this nevertheless leads to a hermitian term in the Hamiltonian, as required. Indicating the local symmetry eigenspace for site k by $|\sigma\rangle_k$, the matrix elements of the hopping term in the tensor-product basis $|\sigma_{k+1}\rangle|\sigma_k\rangle$ (in this order, assuming site $k+1$ is added after site k) are given by

$$\langle\sigma_k|\langle\sigma_{k+1}|\hat{\psi}_k^\dagger\hat{\psi}_{k+1}|\sigma'_{k+1}\rangle|\sigma'_k\rangle = \psi_k^\dagger \otimes [z\psi]_{k+1}, \quad (\text{A.64})$$

where the ψ 's to the right without the hat denote the matrix elements in the local $|\sigma\rangle$ basis. Note, that fermionic signs apply, when $\hat{\psi}_k^\dagger$ is moved, for example, to the left of $\langle\sigma_{k+1}|$, such that the tensor-product on the r.h.s. of Eq. (A.64) contains $[z\psi]_{k+1}$ rather than ψ_{k+1} , where $\hat{z}_k \equiv (-1)^{\hat{n}_k}$ is diagonal in $|\sigma_k\rangle$ and adds signs corresponding to the number of particles in $|\sigma_k\rangle$. Note that with the particle number being related to $\hat{C}_z = \frac{1}{2}(\hat{n} - 1)$, the operator \hat{z} is well-defined in terms of the symmetry labels. It is a scalar operator, since $(-1)^{\hat{n}-1} = (-1)^{(\hat{n}-1)^2} = (-1)^{4\hat{C}_z^2}$, hence does not alter the Clebsch–Gordan content of the operator $\hat{\psi}$ but rather acts on the multiplet level only. For the hopping $\hat{\psi}_k^\dagger\hat{\psi}_{k+1}$ between two nearest-neighbor sites, Eq. (A.63) finally leads to

$$H_{k,k+1} = \begin{pmatrix} 0 & \sqrt{2} \\ s_k\sqrt{2} & 0 \end{pmatrix} \otimes \underbrace{\begin{pmatrix} -1 & 0 \\ 0 & 1 \end{pmatrix}}_{= \begin{pmatrix} 0 & -s_{k+1}\sqrt{2} \\ \sqrt{2} & 0 \end{pmatrix}} \begin{pmatrix} 0 & s_{k+1}\sqrt{2} \\ \sqrt{2} & 0 \end{pmatrix},$$

written as a plain tensor product on the level of the multiplet spaces of two fermionic sites. For the sake of the argument, the product space here is not yet described in terms of proper combined symmetry multiplets of sites k and $k+1$.

With $s_k = (-1)^k$, $H_{k,k+1}$ in the last equation clearly yields a hermitian object for all iterations. For example, for even k , the hopping term is given by

$$H_{k,k+1}^{[k \text{ even}]} = \begin{pmatrix} 0 & \sqrt{2} \\ \sqrt{2} & 0 \end{pmatrix} \otimes \begin{pmatrix} 0 & \sqrt{2} \\ \sqrt{2} & 0 \end{pmatrix}$$

similar in structure to a hermitian object of the type $\tau_x \otimes \tau_x$ in terms of Pauli matrices, while for odd k ,

$$H_{k,k+1}^{[k \text{ odd}]} = \begin{pmatrix} 0 & \sqrt{2} \\ -\sqrt{2} & 0 \end{pmatrix} \otimes \begin{pmatrix} 0 & -\sqrt{2} \\ \sqrt{2} & 0 \end{pmatrix}$$

similar in structure to the hermitian $(i\tau_y) \otimes (i\tau_y) = -\tau_y \otimes \tau_y$. Hence for every even (odd) iteration, one has a $\tau_x \otimes \tau_x$ ($\tau_y \otimes \tau_y$) structure, respectively, a prescription that is periodic with every pair of iterations. This intrinsic even–odd behavior is not specifically surprising, considering, for example, that two particles are needed to return to the same charge quantum numbers related to particle–hole symmetry.

In summary, using Eq. (A.60), the hopping in the Hamiltonian is given by

$$\hat{H} = \sum_k t_k \hat{\psi}_k^\dagger \hat{\psi}_{k+1}. \quad (\text{A.65})$$

In a sense, the net effect of incorporating spin SU(2) was to eliminate the spin index, while incorporation of particle–hole SU(2) eliminates the hermitian conjugate term in the Hamiltonian. Together they reduce the four terms initially required for a single hopping in Eq. (A.46) to the single scalar term $\hat{\psi}_k^\dagger \hat{\psi}_{k+1}$.

A.9.3. Particle-hole SU(2) symmetry for several channels

The alternating sign in the raising operator $\hat{c}_{k,+} = s\hat{c}_\uparrow^\dagger \hat{c}_\downarrow^\dagger$ in Eq. (A.52) defines the doubly occupied states as $|\frac{1}{2}; \frac{\pm 1}{2}\rangle = \hat{c}_{k,+} |\frac{1}{2}; \frac{\mp 1}{2}\rangle = s\hat{c}_\uparrow^\dagger \hat{c}_\downarrow^\dagger |0\rangle$; for even sites, $s = +1$, therefore $|\frac{1}{2}; \frac{\pm 1}{2}\rangle = \hat{c}_\uparrow^\dagger \hat{c}_\downarrow^\dagger |0\rangle$. For odd sites, on the other hand, $|\frac{1}{2}; \frac{\pm 1}{2}\rangle = -\hat{c}_\uparrow^\dagger \hat{c}_\downarrow^\dagger |0\rangle = \hat{c}_\downarrow^\dagger \hat{c}_\uparrow^\dagger |0\rangle$. In practice, for consistency, usually a certain well-defined fermionic order is adopted. Above raising operator $\hat{c}_{k,+}$ thus suggests that it may be useful to *reverse the fermionic order of every other site* for the local state space included there.

Fully reversing the fermionic order of a given site k with several fermionic channels $i = 1, \dots, m$ implies for the *matrix elements* for particle creation or annihilation operators,

$$\begin{aligned} c_{k,i\sigma} &\rightarrow \tilde{c}_{k,i\sigma} \equiv z_k c_{k,i\sigma} \\ c_{k,i\sigma}^\dagger &\rightarrow \tilde{c}_{k,i\sigma}^\dagger \equiv -z_k c_{k,i\sigma}^\dagger. \end{aligned}$$

This transformation is equivalent to a unitary transformation local to site k . Similar to Eq. (A.64), $\hat{z}_k \equiv (-1)^{\hat{n}_k}$ with $\hat{n}_k \equiv \sum_{i\sigma} \hat{n}_{k,i\sigma}$ and $\hat{n}_{k,i\sigma} \equiv \hat{c}_{k,i\sigma}^\dagger \hat{c}_{k,i\sigma}$ again takes care of fermionic signs for the full multi-level site k . Being a scalar operator, \hat{z}_k is independent of the fermionic order.

Now consider the effect of flipping the fermionic order for the odd sites in the tight-binding chain that carry the sign $s = -1$, assuming particle-hole symmetry in every channel. For a specific channel, this (i) takes away the sign in the raising operator $\hat{c}_{k,+}$, and (ii) implies, for example, for the 4-component spinor in Eq. (A.59) for a single channel,

$$\hat{\psi}_{CS,k \text{ odd}} \equiv \begin{pmatrix} -\hat{c}_\uparrow^\dagger \\ \hat{c}_\downarrow \\ -\hat{c}_\downarrow^\dagger \\ -\hat{c}_\uparrow \end{pmatrix} \rightarrow \begin{pmatrix} +\hat{z}\hat{c}_\uparrow^\dagger \\ \hat{z}\hat{c}_\downarrow \\ +\hat{z}\hat{c}_\downarrow^\dagger \\ -\hat{z}\hat{c}_\uparrow \end{pmatrix} \equiv \hat{z}_k \hat{\psi}_{CS,k \text{ even}}, \quad (\text{A.66})$$

having intermittently dropped the index k for readability. Therefore, up to the local operator \hat{z}_k which assigns fermionic signs to the full Hilbert space of a local site, the matrix elements of the spinor for the odd sites are *exactly* the same as the matrix elements of the spinor for even sites. Therefore with $\hat{\psi}$ taken as the spinor for even sites in the chain, the required spinor for odd sites becomes $\hat{z}\hat{\psi}$. Together with the additional fermionic signs in the nearest-neighbor hopping term as already encountered in Eq. (A.64), the hopping structure $\hat{h}_{k,k+1}$ of the tight-binding Hamiltonian in Eq. (A.65) becomes,

$$\begin{aligned} \psi_k^\dagger \otimes [z \cdot (z\psi)]_{k+1} &= \psi_k^\dagger \otimes \psi_{k+1} \quad \text{for } k \text{ even} \\ (z\psi)_k^\dagger \otimes [z \cdot \psi]_{k+1} &= (z\psi)_k^\dagger \otimes (z\psi)_{k+1} \quad \text{for } k \text{ odd}. \end{aligned}$$

This result generalizes to any number of channels with particle-hole symmetry. As such it much simplifies the structure and thus the treatment of the two different kinds of spinors for even and odd sites, respectively, that had been required initially.

A.9.4. Symmetric three-channel system

Consider the generalization of the spinful one-channel setup in Eq. (A.46) to a spinful three-channel system,

$$\hat{H} = \sum_k t_k \cdot \underbrace{\sum_{i=1}^{m=3} \sum_\sigma (\hat{c}_{k,i\sigma}^\dagger \hat{c}_{k+1,i\sigma} + \text{H.c.})}_{\equiv \hat{h}_{k,k+1}}, \quad (\text{A.67})$$

where $\hat{c}_{k,i\sigma}^\dagger$ creates a particle at site k in channel i with spin σ . This model is relevant for the system analyzed in the main body of the paper where the specific number of three channels, for example, originates from the underlying orbital band structure in terms of a partially filled d-shell. The Hamiltonian in Eq. (A.67) can also be complemented with interaction terms that are compatible with the symmetries discussed in the following. This can include onsite interaction U at half-filling

[cf. Eq. (A.58)], or uniform local Hund's coupling J_H [e.g. see Eq. (27b)]. Here, however, the focus of the discussion is on symmetries, for which the Hamiltonian in Eq. (A.67) suffices.

The Hamiltonian in Eq. (A.67) possesses SU(2) spin symmetry, SU(2) particle–hole symmetry in each channel, and also SU(3) channel symmetry, while not all of these symmetries necessarily are independent of, *i.e.* commute with each other. All of these symmetries can be defined within the Hilbert space of a local site, hence again focusing the discussion on a single site k in the following, while dropping the site index k , for simplicity. For each of the three channels, the associated spinful fermionic level is represented by the four states as in Eq. (A.62), leading to a total of $4^3 = 64$ state for a given site.

The total spin-SU(2) symmetry of a site is described by the generators

$$\begin{aligned}\hat{S}_+ &= \sum_i \hat{S}_{i+} = \sum_i \hat{c}_{i\uparrow}^\dagger \hat{c}_{i\downarrow} \\ \hat{S}_z &= \sum_i \hat{S}_{iz} = \frac{1}{2} \sum_i (\hat{n}_{i\uparrow} - \hat{n}_{i\downarrow}),\end{aligned}\tag{A.68}$$

where $\hat{S}_{i\sigma}$ represents the spin operators for the fermionic level i , with $\hat{S}_z = \frac{1}{2}[\hat{S}_+, \hat{S}_+^\dagger]$, as expected for SU(2).

The particle–hole symmetry exists for every channel i , and is described by the SU(2) symmetry,

$$\begin{aligned}\hat{C}_{i+} &= s \hat{c}_{i\uparrow}^\dagger \hat{c}_{i\downarrow}^\dagger \\ \hat{C}_{iz} &= \frac{1}{2} [\hat{C}_{i+}, \hat{C}_{i+}^\dagger] = \frac{1}{2} (\hat{n}_i - 1),\end{aligned}\tag{A.69a}$$

which includes the same sign-factor $s_k = (-1)^k$ as in Eq. (A.52) to correctly represent the hopping structure in the Hamiltonian equation (A.67). The total charge relative to half-filling is given by (up to a factor of 2)

$$\hat{C}_z \equiv \sum_i \hat{C}_{iz}.\tag{A.69b}$$

Finally, the channel symmetry is given by the minimal set of two raising operators $\{\hat{T}_+, \hat{U}_+\} \equiv \{\hat{S}_{12}, \hat{S}_{23}\}$ together with the z-operator $\{\hat{T}_z, \hat{Y}\} \equiv \{\hat{Z}_1, \hat{Z}_2\}$ as introduced through Eq. (A.28) in Eq. (A.30),

$$\begin{aligned}\hat{T}_+ &= \sum_\sigma \hat{c}_{1\sigma}^\dagger \hat{c}_{2\sigma}, \quad \hat{T}_z = \sum_\sigma (\hat{n}_{1\sigma} - \hat{n}_{2\sigma}), \\ \hat{U}_+ &= \sum_\sigma \hat{c}_{2\sigma}^\dagger \hat{c}_{3\sigma}, \quad \hat{Y} = \sum_\sigma (\hat{n}_{1\sigma} + \hat{n}_{2\sigma} - 2\hat{n}_{3\sigma}).\end{aligned}\tag{A.70}$$

Here the notation for the generators of SU(3) has been changed to another notation frequently also found in the literature, so these generators can be better distinguished from the generators for spin and particle–hole symmetry. In particular, the operators \hat{T}_+ and \hat{T}_z generate an SU(2) subalgebra, that is linked to the full SU(3) symmetry through the generators \hat{U}_+ and \hat{Y} . The normalization of the z-operators, however, has been chosen consistent with Eq. (A.28), such that plain integer matrix elements arise.

The spin symmetry clearly commutes with the particle–hole symmetry in each channel, which follows from the previous one-channel discussion in Eqs. (A.57). Therefore it remains to analyze the compatibility of the SU(3) channel symmetry. All z-operators clearly commute. For the SU(3) raising operators, it follows with respect to the spin symmetry,

$$\begin{aligned}[\hat{T}_+, \hat{S}_+] &= \sum_{\sigma, i} [\hat{c}_{1\sigma}^\dagger \hat{c}_{2\sigma}, \hat{c}_{i\uparrow}^\dagger \hat{c}_{i\downarrow}] \\ &= \sum_\sigma (\delta_{\sigma\uparrow} - \delta_{\sigma\downarrow}) \cdot \hat{c}_{1\uparrow}^\dagger \hat{c}_{2\downarrow} = 0\end{aligned}\tag{A.71}$$

with a similar expression for \hat{U}_+ instead of \hat{T}_+ with a shift in the channel indices. Note that in order for the *r.h.s.* to vanish, the sum over the spin σ is essential which shows the importance of the summation

over σ in Eqs. (A.70). As a consequence, the SU(3) channel symmetry in Eq. (A.70) commutes with the SU(2) spin symmetry, indeed.

The compatibility of the SU(3) channel symmetry with the SU(2) particle-hole symmetry, however, cannot be established, since

$$\begin{aligned} [\hat{T}_+, \hat{C}_{i+}] &= \sum_{\sigma} [c_{1\sigma}^\dagger \hat{c}_{2\sigma}, s \hat{c}_{1\uparrow}^\dagger \hat{c}_{1\downarrow}^\dagger] \\ &= s \delta_{i2} (\hat{c}_{1\uparrow}^\dagger \hat{c}_{2\downarrow}^\dagger - \hat{c}_{1\downarrow}^\dagger \hat{c}_{2\uparrow}^\dagger) \neq 0 \end{aligned} \quad (\text{A.72})$$

cannot be made to vanish for all channels i at the same time. Therefore the non-abelian channel and particle-hole symmetries cannot coexist independently of each other. Nevertheless, the generators of each individual symmetry do commute with the Hamiltonian, which thus suggests a larger symmetry, with Eq. (A.72) already indicating one of the additional generators. As it turns out, this symmetry is $\text{Sp}(2m)$ with m the number of channels [30]. This symmetry will be introduced and discussed in the next section.

By reducing the non-abelian particle-hole symmetry to its abelian conservation of total charge, however, this abelian symmetry does commute with the SU(3) channel symmetry,

$$\begin{aligned} \sum_i [\hat{T}_+, \hat{C}_{iz}] &= \sum_{\sigma, i\sigma'} \frac{1}{2} [c_{1\sigma}^\dagger \hat{c}_{2\sigma}, c_{i\sigma'}^\dagger \hat{c}_{i\sigma'}] \\ &= \sum_i \frac{1}{2} (\delta_{i2} - \delta_{i1}) \sum_{\sigma} \hat{c}_{1\sigma}^\dagger \hat{c}_{2\sigma} = 0. \end{aligned}$$

In order to get a commuting abelian charge symmetry, the z -operators for the channel-specific particle-hole symmetry must be summed over all channels i . With all commuting symmetries combined, this leads to the overall symmetry $\text{SU}(2)_{\text{spin}} \otimes \text{U}(1)_{\text{charge}} \otimes \text{SU}(3)_{\text{channel}}$, consisting of the SU(2) total spin symmetry in Eq. (A.68), the abelian total charge of the system in Eq. (A.69b), and the channel SU(3) symmetry in Eq. (A.70).

A more conventional symmetry setup can be obtained by giving up the channel SU(3) symmetry. Bearing in mind that the channel-specific SU(2) particle-hole symmetries commute with total spin, this also allows the symmetry setup $\text{SU}(2)_{\text{spin}} \otimes \text{SU}(2)_{\text{charge}}^{\otimes 3}$.

The symmetry combinations above can be motivated also by a simple counting argument with respect to conserved abelian quantum numbers. Note that the preserved abelian quantum numbers in the Hamiltonian equation (A.67) are the particle number in each of the three channels together with the total spin S_z . This results in a total of four z -operators, and thus four z -labels. Now, by including non-abelian flavors, the number of z -operators clearly cannot increase, but will remain the same. Total spin has one z -operator, the channel SU(3) symmetry has two z -operators, and the channel-specific particle-hole symmetries have three z -operators, which combined results in $1 + 2 + 3 = 6$ z -operators. This set of z -operators therefore *cannot be independent* of each other, as already seen in the earlier discussion. Yet, in fact, both of the alternative symmetry setups above do have a total of four z -operators. For $\text{SU}(2)_{\text{spin}} \otimes \text{U}(1)_{\text{charge}} \otimes \text{SU}(3)_{\text{channel}}$, these are $1 + 1 + 2$ from spin, charge, and channel symmetry, respectively, while for $\text{SU}(2)_{\text{spin}} \otimes \text{SU}(2)_{\text{charge}}^{\otimes 3}$ these are $1 + 3$ from spin and each channel.

For the symmetry setting $\text{SU}(2)_{\text{spin}} \otimes \text{U}(1)_{\text{charge}} \otimes \text{SU}(3)_{\text{channel}}$ then, the hopping term in the Hamiltonian in Eq. (A.67) is described by a 6-component IROP $\hat{\psi}_k^{[6]}$ (annihilation operators for spin-up and spin-down combined), that can be obtained, for example, numerically as described in Appendix B.2. This leads to

$$\hat{h}_{k,k+1} = \hat{\psi}_n^{[6]\dagger} \cdot \hat{\psi}_k^{[6]} + \text{H.c.} \quad (\text{A.73a})$$

In contrast, for the second symmetry setting $\text{SU}(2)_{\text{spin}} \otimes \text{SU}(2)_{\text{charge}}^{\otimes 3}$, the IROPs $\hat{\psi}_{k,i}^{[4]}$ required for the hopping term are already exactly the 4-component spinors in Eq. (A.59), i.e. one for each individual channel, $i = 1, \dots, 3$. The hopping in the Hamiltonian is thus described by

$$\hat{h}_{k,k+1} = \sum_{i=1}^{m=3} \hat{\psi}_{k,i}^{[4]\dagger} \hat{\psi}_{k+1,i}^{[4]}, \quad (\text{A.73b})$$

i.e. without the hermitian conjugate part as this is already included through particle–hole symmetry. Furthermore, note that particle–hole symmetry also acquires even–odd alternations for the spinors along a chain [see Appendix A.9.2].

A.10. The symplectic group $\text{Sp}(2m)$

All Hamiltonians considered in this paper are time-independent, hence obey time-reversal symmetry. Time-reversal symmetry then is described by an anti-unitary operator $\hat{T} = \hat{\Sigma}_y \hat{K}$ [32], that includes a standard unitary operation $\hat{\Sigma}_y$ together with the operator \hat{K} , which stands for complex conjugation [the notation of $\hat{\Sigma}_y$ has been chosen for latter convenience; see Eq. (A.77) below]. The time-reversal operator obeys $\hat{T}^2 = \pm 1$, where for spin-half particles, such as electrons as considered throughout in this paper, it holds $\hat{T}^2 = -1$. The latter is important for the symmetry $\text{Sp}(2m)$, since it implies that the unitary $\hat{\Sigma}_y$ must be antisymmetric. This follows simply by looking at the matrix elements of the time-reversal operator for arbitrary states $|a\rangle$ and $|b\rangle$ in some real basis i ,

$$\langle a|\hat{T}b\rangle = \sum_{i,j} a_i^*(\Sigma_y)_{ij} b_j^*,$$

yet it also holds,

$$\langle a|\hat{T}b\rangle = \underbrace{\langle \hat{T}^2}_{-1} b|\hat{T}a\rangle = - \sum_{i,j} b_j^*(\Sigma_y)_{ji} a_i^*.$$

As this applies for arbitrary states $|a\rangle$ and $|b\rangle$, this shows that, given $\hat{T}^2 = -1$, the unitary $\hat{\Sigma}_y$ must be antisymmetric, indeed.

Since a time-independent Hamiltonian obviously commutes with the time-reversal operator, it follows that all eigenstates of the Hamiltonian can also be written as eigenstates of the time-reversal operator \hat{T} . As a consequence, all unitary symmetry operations $\hat{G} = \exp(i \sum_\sigma a_\sigma \hat{S}_\sigma)$ can be constrained to unitaries which also leave the time-reversal operator invariant. That is,

$$\begin{aligned} \hat{T} &\stackrel{!}{=} \hat{G}\hat{T}\hat{G}^{-1} = \hat{G}\hat{\Sigma}_y \underbrace{\hat{K}\hat{G}}_{=\hat{G}^T\hat{K}} \\ &\Rightarrow \hat{\Sigma}_y = \hat{G}\hat{\Sigma}_y\hat{G}^T. \end{aligned} \quad (\text{A.74})$$

For the generators \hat{S}_σ of a symmetry group this implies (e.g. by expansion of the exponential in \hat{G} to first order in a_σ), that

$$\hat{S}_\sigma \hat{\Sigma}_y + \hat{\Sigma}_y \hat{S}_\sigma^T = 0. \quad (\text{A.75})$$

This exactly corresponds to the definition of the Lie algebra $\text{Sp}(2m)$. Having a unitary, i.e. non-singular, yet also antisymmetric $\hat{\Sigma}_y$, this requires a global Hilbert space of even dimension N , since $\det(\Sigma_y) = \det(\Sigma_y^T) = (-1)^N \det(\Sigma_y) \neq 0$. While this argument holds on the entire Hilbert space, for a specific symmetry subspace (carrier space) of an irreducible representation of $\text{Sp}(2m)$ this is not necessarily the case. Specifically, there are IREPs with odd dimensions, a simple example being the scalar representation with dimension 1. Within such an irreducible representation, a non-singular antisymmetric Σ_y does not exist. This is not a problem, however, since the existence of Σ_y is required only globally, and also in the defining representation, which thus has to be of even dimension.

Consider such a matrix representation of $\text{Sp}(2m)$ of even dimension, which allows to explicitly construct the non-singular antisymmetric Σ_y . In this case, an arbitrary matrix $S_{(\sigma)}$ within the space of the generators of the symmetry can be written as a tensor-product with a two-dimensional space, which itself can be expanded in terms of the Pauli matrices τ_σ [cf. Eq. (A.6)],

$$S_{(\sigma)} \equiv \sum_{x=0}^3 \tau_x \otimes S_x^{(\sigma)}, \quad (\text{A.76})$$

where $x \in \{0, 1, 2, 3\} \equiv \{0, x, y, z\}$ and $\tau_0 \equiv 1^{(2)}$ the two-dimensional identity matrix. Here the same letter S is used left and right in Eq. (A.76), as their interpretation is related. Nevertheless, they refer to different objects. So in order to distinguish them, the generators on the *l.h.s.* are written with Greek-letter subscripts (σ), while their decomposition $S_x^{(\sigma)}$ is denoted in roman font with roman or numeric subscripts. Moreover, for readability, the index σ referring to a specific generator will be skipped in the following where not explicitly required (hence the σ has been put in brackets).

Now, with representations of a symmetry unique up to similarity transformation, one is free to choose the form of the matrix representation of the operator $\hat{\Sigma}_y$ in Eq. (A.75). In the two-dimensional (block) space described by the Pauli matrices then, Σ_y is chosen as follows [66,67],

$$\Sigma_y = \tau_y \otimes 1^{(m)} \equiv \begin{pmatrix} 0^{(m)} & -i1^{(m)} \\ i1^{(m)} & 0^{(m)} \end{pmatrix}, \quad (\text{A.77})$$

where the last term explicitly denotes the tensor block-decomposition of $m \times m$ matrices, with $0^{(m)}$ [$1^{(m)}$] an $m \times m$ dimensional zero [identity] matrix, respectively. This Σ_y fulfills the minimal requirement that it is (i) unitary and (ii) antisymmetric. Using the Σ_y in Eq. (A.77) in the defining equation for $\text{Sp}(2m)$, Eq. (A.75), and the fact that the generators $S_{(\sigma)}$ in Eq. (A.76) shall refer to hermitian operators to start with, this implies for the decomposition S_x , that $S_0 \equiv iA$ is a purely imaginary and antisymmetric matrix, while the remaining S_x for $x = (1, 2, 3)$ must be real symmetric matrices. In summary, this allows to rewrite the matrix block-decomposition in Eq. (A.76) in the form [66,67],

$$S = \begin{pmatrix} iA + S_3 & S_1 - iS_2 \\ S_1 + iS_2 & iA - S_3 \end{pmatrix} \equiv \begin{pmatrix} C & D^\dagger \\ D & -C^T \end{pmatrix}, \quad (\text{A.78})$$

where $C \equiv iA + S_3$ ($D \equiv S_1 + iS_2$) is an arbitrary hermitian (symmetric) $m \times m$ matrix, respectively. The resulting number of free parameters is $m^2 + m$ for the matrix D (where the $+m$ comes from the fact that the diagonal can be fully complex), and m^2 for the hermitian matrix C . The total number of free parameters of the ($N \equiv 2m$)-dimensional matrices therefore is,

$$g = m(2m + 1) \equiv \frac{N}{2}(N + 1). \quad (\text{A.79})$$

In the case of the defining representation, by construction, this also corresponds to the dimension of the symmetry group $\text{Sp}(2m)$. For comparison, for example, the orthogonal group $O(N)$ has dimension $\frac{N}{2}(N - 1)$.

Setting the off-diagonal block-matrix D in Eq. (A.78) to zero, and using arbitrary hermitian yet *also traceless* matrices C , this directly demonstrates that $SU(m)$ is contained as a subalgebra within $\text{Sp}(2m)$. This subalgebra $SU(m)$ has rank $m - 1$, *i.e.* has $m - 1$ z -operators. Now, the full $\text{Sp}(2m)$ symmetry also includes the *tracefull* hermitian matrix C . This introduces the remaining m -th z -operator, $Z_m = \tau_z \otimes 1^{(m)}$. With a total of mz -operators, $\text{Sp}(2m)$ therefore has rank m , with the z -operators given by

$$Z_k \equiv \tau_z \otimes Z_k^{(m)}, \quad (\text{A.80a})$$

where

$$Z_k^{(m)} = \begin{cases} (Z_k^{(m)})^{\text{SU}(m)} & k = 1, \dots, m - 1 \\ 1^{(m)} & k = m, \end{cases} \quad (\text{A.80b})$$

with $(Z_k^{(m)})^{\text{SU}(m)}$ the standard $m \times m$ dimensional z -operators for $SU(m)$. By construction, all of these z -operators can be considered diagonal, as they form a mutually commuting set of matrices.

Leaving the space of strictly hermitian generators, the canonical RLOs from the $SU(m)$ subalgebra are given by

$$S_{ij} \equiv \begin{pmatrix} S_{ij} & 0 \\ 0 & -S_{ij}^T \end{pmatrix}, \quad (i \neq j) \quad (\text{A.81})$$

with $S_{ij} \equiv E_{ij}$ given by the non-symmetric matrices in Eq. (A.27b). This encodes both, raising and lowering operators, depending on $i < j$ or $i > j$, respectively. Having $(m^2 - 1) + 1 = m^2$ generators from the $SU(m)$ subalgebra together with Z_m , the remaining $m(m+1)$ operators are split equally into complimentary raising and lowering operators. The corresponding canonical RLOs can be chosen as follows [66,67],

$$\tilde{S}_{ij}^\pm \equiv \frac{1}{2} (\tau_x \pm i\tau_y) \otimes \tilde{S}_{ij}, \quad (\text{all } i, j) \quad (\text{A.82})$$

with the symmetric matrices $\tilde{S}_{ij} \equiv \frac{1}{2}(E_{ij} + E_{ji})$. Here the tilde serves to differentiate the RLOs from the $SU(m)$ subalgebra in Eq. (A.81). Having symmetric \tilde{S}_{ij} , i.e. $\tilde{S}_{ij} = \tilde{S}_{ji}$, this describes a total of $\frac{1}{2}m(m+1)$ raising operators. Complemented by $\frac{1}{2}m(m+1)$ lowering operators, indeed, this completes the group of generators for the Lie algebra $Sp(2m)$.

Using the canonical representation for $SU(m)$ together with above extension to $Sp(2m)$, this provides the canonical representation for $Sp(2m)$ as in Eq. (A.20). For example, with

$$(\vec{z}_i)_k \equiv z_{k,i}^{(m)} \equiv (Z_k^{(m)})_{ii} \quad (\text{A.83})$$

referring to the i -th diagonal matrix element of the diagonal matrices $Z_k^{(m)}$, it follows

$$Z_k^{(m)} \tilde{S}_{ij} = \tilde{S}_{ij} Z_k^{(m)} = \underbrace{(z_{k,i}^{(m)} + z_{k,j}^{(m)})}_{\equiv (\vec{z}_i + \vec{z}_j)_k} \cdot \tilde{S}_{ij},$$

and thus

$$\begin{aligned} [Z_k, \tilde{S}_{ij}^\pm] &= \left[\tau_z \otimes Z_k^{(m)}, \frac{1}{2}(\tau_x \pm i\tau_y) \otimes \tilde{S}_{ij} \right] = \underbrace{\frac{1}{2}[\tau_z, \tau_x \pm i\tau_y]}_{=\pm(\tau_x \pm i\tau_y)} \otimes ((\vec{z}_i + \vec{z}_j)_k \tilde{S}_{ij}) \\ &= \pm(\vec{z}_i + \vec{z}_j)_k \cdot \tilde{S}_{ij}^\pm, \end{aligned} \quad (\text{A.84a})$$

(no summation over i or j). Similarly, for the RLOs S_{ij} from the $SU(m)$ subalgebra, with

$$[Z_k^{(m)}, S_{ij}] = (\vec{z}_i - \vec{z}_j)_k \cdot S_{ij}$$

it follows,

$$\begin{aligned} [Z_k, S_{ij}] &= \left[\tau_z \otimes Z_k^{(m)}, \begin{pmatrix} S_{ij} & 0 \\ 0 & -S_{ij}^T \end{pmatrix} \right] = \left(\begin{matrix} [Z_k^{(m)}, S_{ij}] & 0 \\ 0 & [Z_k^{(m)}, S_{ij}^T] \end{matrix} \right) \\ &= (\vec{z}_i - \vec{z}_j)_k \cdot S_{ij}, \end{aligned} \quad (\text{A.84b})$$

since $[Z, S^T] = -[Z, S]^T$. This confirms that the z -operators together with the raising and lowering operators are in the expected canonical form, indeed.

A.10.1. Internal multiplet ordering

The block-decomposition of Eq. (A.76) is not yet ordered w.r.t. to the RLOs, i.e. the z -labels [here, by definition, it is assumed that a raising (lowering) operator leads to a larger (smaller) z -label in root space which directly links to the underlying sorting implemented in root space]. The starting point, however, is correct: (i) The ($D = 2m$) dimensional first state $|e_1\rangle$ [cf. Eq. (A.27a)] does represent the maximum weight state, indeed, and (ii) by applying the $m - 1$ lowering operators from the $SU(m)$ subalgebra, this iteratively demotes the MW-state through the states $|e_2\rangle, \dots, |e_m\rangle$. So far the state order is correct.

However, the next lower state is obtained by the m -th lowering operator, i.e. the one that links to the full $Sp(2m)$ symmetry. This will generate the state $|e_D\rangle$, which thus is not in order. Through another sequence of lowering operators from the $SU(m)$ subalgebra, finally this proceeds through the

states $|e_{D-1}\rangle, \dots, |e_{D-m+1}\rangle$ with additional alternating signs. The full sequence of normalized states thus obtained starting from the MW-state, can be collected as columns into a unitary matrix U ,

$$U \equiv \begin{pmatrix} 1^{(m)} & 0 \\ 0 & \Sigma^{(m)} \end{pmatrix}, \quad (\text{A.85a})$$

with the $m \times m$ dimensional matrix $\Sigma^{(m)}$

$$\Sigma^{(m)} \equiv \begin{pmatrix} \cdot & \cdot & \cdot & \cdot \\ \cdot & \cdot & +1 & \cdot \\ \cdot & -1 & \cdot & \cdot \\ +1 & \cdot & \cdot & \cdot \end{pmatrix}, \quad (\text{A.85b})$$

to be distinguished from Σ_y in Eq. (A.77) associated with time-reversal symmetry. The unitary U in Eq. (A.85a) maps the basis into the correct order w.r.t. to sorted z -labels, as is assumed throughout this paper. Therefore this basis convention will be used henceforth, which requires U to be applied to all generators.

The transformation of an arbitrary symmetry operation S in Eq. (A.78) then leads to $S \rightarrow U^\dagger S U$, that is

$$\begin{pmatrix} C & D^\dagger \\ D & -C^T \end{pmatrix} \rightarrow \begin{pmatrix} C & (\Sigma^T D)^\dagger \\ \Sigma^T D & -C^t \end{pmatrix}. \quad (\text{A.86})$$

In $\Sigma^T D$, Σ^T flips the order of the rows in D with alternating signs, starting with $+1$ on the new first row. The transformation $C^t \equiv \Sigma^T C^T \Sigma$ in the lower right block, finally, corresponds to inversion of C w.r.t. its center with alternating checker-board like minus signs applied, starting with plus signs along the regular matrix diagonal. With C hermitian, when taken real, C^t is equivalent to transposition w.r.t. the minor diagonal [67], thus indicated by superscript lowercase t [this is in contrast to the standard transposition $(\cdot)^T$ around the regular diagonal].

All generators inherited from the $SU(m)$ subalgebra thus become

$$S \rightarrow \begin{pmatrix} S_i & 0 \\ 0 & -S_i^t \end{pmatrix}. \quad (\text{A.87})$$

In particular, all z -operators have the diagonal in the lower-right diagonal flipped to reverse order. The *simple* RLOs from the $SU(m)$ subalgebra now have two strictly positive entries $+1$ at the first upper subdiagonal at symmetric positions w.r.t. the *center* of the matrix. The remaining simple raising operator completing the $Sp(2m)$ algebra (see below) is given by the matrix $\tilde{S}_{mm} = E_{mm} \rightarrow E_{mm} \Sigma = +E_{m1}$ in the upper right block, thus naturally completing the set of simple raising operators of the type

$$S_{(\alpha=1)}^+ = \begin{pmatrix} 0 & 1 & \cdot & \cdot & \cdot & \cdot \\ \cdot & 0 & 0 & \cdot & \cdot & \cdot \\ \cdot & \cdot & 0 & \ddots & \cdot & \cdot \\ \cdot & \cdot & \cdot & \ddots & 0 & \cdot \\ \cdot & \cdot & \cdot & \cdot & 0 & 1 \\ \cdot & \cdot & \cdot & \cdot & \cdot & 0 \end{pmatrix}, \quad (\text{A.88})$$

with $\alpha = 1, \dots, m$ indicating the position of the entries of 1 moving towards the center of the first upper off-diagonal.

A.10.2. Multiplet labels for $Sp(2m)$ for $m = 3$

With the RLOs defined to have at most two matrix elements exactly equal to 1, the canonical commutator relations in Eq. (A.84) directly depict the diagonal elements of the z -matrices. As already indicated in Eq. (A.83), these diagonals can be combined as rows into an $r \times D$ matrix $z_{k,i}$, to be referred to as z -matrix, with $r = m$ being the rank of the symmetry and $D = 2m$ the dimension of the

defining matrix representation. The vectors \vec{z}_i in Eq. (A.83) thus refer to the *columns* in the z -matrix, and therefore directly reflect the q_z -labels, *i.e.* the root space.

For $\text{Sp}(6)$, this 3×6 dimensional z -matrix reads

$$z = \underbrace{\begin{pmatrix} 1 & -1 & 0 \\ 1 & 1 & -2 \\ 1 & 1 & 1 \end{pmatrix}}_{\equiv \tilde{z}} \begin{pmatrix} 0 & 1 & -1 \\ 2 & -1 & -1 \\ -1 & -1 & -1 \end{pmatrix}. \quad (\text{A.89})$$

By construction, all matrix elements are integers, for simplicity. The z -labels of the defining representation are *directly* specified by the columns \vec{z}_i of the z -matrix. Moreover, since the z -labels are additive for tensor-product spaces, this implies that the z -labels for *arbitrary* IREPs also contain integers only.

Consequently, the root space is fully spanned by simple linear integer combinations of the vectors \vec{z}_i . Furthermore, also the action of the RLOs themselves can be expressed as simple shifts in root space [cf. Eq. (A.84)]. While in the defining representation, the z -labels in the carrier space are clearly unique, they are not linearly independent. In particular, it is sufficient to focus the discussion on the linearly independent subset of the vectors \vec{z}_i in terms of the leading 3×3 block \tilde{z} of the z -matrix in Eq. (A.89).

In terms of the three column vectors \vec{z}_i in \tilde{z} , the simple roots are given (i) by the simple roots of $\text{SU}(m)$, which (ii) is complemented by one further root involving \vec{z}_3 ,

$$\begin{aligned} \vec{\alpha}_1 &= \vec{z}_1 - \vec{z}_2 = (-2, 0, 0)^T \hat{=} S_{12} \\ \vec{\alpha}_2 &= \vec{z}_2 - \vec{z}_3 = (-1, 3, 0)^T \hat{=} S_{23}, \\ \vec{\alpha}_3 &= 2\vec{z}_3 = (0, -4, 2)^T \hat{=} \tilde{S}_{33}^+ \end{aligned} \quad (\text{A.90})$$

where the correspondence with the raising operators indicated in the last column follows from Eq. (A.84). Having $\vec{\alpha}_i \cdot \vec{\alpha}_j \leq 0$ for $i \neq j$ together with taking smallest integer combinations derived from the action of RLOs in Eq. (A.84), this suggests *simple* roots [66,67].

Similar to $\text{SU}(N)$, the convention on the sorting of the z -labels is chosen lexicographic, yet as always, starting from the last z -label. In this sense, the vectors $\vec{\alpha}_i$ in Eq. (A.90) are greater than $(0, 0, 0)^T$, hence positive. The corresponding operators thus *increase* the z -labels, *i.e.* correspond to raising operators, indeed. Moreover, having reduced the symmetry to its simple roots, equivalently, this also defines the set of *simple* RLOs that are sufficient to fully explore multiplet spaces. Note that above convention on the sorting of the z -labels is already also consistent with the state order in the defining representation in Eq. (A.89): the z -labels strictly decrease, starting from the MW-state (the very left column) all the way to the last state represented by the very right column.

In principle, the z -labels of the MW-state already could be used as labels for the entire multiplet. However, using the vectors \vec{z}_i as (non-)orthogonal basis that spans the root space, also $\vec{q} \equiv \tilde{z}^{-1} \max \{\tilde{z}\}$ could be used as multiplet label, instead. The latter has the advantage that it guarantees that the multiplet labels are strictly positive integers or zero. For consistency with the literature, however, the multiplet labels for $\text{Sp}(2m)$ are still modified somewhat further, and thus finally derived from the MW-state as follows,

$$\vec{q} \equiv \underbrace{M\tilde{z}^{-1}}_{\equiv Q} \cdot \max \{\tilde{z}\} \quad (\text{A.91a})$$

where the matrix M ,

$$M \equiv \begin{pmatrix} 1 & -1 & 0 \\ 0 & 1 & -1 \\ 0 & 0 & 1 \end{pmatrix}, \quad (\text{A.91b})$$

has been added as a further minor modification for consistency with the standard literature [68] which further ensures that the multiplet labels lie dense, *i.e.* with $q = (q_1, q_2, q_3)$ any $q_i \geq 0$ will result in a valid multiplet. Overall,

$$Q \equiv \begin{pmatrix} 1 & 0 & 0 \\ -\frac{1}{2} & \frac{1}{2} & 0 \\ 0 & -\frac{1}{3} & \frac{1}{3} \end{pmatrix}. \quad (\text{A.91c})$$

For example, when applied from the right to the z -matrix in Eq. (A.89), all resulting matrix elements (z -labels) are either ± 1 or 0. In particular, the MW-state of the defining representation of $\text{Sp}(2 \cdot 3)$ has the q -labels $(1, 0, 0)$.

A.10.3. Construction of $\text{Sp}(2m)$ for m -channel setup

Given the three-channel setup in the previous section with $m = 3$, the resulting defining representation for $\text{Sp}(2m)$ is $(2m = 6)$ -dimensional. As seen from the earlier introduction of this model in Appendix A.9.4, this contains an $\text{SU}(3)$ subalgebra, together with a third z -operator, namely total particle conservation. This subalgebra of a total of 9 generators can now be completed by 6 raising operators together with their hermitian conjugates, *i.e.* their corresponding lowering operators. This leads to a total of 21 generators, consistent with the dimension of the group $\text{Sp}(2 \cdot 3)$.

Using a sorted z -label space, this requires that the unitary U in Eq. (A.85a) is applied to all generators of the defining representation, as well as to the initial spinor $\hat{\psi}^{[2m]} \equiv (\hat{c}_{1\uparrow}, \dots, \hat{c}_{m\uparrow}, \hat{c}_{1\downarrow}^\dagger, \dots, \hat{c}_{m\downarrow}^\dagger)^T$ derived from Eq. (A.76). In the case of $m = 3$, the properly sorted 6-dimensional spinor (IROP) spinor becomes,

$$\hat{\psi}_{(\uparrow)}^{[6]} \equiv \begin{pmatrix} \hat{c}_{1\uparrow} \\ \vdots \\ \hat{c}_{m\uparrow} \\ +\hat{c}_{m\downarrow}^\dagger \\ -\hat{c}_{m-1,\downarrow}^\dagger \\ \vdots \\ (-1)^{m-1}\hat{c}_{1\downarrow}^\dagger \end{pmatrix}. \quad (\text{A.92})$$

This naturally generalizes particle-hole symmetry in the presence of channel symmetry. The symmetry preserving hopping term in Eq. (A.67), for example, can now be written as scalar contraction $\hat{h}_{k,k+1} = \sum_\sigma (\hat{\psi}_{k\sigma}^{[6]})^\dagger \cdot \hat{\psi}_{k+1,\sigma}^{[6]}$. Note that if, in addition, also $\text{SU}(2)_{\text{spin}}$ is present, this would further double the dimension of the IROP in Eq. (A.92) to a set of 12 operators, such that the hopping term in Eq. (A.67) can be written as single scalar contraction $\hat{h}_{k,k+1} = (\hat{\psi}_k^{[12]})^\dagger \cdot \hat{\psi}_{k+1}^{[12]}$.

All generators are given in second quantization by the quadratic form $\hat{S}_\sigma \equiv \hat{\psi}^\dagger S_\sigma \hat{\psi}$, with S_σ a $2m$ -dimensional generator from the defining representation. Specifically, the remaining $\frac{1}{2}m(m+1)$ raising operators for the m -channel setup in Eq. (A.82) that complete $\text{Sp}(2m)$ are given by

$$\tilde{S}_{ij}^+ = \frac{1}{2} (\tau_x + i\tau_y) \otimes (\tilde{S}_{ij} \Sigma) \equiv \begin{pmatrix} 0 & \tilde{S}_{ij} \Sigma \\ 0 & 0 \end{pmatrix}, \quad (\text{A.93})$$

which leads to

$$\hat{S}_{ij}^+ \equiv \hat{\psi}^\dagger \tilde{S}_{ij}^+ \hat{\psi} = \frac{1}{2} (\hat{c}_{i\uparrow}^\dagger \hat{c}_{j\downarrow}^\dagger + \hat{c}_{j\uparrow}^\dagger \hat{c}_{i\downarrow}^\dagger) \quad (\text{all } i, j). \quad (\text{A.94})$$

This generates a pair of particles, the nature of which originates from the underlying general particle-hole symmetry. With $\{\hat{\psi}_i, \hat{\psi}_j^\dagger\} = \delta_{ij}$ for $v = 1, \dots, 2m$, and therefore

$$\begin{aligned} [\hat{S}_\sigma, \hat{S}_{\sigma'}] &\equiv [\hat{\psi}_i^\dagger (S_\sigma)_{ij} \hat{\psi}_j, \hat{\psi}_{i'}^\dagger (S_{\sigma'})_{i'j'} \hat{\psi}_{j'}] \\ &= \hat{\psi}^\dagger [S_\sigma, S_{\sigma'}] \hat{\psi}, \end{aligned} \quad (\text{A.95})$$

the commutator relations within the matrix representations of the defining representation earlier directly carry over to the quadratic second-quantized operators as in Eq. (A.94).

Appendix B. Numerical implementation

Tensor-product spaces are an essential ingredient to numerical renormalization group techniques such as NRG or DMRG. State spaces are enlarged iteratively by adding a small local state space at a time, *i.e.* a physical site with a few degrees of freedom. With respect to the description of strongly-correlated entangled quantum many-body states, this leads to a description which is well-known as matrix product states (MPSs). Both, the existing state space (iteratively constructed itself) as well as the newly added state-space, have finite dimension and well-defined symmetry labels. New representations can therefore only emerge through the tensor product of the two spaces. In particular, all iteratively constructed quantum many body states strictly derive from the IREPs of the elementary sites. With operators usually acting locally, these are also expressed in the symmetries of the local basis. Furthermore, the local state space of a site is usually small. For example, a fermionic site has the four states described in Eq. (A.62). Therefore the IREPs present within the local state space are usually just the smallest non-trivial IREPs, often just the defining representation itself. For identical sites, the local symmetry space can be setup once and for all at the beginning of the calculation.

Having identified and labeled all symmetries on the local site level, this sets the stage for generic iterative algorithms such as NRG or DMRG. The remainder is a large exercise on tensor-product spaces. By construction, the iteratively combined spaces are finite, yet as they grow rapidly, they are eventually truncated on the multiplet level while leaving the symmetry content of the individual multiplets, *i.e.* the CGC spaces, fully intact.

B.1. Tensor product decomposition of symmetry spaces

The decomposition of the tensor-product space of two IREPs into irreducible multiplets has already been discussed more generally in Appendices A.5 and A.6. In the actual numerical implementation, however, in particular the presence of inner and out multiplicity must be taken care of meticulously for overall consistency. This will be discussed in the following.

Similar to Appendix A.6, consider a specific arbitrary non-abelian symmetry group δ whose Clebsch–Gordan coefficients may not necessarily be easily accessible analytically for arbitrary multiplets. Assume two of its IREPs, q_1 and q_2 , with dimensions d_{q_1} and d_{q_2} , respectively, are known together with their irreducible representations of the generators $I_\sigma^{[q_1]}$ and $I_\sigma^{[q_2]}$, specifically the z-operators (Cartan subalgebra) and the simple RLOs (simple roots). In practice, these representations either refer to small IREPs such as the defining representation, or have been generated through prior iterative calculations. As in Eq. (A.36), consider their tensor-product,

$$R_\sigma^{\text{tot}} \equiv I_\sigma^{[q_1]} \otimes \mathbf{1}^{[q_2]} + \mathbf{1}^{[q_1]} \otimes I_\sigma^{[q_2]}, \quad (\text{B.1})$$

resulting in matrices of dimension $D = d_{q_1}d_{q_2}$. Clearly the commutator relations are preserved, and the z-labels are *additive* under this operation [cf. Appendix A.6].

In order to determine the decomposition into IREPs, a tempting route may be through the construction of the group's Casimir operators in the combined state space and their simultaneous diagonalization together with the z-operators. However, in the presence of outer or inner multiplicity, subspaces exist that are fully degenerate in Casimir operators as well as in the z-operators. In this case, for overall consistency a *unique deterministic* algorithm must be constructed that (i) separates multiplets in the presence of outer multiplicity, and (ii) fixes a choice of basis for degenerate spaces within a multiplet in the presence of inner multiplicity. Moreover, the explicit construction of the Casimir operators bears some efforts of its own. In practice, therefore a more straightforward approach has been adopted, instead, as will be explained in the following.

The main hurdles in the decomposition of the tensor-product in Eq. (B.1) into IREPs is the possible occurrence of outer and inner multiplicities. The strategy employed here to deal with this situation is based on the uniqueness and accessibility of the MW (maximum-weight) states as introduced in Appendix A.3.3. For this, throughout the procedure below, the *same* lexicographic sorting scheme of the z-labels, used to obtain the MW-state in Eq. (A.26), is employed to order all states within an IREP. The sorting is descending, such that the MW-state appears *first* within a multiplet.

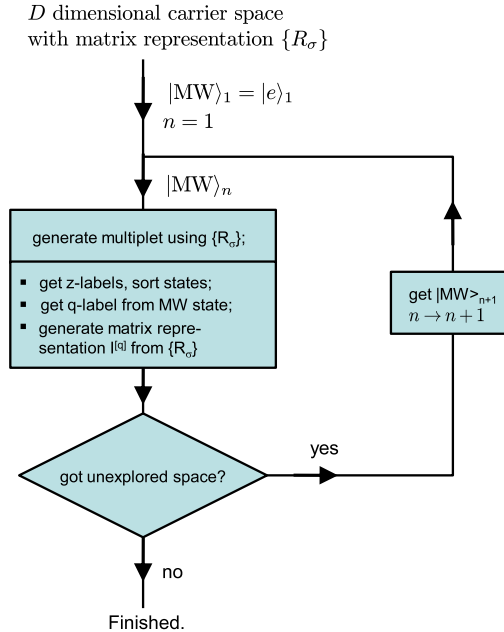


Fig. B.13. Schematic procedure of state space decomposition of given D dimensional vector space with known set of generators $\{R_\sigma^{(\text{tot})}\}$.

Since the z -labels are additive, it also follows for a tensor product of two such representations that the first state automatically also represents a MW-state of some multiplet,

$$|\text{MW}\rangle_1 \equiv |e_1\rangle, \quad (\text{B.2})$$

where the vectors $|e_k\rangle$ [cf. Eq. (A.27a)] form the cartesian basis for the D -dimensional space of the representation R_σ^{tot} in Eq. (B.1). Given that the MW-state of a representation is guaranteed to be unique [38,66,67], the state $|\text{MW}\rangle_1$ is already a proper symmetry eigenstate, i.e. an eigenstate of all z -operators. This was always double checked, in practice, as a safety measure. The further procedure then is schematically depicted in the work flow diagram in Fig. B.13: starting with $|\text{MW}\rangle_{n=1}$,

1. the symmetry eigenstate $|\text{MW}\rangle_n$ is used as the *seed state* to sequence its complete IREP (the *current multiplet*). This is done by repeatedly applying an *arbitrary but fixed order of simple lowering operators only* to the current set of vectors in the multiplet. Therefore starting with the MW-state $|\text{MW}\rangle_n$ and adding the newly acquired symmetry states one at a time, this introduces a well-defined state order, independent of whether their z -labels are degenerate or not. In the presence of inner multiplicity, it is important to notice, however, that it is not guaranteed that a newly acquired state is automatically orthogonal to the already existing states within the current multiplet. Therefore, a newly acquired state, if it represents a new vector space component, must be orthonormalized with respect to the existing states. This is repeated, until the current multiplet space is exhausted.
2. The states in the multiplet thus generated, by construction, already have well-defined z -labels (this again was double-checked, in practice); the states are sorted with respect to these labels in descending lexicographic order while keeping subspaces that are degenerate in the z -labels in their *original order* in order to remain deterministic. Within this order, the first state defines the label for the generated multiplet, i.e. $q = q_{\text{MW}}$. In addition, the matrix representation in Eq. (B.1), when cast into the current IREP space results in the newly generated irreducible matrix representation $\hat{I}_\sigma^{[q]}$.
3. If the D -dimensional vector space is not fully exhausted yet, a new seed state is determined by finding the *smallest* k for which $|e_k\rangle$ exhibits a new vector component w.r.t. the symmetry states

already collected. Having started with $k = 1$ above, it follows $k > 1$. After proper orthonormalization with respect to the previously explored space, this state becomes the next seed state. If it already does represent a MW-state, which is typically the case in that it is destroyed by all raising operators, then $|\text{MW}\rangle_{n+1}$ has been found. Otherwise repeatedly apply simple raising operators on the current seed state until the unique new maximum weight state $|\text{MW}\rangle_{n+1}$ is reached. Continue with (1), setting $n \rightarrow n + 1$.

4. If on the other hand, the D -dimensional vector space in Eq. (B.1) is already fully exhausted, the decomposition of the tensor-product space into n irreducible representations is completed, and the procedure terminates.

Note that no explicit reference to z -labels has been made, except for step (2). That step, however, is actually not required right away for the decomposition, with its results only relevant for subsequent calculations. By construction, therefore this procedure is deterministic and does not depend on dealing with degeneracies in the z -labels or inner and outer multiplicities. The MW-states are accessible by keeping IREPs sorted in their z -labels throughout. They represent the entry point in sequencing its IREP, which guarantees that inner and outer multiplicities are dealt with in a consistent fashion. Finally, note that the choice of the seed states $|\text{MW}\rangle_n$, i.e. starting with $+|e\rangle_k$, also provides the sign convention.

The resulting unitary transformation into the irreducible symmetry subspaces directly determines (i) the Clebsch–Gordan coefficients, and (ii) the matrix-representations of the newly generated IREPs. With only a few Clebsch–Gordan coefficients usually unequal to zero and of order 1, small numbers below a numerical noise threshold for double-precision (10^{-12}) are neglected, i.e. set to zero. Moreover, a non-zero Clebsch–Gordan coefficient can typically be expressed as a rational number, or the square root of a rational number, an efficient approximation of which can be found through continued fraction techniques. Therefore if an excellent fractional approximation was found within the same accuracy of 10^{-12} , this rational approximation also was used, instead.

B.2. State space initialization and operator compactification

In the presence of several symmetries, a given state space is represented by a certain set of multiplet combinations. For a single fermionic site in the presence of spin-symmetry and particle–hole symmetry, this still can be easily characterized by hand [cf. Eq. (A.62)]. The situation, however, can quickly become more involved. For example, for a spinful three-channel calculation with $SU(3)$ channel symmetry as in Eq. (27a), a site is represented by $4^3 = 64$ states (4 fermionic states for each of the 3 channels). If for example, particle number, spin symmetry and channel symmetry is preserved, then this system exhibits $SU(2)_{\text{spin}} \otimes U(1)_{\text{charge}} \otimes SU(3)_{\text{channel}}$ symmetry, as discussed in Appendix A.9.4. Given these symmetries, the 64-dimensional Hilbert space of a site cannot be decomposed into a tensor product of convenient smaller units with already well-defined $SU(2)_{\text{spin}} \otimes U(1)_{\text{charge}} \otimes SU(3)_{\text{channel}}$ symmetry labels themselves. For the channel symmetry it is essential, of course, that all three channels are present, while it is also essential for the spin symmetry that both spin species are present. Therefore in the example above, the 64-dimensional space of site already appears as the smallest building block. It can be reduced to a set of irreducible multiplet combinations, of course, but explicit determination can quickly become tedious if done by hand, while the problem can be tackled completely generally and straightforwardly on a numerical level.

In order to get started numerically, a simple and natural starting point is the Fock space representation. While this usually does not represent the symmetry eigenbasis, of course, nevertheless all generators of the symmetries present, in particular its raising, lowering, and z -operators, are known in second-quantized form and can be equally constructed in Fock space.

The z -operators typically have a simple form. In particular, for 3-channel setup mentioned above, the z -operators are already all diagonal in the Fock space, cf. Eq. (A.68), (A.69b), or (A.70). This thus already provides the z -labels. Next, note that the order of the states w.r.t. to their z -labels is important for consistency with the Clebsch–Gordan coefficients later, which suggests using the same lexicographic order as for the determination of the MW-states. Sorting the states in this order and

applying the same prescription for state space decomposition as explained in [Appendix B.1](#), this suffices to fully identify all symmetry multiplets within the given D -dimensional Hilbert space.

B.2.1. Compactifying operators using Wigner–Eckart theorem

Irreducible operator sets can be equally constructed starting from the Fock space representation of a *seed operator* that is part of some irreducible operator set. This seed operator is typically known, yet can be completed to an IROP set, by using the RLOs in Fock space representation and numerically evaluating the commutators in Eq. [\(A.42\)](#) (see also subsequent discussion in [Appendix A.7.1](#)). Using the same unitary transformation that brings the Fock space into the correct symmetry eigenbasis as described above, the IROP set is rotated into the space of symmetry eigenstates. With this, however, this IROP set is still represented in the *fully expanded* multiplet space, *i.e.* this space still references both multiplet labels and their corresponding z-labels on the same flat level. However, through the Wigner–Eckart theorem, Eq. [\(A.43\)](#),

$$\langle qq_z | \hat{F}_{q_{1z}}^{q_1} | q_2 q_{2z} \rangle = \langle q | \hat{F}^{q_1} | q_2 \rangle \cdot C_{q_{1z} q_{2z}(\sigma)}^{[q_{2z}]}, \quad (\text{B.3})$$

many of the matrix elements can be related to each other through Clebsch–Gordan coefficients. The IROP set can therefore be *compactified* as a tensor-product of reduced matrix-elements $\langle q | \hat{A}_{q_1} | q_2 \rangle$ in the multiplet space times the CGC space $C_{q_{1z} q_{2z}(\sigma)}^{[q_{2z}]}$.

The CGC spaces are known from a separate numerical calculation, *e.g.* they can be generated by several iterations of tensor-product decompositions starting from the defining representation. Therefore, the final compactification in Eq. [\(B.3\)](#) of the fully expanded matrix elements of the IROP also serves as a major consistency check. The first non-zero matrix-element $\langle qq_z | \hat{F}_{q_{1z}}^{q_1} | q_2 q_{2z} \rangle$ for the already known multiplet spaces $(q; q_1, q_2)$ can be used to determine the reduced matrix element $\langle q | \hat{F}^{q_1} | q_2 \rangle$, with its corresponding Clebsch–Gordan coefficient known. This, however, immediately predicts the existence of a set of other non-zero matrix elements within the same multiplet spaces $(q; q_1, q_2)$. These matrix elements must exist and agree within numerical noise. The matched matrix elements are marked and considered taken care of. If the same value of a matrix element occurs several times within the multiplets $(q; q_1, q_2)$ for the same z-labels, the first one that matches is taken. This check is thus not entirely unique, but nevertheless a strong one, and sufficient to obtain the space of reduced matrix elements. Finally, having identified all non-zero matrix elements, the multiplet matrix element space $\langle q | \hat{F}^{q_1} | q_2 \rangle$ are stored together with their referenced CGC space in terms of a QSpace as discussed in the main text.

Appendix C. Example QSpaces

QSpaces represent an efficient numerical description of tensors of arbitrary rank in the presence of arbitrary quantum symmetries [*cf.* Eq. [\(5\)](#)]. This includes both abelian and non-abelian symmetries, with the extension to further symmetries such as point symmetries being straightforward. The QSpaces are decomposed into a set of reduced multiplet spaces together with their respective CGC (Clebsch–Gordan coefficient) spaces. In the following several elementary examples of QSpaces are given as they appeared in practice. Elementary QSpaces typically have rank-2 (such as scalar operators with identity CGC spaces) or rank-3 (IREPs and IROPs with reference to standard rank-3 CGC spaces), while combinations of these through subsequent algebraic operations can easily result in higher-rank intermediate objects.

The notation regarding the elementary data arrays will be as follows. Plain matrices of dimension $m \times n$ will be written as $a = [a_{11}, \dots, a_{1n}; \dots; a_{m1}, \dots, a_{mn}]$, *i.e.* m rows of equal length n separated by semicolons. The commas within a row are considered optional. In order to deal with $m \times n \times k$ dimensional rank-3 objects, the notation $\{a_1, a_2, \dots, a_k\}$ is used, which shall indicate that the matrices a_1, \dots, a_k , all of the same dimension $m \times n$, are concatenated along the third dimension. Trailing singleton dimensions will be considered implicit if required, *e.g.* a scalar such as 1. can stand for an arbitrary rank-r object in that a number also represents a $1 \times 1 \times \dots \times 1$ object. Identity matrices of dimension n will be denoted by $\mathbf{1}^{(n)}$.

C.1. Fermionic site with $U(1)_{\text{charge}} \otimes SU(2)_{\text{spin}}$ symmetry

Consider the state space of a single fermionic site with the four states: empty $|0\rangle$, singly occupied $|\uparrow\rangle$ and $|\downarrow\rangle$, and double occupied $|\uparrow\downarrow\rangle$. The symmetries considered are particle conservation $U(1)_{\text{charge}}$, and full spin symmetry $SU(2)_{\text{spin}}$. The z-operators are $\hat{C}_z \equiv \frac{1}{2}(\hat{n}_\uparrow + \hat{n}_\downarrow - 1)$ and $\hat{S}_z \equiv \frac{1}{2}(\hat{n}_\uparrow - \hat{n}_\downarrow)$, with the corresponding quantum labels C_z for charge and S for total spin. For consistency with later discussion to follow, here the charge is treated as the reduction of the non-abelian particle-hole symmetry to its abelian part, which also reduces the set of symmetry operations to the z-operator \hat{C}_z only [hence the factor $\frac{1}{2}$]. Consequently, the z-label of the underlying non-abelian symmetry is promoted into a q -label, while the CGC space becomes trivial (1.) with internal multiplet dimension of 1. In order to stress the difference between the original z-label which can become negative, and the $SU(2)q$ -labels of multiplets which are positive, by definition, the q -labels are therefore written as $(+C_z, S)$, emphasizing the origin of the q -label C_z being derived from a z-operator.

C.1.1. Symmetry space and operators of one site

The states $|0\rangle$, $|\uparrow\rangle$, $|\downarrow\rangle$, and $|\uparrow\downarrow\rangle$ already represent the correct symmetry eigenstates [cf. Eq. (A.62)],

multiplet space $ C_z; S\rangle$	dimension $d_{C_z} \times d_S = d_{\text{tot}}$
$ \mp\frac{1}{2}; 0\rangle$	$1 \times 1 = 1$
$ \pm\frac{1}{2}; 0\rangle$	$1 \times 1 = 1$
$ 0; \frac{1}{2}\rangle \equiv \{ \uparrow\rangle, \downarrow\rangle\}$	$1 \times 2 = 2$

(C.1)

The matrix elements of a generic Hamiltonian in this basis can be written as QSpace [see definition in Eq. (5)],

$$H \equiv \left\{ \begin{array}{cc|cc|c} (C_z; S) & (C'_z; S') & \|H\| & \text{CGC spaces} \\ \hline -\frac{1}{2}; 0 & -\frac{1}{2}; 0 & h_{-\frac{1}{2}, 0} & 1. & 1. \\ +\frac{1}{2}; 0 & +\frac{1}{2}; 0 & h_{+\frac{1}{2}, 0} & 1. & 1. \\ 0; \frac{1}{2} & 0; \frac{1}{2} & h_{0, \frac{1}{2}} & 1. & \mathbf{1}^{(2)} \end{array} \right\}. \quad (\text{C.2})$$

The Hamiltonian is a scalar operator, hence its rank as an IROP can be reduced from three to two, as it is the only operator in its irreducible set. Consequently, all CGC spaces reduce to the identity, as reflected in the last two columns of the QSpace (C.2). Each of the remaining two indices explicitly refers to symmetry states, hence the QSpace requires the two sets of q -labels $q \equiv (C_z; S)$ and $q' \equiv (C'_z; S')$ referring to the first (second) index shown in the first (second) column, respectively. With the Hamiltonian preserving the symmetries, it must be block-diagonal, i.e. $q = q'$ for all records in (C.2). Both of the symmetry spaces $(\pm\frac{1}{2}; 0)$ have a single state only, therefore the corresponding entries in the multiplet space $h_{\pm 1/2, 0}$ are 1×1 dimensional blocks, i.e. numbers. The last symmetry multiplet $(0; \frac{1}{2})$ has two states owing to the $SU(2)$ symmetry [see (C.1)]. By means of the Wigner-Eckart theorem, the space of reduced matrix elements, $h_{0, 1/2}$, is therefore again a number while the CGC space becomes a 2-dimensional identity matrix. Therefore the most general representation of a scalar operator for a single fermionic level in the presence of $U(1)_{\text{charge}} \otimes SU(2)_{\text{spin}}$ symmetry is given by the three numbers $\{h_{-1/2, 0}, h_{+1/2, 0}, h_{0, 1/2}\}$ in the multiplet space. The remaining matrix elements are constrained due to symmetry.

As an example for a non-scalar IROP, consider the spinor of particle creation operators $\hat{\psi}_S^\dagger = \{\hat{c}_\uparrow^\dagger, \hat{c}_\downarrow^\dagger\}$ that encodes $SU(2)$ spin symmetry [cf. Eq. (A.49)], with its QSpace representation shown in (C.3a). The z-labels of the IROP set $\hat{\psi}_S^\dagger$ are determined through the z-operators \hat{C}_z and \hat{S}_z acting on the components of $\hat{\psi}_S^\dagger$,

$$\begin{aligned} [\hat{C}_z, \hat{c}_\sigma^\dagger] &= \frac{\pm 1}{2} \cdot \hat{c}_\sigma^\dagger \\ [\hat{S}_z, \hat{c}_\sigma^\dagger] &= \frac{\sigma}{2} \cdot \hat{c}_\sigma^\dagger, \end{aligned}$$

Table C.1

Example QSpaces in the presence of $U(1)_{\text{charge}} \otimes SU(2)_{\text{spin}}$ symmetry for a single fermionic site. Having the two symmetries of abelian $U(1)_{\text{charge}}$ and non-abelian $SU(2)_{\text{spin}}$, the respective CGC spaces C (trivial) and S appear in the right columns. The record index ν in the first column, as well as the explicit specification of the dimensions of the reduced multiplet space and the combined CGC spaces are just added for better clarity. The specific order of the records, however, is irrelevant and hence chosen as convenient. (C.3) shows the QSpaces for $\hat{\psi}_S^\dagger = \{\hat{c}_\uparrow^\dagger, \hat{c}_\downarrow^\dagger\}$ and $\hat{\psi}_S = \{-\hat{c}_\downarrow; \hat{c}_\uparrow\}$; cf. Eq. (A.49)]. (C.4) shows the identity A-tensor for the combination of the state spaces of two sites. For comparison, Table C.2 shows how the QSpaces (C.3a) and (C.4) are modified for the case that the abelian charge symmetry also becomes a non-abelian $SU(2)_{\text{charge}}$ particle-hole symmetry.

record index ν				reduced matrix elements		CGC spaces		
	$(C_z; S)$	$(C'_z; S')$	$(C''_z; S'')$	$\ \psi_S^\dagger\ $,	dimension	C	S	dimension
1.	$0; \frac{1}{2}$	$\frac{-1}{2}; 0$	$\frac{+1}{2}; \frac{1}{2}$	1.	$1 \times 1 \times 1$	1.,	$\{[1; 0], [0; 1]\}$	$2 \times 1 \times 2$
	$\frac{+1}{2}; 0$	$0; \frac{1}{2}$	$\frac{+1}{2}; \frac{1}{2}$	$\sqrt{2}$	$1 \times 1 \times 1$	1.,	$\frac{1}{\sqrt{2}}\{[0; 1], [-1; 0]\}$	$1 \times 2 \times 2$

(C.3a)

record index ν				reduced matrix elements		CGC spaces		
	$(C_z; S)$	$(C'_z; S')$	$(C''_z; S'')$	$\ \psi_S\ $,	dimension	C	S	dimension
1.	$0; \frac{1}{2}$	$\frac{-1}{2}; 0$	$\frac{-1}{2}; \frac{1}{2}$	1.	$1 \times 1 \times 1$	1.,	$\{[1; 0], [0; 1]\}$	$2 \times 1 \times 2$
	$\frac{-1}{2}; 0$	$0; \frac{1}{2}$	$\frac{-1}{2}; \frac{1}{2}$	$-\sqrt{2}$	$1 \times 1 \times 1$	1.,	$\frac{1}{\sqrt{2}}\{[0; 1], [-1; 0]\}$	$1 \times 2 \times 2$

(C.3b)

record index ν	site 1	site 2	combined	multiplet space $\ A\ $	dimension	CGC Spaces		
	$(C_z; S)$	$(C'_z; S')$	$(C''_z; S'')$			C	S	dimension
1.	$\frac{-1}{2}; 0$	$\frac{-1}{2}; 0$	$-1; 0$	1.	$1 \times 1 \times 1$	1.	1.	$1 \times 1 \times 1$
2.	$\frac{-1}{2}; 0$	$0; \frac{1}{2}$	$\frac{-1}{2}; \frac{1}{2}$	$\{[1], [0]\}$ $\{[0], [1]\}$	$1 \times 1 \times 2$	1.	$\{[1; 0], [0; 1]\}$	$1 \times 2 \times 2$
3.	$0; \frac{1}{2}$	$\frac{-1}{2}; 0$	$\frac{-1}{2}; \frac{1}{2}$		$1 \times 1 \times 2$	1.	$\{[1; 0], [0; 1]\}$	$2 \times 1 \times 2$
4.	$\frac{-1}{2}; 0$	$\frac{1}{2}; 0$	$0; 0$		$1 \times 1 \times 3$	1.	1.	$1 \times 1 \times 1$
5.	$0; \frac{1}{2}$	$0; \frac{1}{2}$	$0; 0$		$1 \times 1 \times 3$	1.	$[0; \frac{-1}{\sqrt{2}}, \frac{1}{\sqrt{2}}; 0]$	$2 \times 2 \times 1$
6.	$\frac{1}{2}; 0$	$\frac{-1}{2}; 0$	$0; 0$		$1 \times 1 \times 3$	1.	1.	$1 \times 1 \times 1$
7.	$0; \frac{1}{2}$	$0; \frac{1}{2}$	$0; 1$		$1 \times 1 \times 1$	1.	$\{[1; 0; 0], [0; \frac{1}{\sqrt{2}}, \frac{1}{\sqrt{2}}; 0], [0; 0; 1]\}$	$2 \times 2 \times 3$
8.	$0; \frac{1}{2}$	$\frac{1}{2}; 0$	$\frac{1}{2}; \frac{1}{2}$		$1 \times 1 \times 2$	1.	$\{[1; 0], [0; 1]\}$	$2 \times 1 \times 2$
9.	$\frac{1}{2}; 0$	$0; \frac{1}{2}$	$\frac{1}{2}; \frac{1}{2}$		$1 \times 1 \times 2$	1.	$\{[1; 0], [0; 1]\}$	$1 \times 2 \times 2$
10.	$\frac{1}{2}; 0$	$\frac{1}{2}; 0$	$+1; 0$		$1 \times 1 \times 1$	1.	1.	$1 \times 1 \times 1$

(C.4)

with $\sigma \equiv \{\uparrow, \downarrow\} \equiv \{+1, -1\}$. The IROP $\hat{\psi}_S^\dagger$ is therefore identified with the multiplet $q'' \equiv (C''_z; S'') = (\frac{+1}{2}; \frac{1}{2})$, as indicated in the third column of (C.3a). The QSpace representation of $\hat{\psi}_S^\dagger$ derives from the matrix-elements

$$\psi_S^\dagger \rightarrow \langle C_z S | \cdot \left((\hat{\psi}_S^\dagger)^{(\frac{+1}{2}; \frac{1}{2})} | C'_z S' \right) \rangle$$

using the Wigner-Eckart theorem as in Eq. (A.43).

The operator index in the QSpace (C.3a) is listed third, by convention. The two non-zero matrix elements of each \hat{c}_σ^\dagger within the four-dimensional space of single fermionic site implies a total of four non-zero matrix elements in ψ_S^\dagger , all having norm 1, with one matrix-element being negative. These matrix elements can be directly identified in QSpace (C.3a). Since the reduced matrix elements $\|\psi_S^\dagger\|$ and the CGC spaces are to be interpreted as tensor product, the $\sqrt{2}$ factors in the last line cancel. With $\hat{\psi}_S^\dagger$ representing non-hermitian operators, the first column $q \equiv (C_z; S)$ is in general different from the second column $q' \equiv (C'_z; S')$. Moreover, since $\hat{\psi}_S^\dagger$ creates one particle, the first column, for example, cannot contain the empty state $(\frac{-1}{2}; 0)$, while the second column cannot contain the double occupied state $(\frac{+1}{2}; 0)$.

In contrast, the QSpace representation of the IROP ψ_S , i.e. without the dagger, is shown in (C.3b). Note that for $\hat{\psi}_S \equiv \{-\hat{c}_\downarrow; \hat{c}_\uparrow\}$ to be an irreducible operator as compared to $\hat{\psi}_S^\dagger = \{\hat{c}_\uparrow^\dagger, \hat{c}_\downarrow^\dagger\}$, the reverse

order in spin and the minus sign in the first component is essential [see discussion along with Eq. (A.49)]. In terms of the QSpace (C.3b), this leads to the extra minus signs in the multiplet space of the second row. Moreover, the z-labels of the operator $\hat{\psi}_S$ itself flipped sign w.r.t. $\hat{\psi}_S^\dagger$ as expected as it removes a particle rather than adding one [see the multiplet labels $q'' \equiv (C_z''; S'')$ in the third column of (C.3b)]. This is to emphasize that the application of the Wigner–Eckart theorem must be performed consistently, i.e. switching sides in the application of an operator as in $\langle C_z S | \cdot (\psi^\dagger | C_z' S') = (\psi | C_z S)^\dagger \cdot | C_z' S' \rangle$ must be dealt with carefully.

C.1.2. Identity A-tensor for two fermionic sites

Consider the combination of two fermionic sites. Similar to Fig. 1, let site 1 (2) be described by $|i\rangle$ ($|\sigma\rangle$), respectively, both representing a 4-dimensional state space $\{|0\rangle, |\uparrow\rangle, |\downarrow\rangle, |\uparrow\downarrow\rangle\}$ of their own. The decomposition of the combined space in terms of the overall symmetry $U(1)_{\text{charge}} \otimes SU(2)_{\text{spin}}$ is fully described by the rank-3 QSpace (C.4): site 1 with symmetries $(C_z; S)$ and site 2 with symmetries $(C'_z; S')$ are combined into the global symmetry $(C_z''; S'')$. For better clarity, the records have been sorted with respect to the combined quantum labels $q'' \equiv (C_z''; S'')$, where groups with the same q'' are separated by horizontal lines. The dimensions in the last (third) index are therefore the same within a group that shares the same $(C_z''; S'')$.

Given the $U(1)_{\text{charge}} \otimes SU(2)_{\text{spin}}$ symmetries, the abelian charge quantum number C_z simply adds up, while for the $SU(2)$ spin symmetry, the usual $SU(2)$ addition algebra applies. The overall number of multiplets in the combined space q'' is given by the last number (index 3) in the dimensions specified with the multiplet space. The specific input combinations entering a certain combined space q'' are easily verified. The $q'' = (-\frac{1}{2}; \frac{1}{2})$ sector, for example, derives from the two configurations $\{q, q'\} = \{(-\frac{1}{2}; 0), (0; \frac{1}{2})\}$ and $\{(0; \frac{1}{2}), (-\frac{1}{2}; 0)\}$. Therefore the dimension of the reduced multiplet space for this q'' is 2. Each of these multiplets has an internal z-space which is itself of dimension 2 [last column]. The combined total dimension of the $q'' = (-\frac{1}{2}; \frac{1}{2})$ sector is therefore given by the product $2 \cdot 2 = 4$. Consistently, the dimension of the two 4-dimensional sites combined add up correctly to 16 states total. That is, multiplying the last dimension in the reduced multiplet space with the last dimension in the combined CGC spaces for each block separated by horizontal lines, bearing in mind that the multiplet space and the CGC spaces are to be combined in a tensor-product, yields the overall dimension of the combined space, $1 \cdot 1 + 2 \cdot 2 + 3 \cdot 1 + 1 \cdot 3 + 2 \cdot 2 + 1 \cdot 1 = 16$.

The A-tensor in (C.4) is an identity A-tensor, in that up to permutations, plain identity matrices are split-up on the reduced multiplet level. By considering, for example, the $q'' = (\pm\frac{1}{2}; \frac{1}{2})$ symmetry sector in records 2–3 or 8–9 of the QSpace (C.4), the multiplet space when viewed together, i.e. ignoring all brackets, resemble the structure of a 2-dimensional identity matrix. Similar so for the $q'' = (0; 0)$ space in records 4–6, having essentially a 3-dimensional identity matrix in the multiplet space. Allowing for arbitrary unitaries in the multiplet space in QSpace (C.4), this then becomes the most general unitary transformation of the product space of two fermionic sites that also respects the symmetries considered.

C.2. Fermionic sites in the presence of particle–hole symmetry

The tensors introduced in the previous section for $U(1)_{\text{charge}} \otimes SU(2)_{\text{spin}}$ symmetry can be written more compactly still by assuming the stronger particle–hole $SU(2)_{\text{charge}}$ symmetry instead of the plain abelian $U(1)_{\text{charge}}$. The symmetry considered in the following is therefore $SU(2)_{\text{SC}}^{\otimes 2} \equiv SU(2)_{\text{spin}} \otimes SU(2)_{\text{charge}}$. The z-operator for charge, \hat{C}_z , is now complemented by the raising operator \hat{C}_+ for charge $SU(2)$ [cf. Eq. (A.52)]. The combined symmetries are given by the multiplet label for both charge and spin $SU(2)$, i.e. the non-negative labels $q = (C, S)$ with the z-labels of the charge symmetry now also taken care of by the CGC spaces.

The basis for a single fermionic level given $SU(2)_{\text{SC}}^{\otimes 2}$ symmetry has been introduced in Eq. (A.62). Therefore the full space of the four states $\{0, \uparrow, \downarrow, \uparrow\downarrow\}$ can be reduced to the two symmetry

Table C.2

Example QSpaces in the presence of $SU(2)_{\text{SC}}^{\otimes 2} \equiv SU(2)_{\text{spin}} \otimes SU(2)_{\text{charge}}$ symmetry for a single fermionic site. The CGC spaces for $SU(2)_{\text{charge}}$ and $SU(2)_{\text{spin}}$ are indicated by C and S, respectively. The record index ν as well as the explicit specification of the dimensions are just added for clarity. (C.5) shows the QSpace for the spinor $\hat{\psi}_{\text{CS}}$ defined in Eq. (A.59), with the reduced matrix elements already calculated in Eq. (A.63). The operator index within the IREP is listed third, as usual. (C.5) shows the identity A-tensor for the combination of the state space of two fermionic sites. For comparison, Table C.1 shows the same QSpaces for the case where the particle-hole symmetry is reduced to abelian charge conservation.

ψ_{CS}	record index ν				red. matrix elements $\ \hat{\psi}_{\text{CS}}\ $	CGC spaces C	S	combined dimension	
		$(C; S)$	$(C'; S')$	$(C''; S'')$					
ψ_{CS}	1	$0; \frac{1}{2}$	$\frac{1}{2}; 0$	$\frac{1}{2}; \frac{1}{2}$	$s\sqrt{2}$	$1 \times 1 \times 1$	$\frac{1}{\sqrt{2}}\{[0 \ 1]; [-1 \ 0]\}$	$\{[1 \ 0]; [0 \ 1]\}$	$2 \times 2 \times 4$
	2	$\frac{1}{2}; 0$	$0; \frac{1}{2}$	$\frac{1}{2}; \frac{1}{2}$	$\sqrt{2}$	$1 \times 1 \times 1$	$\{[1 \ 0]; [0 \ 1]\}$	$\frac{1}{\sqrt{2}}\{[0 \ 1]; [-1 \ 0]\}$	$2 \times 2 \times 4$
$A \equiv$	record index ν	site 1 $(C; S)$	site 2 $(C'; S')$	combined $(C''; S'')$	multiplet space $\ A\ $	dimension	CGC spaces C	S	combined dimension
	1	$0; \frac{1}{2}$	$0; \frac{1}{2}$	$0; 0$	$\{[1], [0]\}$	$1 \times 1 \times 2$	1.	$\frac{1}{\sqrt{2}}[0 \ -1; \ 0 \ 1]$	$2 \times 2 \times 1$
	2	$\frac{1}{2}; 0$	$\frac{1}{2}; 0$	$0; 0$	$\{[0], [1]\}$	$1 \times 1 \times 2$	$\frac{1}{\sqrt{2}}[0 \ -1; \ 0 \ 1]$	1.	$2 \times 2 \times 1$
	3	$0; \frac{1}{2}$	$0; \frac{1}{2}$	$0; 1$	1.	$1 \times 1 \times 1$	1.	$\frac{1}{\sqrt{2}}\{[1 \ 0; \ 0 \ 0],$ $[0 \ 1; \ 0 \ 1],$ $[0 \ 0; \ 0 \ 1]\}$	$2 \times 2 \times 3$
	4	$0; \frac{1}{2}$	$\frac{1}{2}; 0$	$\frac{1}{2}; \frac{1}{2}$	$\{[1], [0]\}$	$1 \times 1 \times 2$	$\{[1 \ 0], [0 \ 1]\}$	$\{[1 \ 0], [0; 1]\}$	$2 \times 2 \times 4$
	5	$\frac{1}{2}; 0$	$0; \frac{1}{2}$	$\frac{1}{2}; \frac{1}{2}$	$\{[0], [1]\}$	$1 \times 1 \times 2$	$\{[1 \ 0], [0 \ 1]\}$	$\{[1 \ 0], [0 \ 1]\}$	$2 \times 2 \times 4$
	6	$\frac{1}{2}; 0$	$\frac{1}{2}; 0$	$1; 0$	1.	$1 \times 1 \times 1$	$\frac{1}{\sqrt{2}}\{[1 \ 0; \ 0 \ 0],$ $[0 \ 1; \ 0 \ 1],$ $[0 \ 0; \ 0 \ 1]\}$	1.	$2 \times 2 \times 3$

multiplets

multiplet space $ C, S\rangle$	dimension	
	d_C	$\times d_S = d_{\text{tot}}$
$\left \frac{1}{2}; 0 \right\rangle \equiv \{ 0\rangle, s \uparrow\downarrow\rangle\}$	$2 \times 1 = 2$	
$\left 0; \frac{1}{2} \right\rangle \equiv \{ +\rangle, -\rangle\}$	$1 \times 2 = 2$	

The most general scalar operator such as the Hamiltonian is given by the QSpace,

$$H \equiv \left\{ \begin{array}{c|c|c|cc} (C; S) & (C'; S') & \|H\| & \text{CGC spaces} \\ \hline \frac{1}{2}; 0 & \frac{1}{2}; 0 & h_{\frac{1}{2}, 0} & \mathbf{1}^{(2)} & 1. \\ 0; \frac{1}{2} & 0; \frac{1}{2} & h_{0, \frac{1}{2}} & 1. & \mathbf{1}^{(2)} \end{array} \right\}. \quad (\text{C.8})$$

Thus only the two reduced matrix elements $h_{1/2,0}$ and $h_{0,1/2}$ are left free to choose without compromising $SU(2)_{\text{SC}}^{\otimes 2}$ symmetry.

An example for a non-scalar IROP is given by the 4-component spinor $\hat{\psi}_{\text{CS}}$ in Eq. (A.59), which contains two creation and two annihilation operators. Its symmetries have been identified in Eq. (A.61), leading to the IROP $\hat{\psi}_{\text{CS}}$ with the QSpace presented in (C.5). Note that the size of the third dimension is 4 [see combined CGC dimension in the last column], consistent with the four operators that constitute the IROP. The alternating sign s required with particle-hole symmetry appears with the reduced matrix elements in the first record only [cf. Eq. (A.63); note that the same sign s is also picked up by the double occupied state, cf. Eq. (A.62) or (C.7)].

The QSpace representation for the identity A-tensor combining two fermionic sites is given in (C.6). Again, the symmetry records are sorted with respect the combined symmetry $q'' \equiv (C'', S'')$, where groups with the same (C'', S'') are separated by horizontal lines for clarity. The property of QSpace (C.6) being an identity A-tensor, is seen, for example, in the combined reduced multiplet space of records 1–2, or 4–5). The standard $SU(2)$ addition rules are also quickly confirmed. For

Table C.3

State space of 3-channel site with $SU(2)_{SC}^{\otimes 4} \equiv SU(2)_{\text{spin}} \otimes SU(2)_{\text{charge}}^{\otimes 3}$ symmetry.

Row	Multiplet space						CG dimension	
Index	$ S,$	$C_1,$	$C_2,$	C_3	\rangle	Dim.	$d_S d_{C_1} d_{C_2} d_{C_3} =$	d_{tot}
1	$ 0;$	$0;$	$0;$	$\frac{1}{2}$	\rangle	1	$1 \times 1 \times 1 \times 2 =$	2
2	$ 0;$	$0;$	$\frac{1}{2};$	0	\rangle	1	$1 \times 1 \times 2 \times 1 =$	2
3	$ 0;$	$\frac{1}{2};$	$0;$	0	\rangle	1	$1 \times 2 \times 1 \times 1 =$	2
4	$ 0;$	$\frac{1}{2};$	$\frac{1}{2};$	$\frac{1}{2}$	\rangle	1	$1 \times 2 \times 2 \times 2 =$	8
5	$ \frac{1}{2};$	$0;$	$0;$	0	\rangle	2	$2 \times 1 \times 1 \times 1 =$	2
6	$ \frac{1}{2};$	$0;$	$\frac{1}{2};$	$\frac{1}{2}$	\rangle	1	$2 \times 1 \times 2 \times 2 =$	8
7	$ \frac{1}{2};$	$\frac{1}{2};$	$0;$	$\frac{1}{2}$	\rangle	1	$2 \times 2 \times 1 \times 2 =$	8
8	$ \frac{1}{2};$	$\frac{1}{2};$	$\frac{1}{2};$	0	\rangle	1	$2 \times 2 \times 2 \times 1 =$	8
9	$ 1;$	$0;$	$0;$	$\frac{1}{2}$	\rangle	1	$3 \times 1 \times 1 \times 2 =$	6
10	$ 1;$	$0;$	$\frac{1}{2};$	0	\rangle	1	$3 \times 1 \times 2 \times 1 =$	6
11	$ 1;$	$\frac{1}{2};$	$0;$	0	\rangle	1	$3 \times 2 \times 1 \times 1 =$	6
12	$ \frac{3}{2};$	$0;$	$0;$	0	\rangle	1	$4 \times 1 \times 1 \times 1 =$	4

example, the combined symmetry $q'' = (0, 0)$ [records 1–2] can result from two combinations, namely $(\frac{1}{2}, 0) \otimes (\frac{1}{2}, 0)$, or $(0, \frac{1}{2}) \otimes (0, \frac{1}{2})$, leading to a two dimensional multiplet space. All of this is transparently encoded in given QSpace.

Considering the tensor-product of multiplet and CGC spaces, the combined space has total dimension of $2 \cdot 1 + 1 \cdot 3 + 2 \cdot 4 + 1 \cdot 3 = 16$ as expected for two spinful fermionic levels. Compared to the A-tensor in (C.4) with abelian charge conservation, the number of combined symmetry sectors has been further reduced from 6 to 4 [i.e. number of horizontally separated groups sharing the same q''], with an overall reduction in the number of multiplets present in the QSpace reduced from 10 to 6 [having $1 + 2 + 3 + 1 + 2 + 1 = 10$ in (C.4), and here $2 + 1 + 2 + 1 = 6$].

C.3. Three channels with $SU(3)$ channel symmetry

Consider a system with three spinful particle-hole symmetric channels, as introduced in Appendix A.9.4. A single site then has a full Hilbert space of dimension $4^3 = 64$. Three symmetry settings are analyzed: a set of plain $SU(2)$ symmetries, a combination with the $SU(3)$ channel symmetry, and finally the largest symmetry present which includes the enveloping symplectic symmetry $Sp(6)$. Since the QSpaces in given context are extensive, a more compact comparison of these symmetry settings in the numerical context is given, instead.

The first setting, $SU(2)_{SC}^{\otimes 4} \equiv SU(2)_{\text{spin}} \otimes SU(2)_{\text{charge}}^{\otimes 3}$, is based on four independent $SU(2)$ symmetries. The 64-dimensional state space of single site decomposes into 13 multiplets in 12 symmetry sectors, as listed in Table C.3. All of these contain a single representative multiplet, except for the space $|\frac{1}{2}; 0; 0; 0\rangle$ in row 5, which contains two multiplets. In contrast, using the $SU(2)_{\text{spin}} \otimes U(1)_{\text{charge}} \otimes SU(3)_{\text{channel}}$ symmetry, instead, the 64 states of the three fermionic levels decomposes into the 10 multiplet spaces listed in Table C.4. Thus compared to the $SU(2)_{SC}^{\otimes 4}$ symmetry setting in Table C.3, the number of multiplet spaces is further reduced with all multiplet spaces containing a single multiplet only. This suggests that the latter symmetry including the channel $SU(3)$ is somewhat more efficient as it allows to compactify multiplet spaces more strongly. Given the multiplet space in Table C.4, for example, the most general Hamiltonian in the 64×64 dimensional Hilbert space compatible with given symmetry consists of the 10 reduced matrix elements appearing in the multiplet space only.

A further strong boost in numerical efficiency can be obtained, if the Hamiltonian supports it, by combining the particle-hole symmetry of $SU(2)_{\text{spin}} \otimes SU(2)_{\text{charge}}^{\otimes 3}$ with the channel symmetry in $SU(2)_{\text{spin}} \otimes U(1)_{\text{charge}} \otimes SU(3)_{\text{channel}}$ to their enveloping $Sp(6)$ symmetry. The resulting state space for the state space of a single 3-channel site is given in Table C.5. The 64×64 dimensional Hilbert space has thus been reduced to a total of four multiplets only.

Table C.4

State space of 3-channel site with $SU(2)_{\text{spin}} \otimes U(1)_{\text{charge}} \otimes SU(3)_{\text{channel}}$ symmetry.

Row	Multiplet space					CG dimension	
Index	$ S$	C_z	T	\rangle	dim.	$d_S \cdot d_{C_z} \cdot d_T =$	d_{tot}
1	$ 0;$	$-\frac{3}{2};$	0 0	\rangle	1	$1 \times 1 \times 1 =$	1
2	$ 0;$	$-\frac{1}{2};$	2 0	\rangle	1	$1 \times 1 \times 6 =$	6
3	$ 0;$	$\frac{1}{2};$	0 2	\rangle	1	$1 \times 1 \times 6 =$	6
4	$ 0;$	$\frac{3}{2};$	0 0	\rangle	1	$1 \times 1 \times 1 =$	1
5	$ \frac{1}{2};$	-1;	1 0	\rangle	1	$2 \times 1 \times 3 =$	6
6	$ \frac{1}{2};$	0;	1 1	\rangle	1	$2 \times 1 \times 8 =$	16
7	$ \frac{1}{2};$	1;	0 1	\rangle	1	$2 \times 1 \times 3 =$	6
8	$ 1;$	$-\frac{1}{2};$	0 1	\rangle	1	$3 \times 1 \times 3 =$	9
9	$ 1;$	$\frac{1}{2};$	1 0	\rangle	1	$3 \times 1 \times 3 =$	9
10	$ \frac{3}{2};$	0;	0 0	\rangle	1	$4 \times 1 \times 1 =$	4

Table C.5

State space of 3-channel site with $SU(2)_{\text{spin}} \otimes Sp(6)$ symmetry.

Row	Multiplet space				CG dimension	
index	$ S$	$Sp(6)$	\rangle	dim.	$d_S \cdot d_T =$	d_{tot}
1	$ 0;$	0 0 1	\rangle	1	$1 \times 14 =$	14
2	$ \frac{1}{2};$	0 1 0	\rangle	1	$2 \times 14 =$	28
3	$ \frac{1}{2};$	1 0 0	\rangle	1	$3 \times 6 =$	18
4	$ \frac{3}{2};$	0 0 0	\rangle	1	$4 \times 1 =$	4

All three symmetry settings have been successfully implemented within the NRG framework. By starting with a single site [i.e. the basic fermionic three-level unit as introduced in Appendix A.9.4], and iteratively adding a site within the NRG, new multiplet spaces are quickly explored and built up within the first few NRG iterations. In practice, the CGC spaces of newly generated multiplets are also stored for latter retrieval. Once truncation of the state space within NRG sets in, however, the generation of IREPs eventually saturates to within a finite range of multiplet spaces.

The resulting space for adding up to three further sites without truncation is indicated in Table C.6. With reasonable numerical resources, it is feasible within the $SU(2)_{\text{spin}} \otimes U(1)_{\text{charge}} \otimes SU(3)_{\text{channel}}$ (second) or $SU(2)_{\text{spin}} \otimes Sp(6)$ (third) setting, to keep all states up to three sites total within the NRG, first truncating only when a fourth site is added. This leads to $N_K = 9086$ [$N_K = 1232$] kept multiplets for the second and the third symmetry setting, respectively. The corresponding memory requirements for a general basis transformation for adding another site (A -tensor) then amounts to about 7 G [0.3 G]. The corresponding full NRG iteration for adding another site then takes several hours on a state-of-the-art 8-core workstation.

The same calculation, however, gets quickly impossible as fewer symmetries are available or used in the actual computation as can be seen from Table C.6. For example, if only the abelian part of the symmetry had been accounted for in the computation, the corresponding memory requirement can be estimated by considering the explicit tensor product of the multiplet space with the CGC spaces, leading in terms of the $SU(2)_{\text{SC}}^{\otimes 4}$ setting to about 23 G and 65 T(!) for $n = 3$ and $n = 4$, respectively, the latter being completely hopeless in practice. The explicit treatment of non-abelian symmetries, however, clearly makes the latter case feasible with a reasonable amount of numerical resources.

C.3.1. $SU(3)$ symmetry

The irreducible $SU(3)$ multiplets generated in the actual NRG run using $SU(2)_{\text{spin}} \otimes U(1)_{\text{charge}} \otimes SU(3)_{\text{channel}}$ symmetry as presented in the main text [cf. Section 6], are shown in terms of their weight diagrams in Fig. C.14. For comparison, the $SU(3)$ IREPs present in the description of a single site are $q^{SU(3)} \equiv (q_1, q_2) \in \{(0, 0), (0, 1), (0, 2), (1, 0), (2, 0)\}$, cf. Table C.4. The apparent symmetry w.r.t. to flipping the quantum numbers in (q_1, q_2) is also reflected in the overall set of multiplets generated

within the NRG. As seen in Fig. C.14, all IREPs (q_1, q_2) with $q_1 + q_2 \leq 8$ are present, except for $(0, 8)$ and $(8, 0)$.

Inner multiplicity, as expected for $SU(3)$, is clearly present and depicted in the weight diagrams of Fig. C.14 by the encircled set of points. There the number of points inside a circle stands for the multiplicity of the corresponding z-labels in the multiplet. Inner multiplicity decreases in shells as one moves outward the multiplet, which is seen particularly well for the multiplets $q_1 = q_2$. The states on the outer circumference have no multiplicity, i.e. have unique z-labels, as expected. This demonstrates the uniqueness of the maximum weight state [cf. Appendix A.3.3], which was required for the numerical state space decomposition in Appendix B.1.

Due to the two-dimensional label structure of the $SU(3)$ multiplets together with inner multiplicity, their internal dimensions can get significantly larger as compared to $SU(2)$ multiplets. The largest $SU(3)$ multiplet $(4, 4)$ encountered in the actual NRG run presented in Fig. C.14, for example, has an internal irreducible dimension of $d = 125$ [see also Table C.7]. This implies, for example, that with respect to the diagonalization of a Hamiltonian, a 125-fold degeneracy has been reduced to a single multiplet. In contrast, the multiplet structure for $SU(2)_{\text{SC}}^{\otimes 4}$ is clearly weaker as it only includes $SU(2)$ symmetries. There the largest quantum numbers encountered in an NRG run with comparable number of kept states include $S \leq 6$ in the spin sector, leading to an individual multiplet dimension of at most 13 [see also Table C.7]. In the overall combination of the symmetries, this implies that for comparable number of states, i.e. for a comparable accuracy within the NRG, on average about 50% more multiplets need to be kept within the $SU(2)_{\text{SC}}^{\otimes 4}$ setting as compared to the case when $SU(3)$ is included [see Fig. 11 in the main text].

Finally, the individual weight diagrams in Fig. C.14 show well-known symmetries, such as a reflection symmetry of each diagram around the vertical y -axes, or the reflection symmetry between the multiplets (q_1, q_2) and (q_2, q_1) around the horizontal axis. These *Weyl symmetries* may be used to evaluate or encode CGC spaces more efficiently [39]. For the purpose of this paper, however, these symmetries were not exploited, given also that the pure numerical evaluation of the CGC spaces as outlined earlier was already sufficiently fast.

C.3.2. $\text{Sp}(6)$ symmetry

The complete set of $\text{Sp}(6)$ symmetries generated in the fully converged NRG run (using $\Lambda = 4$ and $E_{\text{trunc}} = 7$ as used in the results in the main text), is listed in Table C.8. All multiplets had been generated within the first four Wilson shells. The fact that the symmetry $\text{Sp}(6)$ fully incorporates non-abelian particle-hole and channel symmetry, manifests itself by observing that all eigenenergies in the multiplet spaces are now strictly *non-degenerate* throughout an entire NRG calculation. Huge degeneracies of several thousands can be split off in terms of tensor products with $\text{Sp}(6)$ multiplets.

For given model, the symmetry $\text{Sp}(6)$ in fact also allowed to reduce the rather coarse discretization of $\Lambda = 4$ in the NRG calculation underlying Table C.8. For comparison, if $\Lambda = 2$ is used, instead, while keeping the same $E_{\text{trunc}} = 7$, it turns out, the largest multiplet generated is $(2, 1, 2)$ of dimension 5720. The largest intermediate product space to be decomposed into IREPs becomes as large as $14 \times 1386 = 19,404$. Having $\Lambda = 2$, this required twice the Wilson chain length for the same range in energy scales, leading to an overall run time of the entire NRG run of about 32 h with still reasonably manageable memory requirements of $\lesssim 20$ G.

As a rough general estimate, typical multiplet dimensions, as they occurred in practice, scale like 10^r where r is the rank of the symmetry. For $SU(2)_{\text{spin}}$, this implies multiplets of dimension $\lesssim 10$, for the $SU(4)_{\text{channel}}$ symmetry, indeed, one had multiplets of dimension of $\lesssim 100$, while now for $\text{Sp}(6)$, a symmetry of rank 3, one easily reaches multiplet dimensions on the order of a few 1000 (cf. Table C.8). Therefore with increasing rank of the symmetry, the numerical effort strongly shifts from the multiplet space to the CGC spaces. For sets of smaller symmetries with rank $r \leq 2$ this leads to a strong gain in numerical efficiency, while the numerical overhead for the CGC spaces remains negligible. Reaching symmetries of rank 3, such as $\text{Sp}(6)$, the numerical effort within the CGC spaces can now become comparable to or even larger than the operations on the higher multiplet level.

Table C.7 summarizes the situation by comparing the maximal multiplet spaces with the corresponding sparsity and memory requirements of the CGC spaces for the first few A -tensors, when

Table C.6

Comparison of different symmetry scenarios for the same underlying physical system of a symmetric 3-channel setup, analyzing the product spaces of up to $n = 4$ sites. Each site represents a Hilbert space of dimension 64, thus n sites amounts to an overall Hilbert space of dimension $D^* = 64^n$ [second column]. This state space can be decomposed into D multiplets in N_S symmetry sectors using an A-tensor for the addition of every new site. These A-tensors are encoded in terms of QSpaces. The total memory requirement for each A-tensor is listed, given sparse CGC representation. In addition, as a comparison to a fully abelian setting, MEM* indicates the memory that had been required if the tensor products between reduced multiplets and CGC-spaces was carried out explicitly [K,M,G,T for kilo-, mega-, giga-, and tera-bytes, respectively]..

Sites	Abelian dim.	$SU(2)_\text{spin} \otimes SU(2)_\text{charge}^{\otimes 3}$						$SU(2)_\text{spin} \otimes U(1)_\text{charge} \otimes SU(3)_\text{channel}$						$SU(2)_\text{spin} \otimes Sp(6)$					
		N_S	D	D^*/D	memory	MEM	N_S	D	D^*/D	memory	MEM	N_S	D	D^*/D	memory	MEM*			
1	$D^* = 64^n$	64	12	13	4.9	<18 K	10	10	6.4	<13 K	>12 M	23	61	67.1	<6 K				
2	4,096	61	388	106	528 K	>8.7 M	69	260	15.8	359 K	>31 G	60	1,232	213	162 K	>34 M			
3	262,144	192	14,229	18.4	27 M	>23 G	226	9,086	28.9	11 M	>85 T	132	31,640	530	7 M	>112 G			
4	16,777,216	469	590,856	28.4	24 G	>65 T	565	366,744	45.7	6.8 G						>355 T			

Table C.7

Comparison of different symmetry scenarios as in Table C.6 in terms of (i) largest multiplet dimension d for each individual symmetry, and (ii), overall average sparsity of the CGC spaces, i.e. the number of non-zero elements divided by the total number of matrix elements. The last columns for each symmetry (CGS/A) shows the memory requirement of all sparse CGC spaces in a given QSpace A_n relative to the entire QSpace. .

Sites	$SU(2)_\text{spin} \otimes SU(2)_\text{charge}^{\otimes 3}$						$SU(2)_\text{spin} \otimes U(1)_\text{charge} \otimes SU(3)_\text{channel}$						$SU(2)_\text{spin} \otimes Sp(6)$					
	d_S	d_C	d_C	d_C	Sparsity	CCS/A	d_S	$d_{U(1)}$	d_C	Sparsity	CCS/A	d_S	$d_{Sp(6)}$	Sparsity	CCS/A			
1	4	2	2	2	0.36	0.8	4	1	8	0.12	0.8	4	14	0.027	0.90			
2	7	3	3	3	0.36	0.8	7	1	27	0.12	0.8	7	126	0.027	0.90			
3	10	4	4	4	0.28	0.11	10	1	64	0.064	0.33	10	616	0.011	0.94			
4	13	5	5	5	0.22	<10 ⁻³	13	1	125	0.039	0.003	13	2457	0.006	0.55			

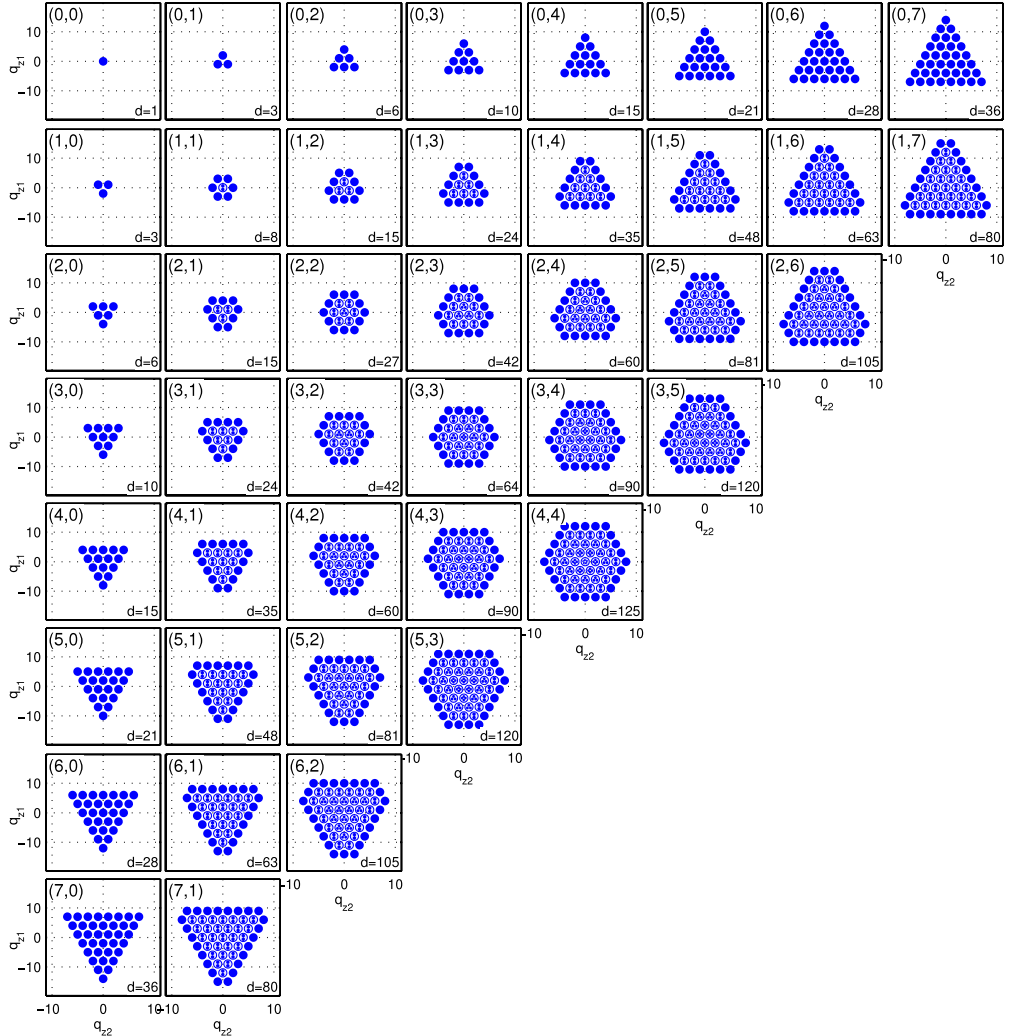


Fig. C.14. Weight diagrams of $SU(3)$ multiplets generated in a typical NRG run for the symmetric 3-channel system including $SU(2)_{\text{spin}} \otimes U(1)_{\text{charge}} \otimes SU(3)_{\text{channel}}$ symmetries ($\Lambda = 4$, $E_{\text{trunc}} = 7$). The multiplet label (q_1, q_2) , as defined in Eq. (A.34), is specified with each multiplet in the upper left corner of its panel. For a weight diagram of a specific IREP (q_1, q_2) , the corresponding z-labels (q_{z1}, q_{z2}) of $SU(3)$ for each individual state within the multiplet are depicted as points in a two-dimensional plot. In the case of inner multiplicity, i.e. that several states within the same IREP share exactly the same z-labels, these states are shown as an encircled group of smaller points. The dimension for every multiplet (number of points drawn within a panel) is indicated to the lower right of each panel. The first panel [multiplet $(0, 0)$] represents the scalar representation with multiplet dimension $d = 1$. Multiplet $(1, 0)$ represents the defining three-dimensional representation [*cf.* Appendix A.4.3], and $(1, 1)$ the regular representation of dimension 8 equal to the dimension of $SU(3)$, i.e. the number of its generators. The largest multiplet encountered in given NRG run is the multiplet $(4, 4)$ with an irreducible dimension of $d = 125$.

combining up to $n = 4$ sites without truncation. As the internal multiplet dimensions quickly grow for higher rank symmetries, nevertheless only an ever smaller fraction of Clebsch–Gordan coefficients are non-zero. As seen from Table C.7, the sparsity roughly grows exponentially with the rank of the symmetry. Nevertheless, with the memory requirement of the sparse CGC for $\text{Sp}(6)$ comparable or even larger than the storage of the reduced matrix elements on the higher multiplet level (see last column in Table C.7), full storage including also the zero CGC spaces would have extremely inflated

Table C.8

$\text{Sp}(6)$ multiplets generated in a fully converged NRG run for the symmetric 3-channel system using $\text{SU}(2)_{\text{spin}} \otimes \text{Sp}(6)$ ($\Lambda = 4$, $E_{\text{trunc}} = 7$). Multiplet $(0, 0, 0)$ represents the scalar representation of dimension 1, multiplet $(1, 0, 0)$ the defining representation of dimension 6, and multiplet $(2, 0, 0)$ the regular representation of dimension 21 which is also equal to the number of generators for $\text{Sp}(6)$. The largest tensor-product decomposition was between the product spaces of IREPs of dimension 14 and 512, yielding a combined product space dimension of 7168. Run time of the bare NRG run was about 2 h on a state-of-the-art 8-core workstation with moderate memory requirements of $\lesssim 4.5$ G.

$\text{Sp}(6)$ multiplet q	Dimension d	$\text{Sp}(6)$ multiplet [cont'd]	Dimension
$(0\ 0\ 0)$	1	$(1\ 2\ 0)$	350
$(1\ 0\ 0)$	6	$(1\ 0\ 2)$	378
$(0\ 0\ 1)$	14	$(0\ 3\ 0)$	385
$(0\ 1\ 0)$	14	$(3\ 1\ 0)$	448
$(2\ 0\ 0)$	21	$(1\ 1\ 1)$	512
$(3\ 0\ 0)$	56	$(3\ 0\ 1)$	525
$(1\ 1\ 0)$	64	$(0\ 1\ 2)$	594
$(1\ 0\ 1)$	70	$(0\ 2\ 1)$	616
$(0\ 0\ 2)$	84	$(2\ 2\ 0)$	924
$(0\ 2\ 0)$	90	$(2\ 0\ 2)$	1078
$(0\ 1\ 1)$	126	$(1\ 3\ 0)$	1344
$(4\ 0\ 0)$	126	$(2\ 1\ 1)$	1386
$(2\ 1\ 0)$	189	$(1\ 2\ 1)$	2205
$(2\ 0\ 1)$	216	$(1\ 1\ 2)$	2240
$(0\ 0\ 3)$	330		

overall storage requirement. In this sense, sparse storage of CGC spaces becomes mandatory for larger-rank symmetries. With the standard CGC spaces already tensors of rank-3, sparse storage of general CGC spaces requires the extension of standard sparse storage and sparse operations to arbitrary-rank tensors. All of these is achieved, in general, by proper efficient permutations in sparse index space which requires a fast sorting scheme, together with reshaping of higher rank-objects to standard two-dimensional sparse objects with fused indices, since this allows to employ efficient algorithms for standard sparse matrix multiplication.

In order to distinguish numerical noise, *i.e.* negligible CGC matrix elements, from actual matrix elements then, this requires an accurate evaluation of the CGC matrix elements. Double precision accuracy as compared to the *exact theoretical* CGCs was sufficient, in practice. In particular, this implies, that also the matrix elements of the generators for given IREPs of the symmetry are known *numerically exact* at any step. In the iterative approach, however, when new multiplets are generated through tensor products with smaller entities, numerical errors can pile up. For large-rank symmetries then the accuracy of the matrix elements of the generators must be better than double precision. For practical purposes, quad precision on matrix elements of the generators turned out sufficient. Alternatively, it is also emphasized that the matrix elements in the numerical representation of the generators *w.r.t.* some given IREP *can actually be corrected even for sizable numerical errors*. The underlying reason is that the generators for a given IREP are unique up to similarity transformation. Nevertheless, the similarity transformation is largely fixed by the construction of the z-operators: these are (i) diagonal, and (ii) their diagonal matrix elements are integer-superpositions of the diagonals of the z-operators in the defining representation, *e.g.* can be chosen to be integer or half-integer valued. Hence small numerical errors $\varepsilon \ll 1$ can be easily corrected *w.r.t.* the z-operators. However, knowing the z-operators exactly, also the matrix elements of the remaining operators can be fixed, in principle, while paying attention to conventions regarding inner multiplicity.

References

- [1] W.M.C. Foulkes, L. Mitas, R.J. Needs, G. Rajagopal, Rev. Modern Phys. 73 (Jan) (2001) 33–83.

- [2] S.R. White, Phys. Rev. Lett. 69 (19) (1992) 2863–2866.
- [3] K.G. Wilson, Rev. Modern Phys. 47 (4) (1975) 773–840.
- [4] P.H. Bonderson, Non-abelian anyons and interferometry (Ph.D. Thesis) California Institute of Technology, 2007.
- [5] R.N.C. Pfeifer, M. Troyer, G. Vidal, Translation invariance, topology, and protection of criticality in chains of interacting anyons, May 2010. [arXiv:1005.5486](https://arxiv.org/abs/1005.5486) V5 [cond-mat.str-el].
- [6] R.N.C. Pfeifer, P. Corboz, O. Buerschaper, M. Aguado, M. Troyer, G. Vidal, Phys. Rev. B 82 (Sep) (2010) 115126.
- [7] R.N.C. Pfeifer, Simulation of anyons using symmetric tensor network algorithms, Ph.D. Thesis, The University of Queensland, May 2011. [arXiv:1202.1522](https://arxiv.org/abs/1202.1522) V2 [cond-mat.str-el].
- [8] S. Singh, R.N.C. Pfeifer, G. Vidal, Phys. Rev. A 82 (5) (2010) 050301.
- [9] S. Singh, H.-Q. Zhou, G. Vidal, New J. Phys. 12 (3) (2010) 033029.
- [10] S. Rommer, S. Östlund, Phys. Rev. B 55 (1997) 2164.
- [11] A. Weichselbaum, F. Verstraete, U. Schollwock, J.I. Cirac, J. von Delft, Phys. Rev. B 80 (16) (2009) 165117.
- [12] A.W. Sandvik, G. Vidal, Phys. Rev. Lett. 99 (22) (2007) 220602.
- [13] V. Murg, F. Verstraete, J.I. Cirac, Phys. Rev. A 75 (3) (2007) 033605.
- [14] J.I. Cirac, F. Verstraete, J. Phys. A: Math. Theor. 42 (2009) 504004.
- [15] J.D. Bekenstein, Phys. Rev. D 7 (8) (1973) 2333–2346.
- [16] M.M. Wolf, F. Verstraete, M.B. Hastings, J.I. Cirac, Phys. Rev. Lett. 100 (7) (2008) 070502.
- [17] J. Eisert, M. Cramer, M.B. Plenio, Rev. Modern Phys. 82 (1) (2010) 277–306.
- [18] G. Vidal, Phys. Rev. Lett. 99 (Nov) (2007) 220405.
- [19] G. Vidal, Phys. Rev. Lett. 101 (11) (2008) 110501.
- [20] E.M. Stoudenmire, S.R. White, Ann. Rev. Condens. Matter Phys. 3 (2012) 111–128.
- [21] I.P. McCulloch, M. Gulcsı, EPL (Europhys. Lett.) 57 (6) (2002) 852.
- [22] I.P. McCulloch, J. Stat. Mech. Theory Exp. 2007 (10) (2007) P10014.
- [23] A.I. Tóth, C.P. Moca, Ö Legeza, G. Zárand, Phys. Rev. B 78 (24) (2008) 245109.
- [24] S. Singh, Tensor network states and algorithms in the presence of abelian and non-abelian symmetries, Ph.D. Thesis, The University of Queensland, Mar. 2012. [arXiv:1203.2222](https://arxiv.org/abs/1203.2222) V2 [quant-ph].
- [25] S. Singh, R.N.C. Pfeifer, G. Vidal, Phys. Rev. B 83 (Mar) (2011) 115125.
- [26] L. De Leo, M. Fabrizio, Phys. Rev. Lett. 94 (Jun) (2005) 236401.
- [27] T.A. Costi, L. Bergqvist, A. Weichselbaum, J. von Delft, T. Micklitz, A. Rosch, P. Mavropoulos, P.H. Dederichs, F. Mallet, L. Saminadayar, C. Bäuerle, Phys. Rev. Lett. 102 (5) (2009) 056802.
- [28] W.J. de Haas, J. de Boer, G.J. van den Berg, Physica 1 (7–12) (1934) 1115–1124.
- [29] J. Kondo, Progr. Theoret. Phys. 32 (1964) 37–49.
- [30] I. Affleck, A.W.W. Ludwig, H.-B. Pang, D.L. Cox, Phys. Rev. B 45 (Apr) (1992) 7918–7935.
- [31] A. Weichselbaum, J. von Delft, Phys. Rev. Lett. 99 (7) (2007) 076402.
- [32] J.J. Sakurai, Modern Quantum Mechanics, Revised Edition, Addison-Wesley Publishing Company, Reading, MA, 1994.
- [33] R. König, B.W. Reichardt, G. Vidal, Phys. Rev. B 79 (May) (2009) 195123.
- [34] A. Fledderjohann, A. Klümper, K.-H. Müttner, J. Phys. A 44 (47) (2011) 475302.
- [35] Zodinmawia, P. Ramadevi, SU(N) quantum racah coefficients & non-torus links, Jul. 2011. [arXiv:1107.3918v4](https://arxiv.org/abs/1107.3918v4) [hep-th].
- [36] U. Schollwöck, Rev. Modern Phys. 77 (1) (2005) 259–315.
- [37] U. Schollwöck, Ann. Phys. 326 (2011) 96–192.
- [38] J.P. Elliott, P.G. Dawber, Symmetry in Physics, Vol. I+II., Oxford University Press, New York, 1979.
- [39] A. Alex, M. Kalus, A. Huckleberry, J. von Delft, J. Math. Phys. 52 (2) (2011) 023507.
- [40] W. Hofstetter, Phys. Rev. Lett. 85 (7) (2000) 1508–1511.
- [41] A. Weichselbaum, Phys. Rev. B 84 (Sep) (2011) 125130.
- [42] Y.-Y. Shi, L.-M. Duan, G. Vidal, Phys. Rev. A 74 (Aug) (2006) 022320.
- [43] V. Murg, F. Verstraete, O. Legeza, R.M. Noack, Phys. Rev. B 82 (Nov) (2010) 205105.
- [44] R. Bulla, T. Costi, T. Pruschke, Rev. Modern Phys. 80 (2008) 395.
- [45] M. Yoshida, M.A. Whitaker, L.N. Oliveira, Phys. Rev. B 41 (1990) 9403.
- [46] R. Žitko, T. Pruschke, Phys. Rev. B 79 (8) (2009) 085106.
- [47] J. Demmel, J. Dongarra, A. Ruhe, H. van der Vorst, Templates for the Solution of Algebraic Eigenvalue Problems: A Practical Guide, Society for Industrial and Applied Mathematics, Philadelphia, PA, USA, 2000.
- [48] F.B. Anders, A. Schiller, Phys. Rev. Lett. 95 (2005) 196801.
- [49] R. Peters, T. Pruschke, F.B. Anders, Phys. Rev. B 74 (24) (2006) 245114.
- [50] R. Bulla, A.C. Hewson, T. Pruschke, J. Phys.: Condens. Matter 10 (1998) 8365.
- [51] J.R. Schrieffer, P.A. Wolff, Phys. Rev. 149 (2) (1966) 491–492.
- [52] A. Freyn, S. Florens, Phys. Rev. B 79 (Mar) (2009) 121102.
- [53] M.C. Bañuls, D. Pérez-García, M.M. Wolf, F. Verstraete, J.I. Cirac, Phys. Rev. A 77 (May) (2008) 052306.
- [54] H. Saberi, A. Weichselbaum, L. Lamata, D. Pérez-García, J. von Delft, E. Solano, Phys. Rev. A 80 (2) (2009) 022334.
- [55] I. Affleck, T. Kennedy, E.H. Lieb, H. Tasaki, Comm. Math. Phys. 115 (1988) 477.
- [56] F. Verstraete, J.I. Cirac, Jul. 2004. [arXiv:0407066](https://arxiv.org/abs/0407066) V1 [cond-mat.str-el].
- [57] F. Verstraete, V. Murg, J. Cirac, Adv. Phys. 57 (2) (2008) 143–224.
- [58] T. Barthel, C. Pineda, J. Eisert, Phys. Rev. A 80 (4) (2009) 042333.
- [59] P. Corboz, R. Orús, B. Bauer, G. Vidal, Phys. Rev. B 81 (16) (2010) 165104.
- [60] C.V. Kraus, N. Schuch, F. Verstraete, J.I. Cirac, Phys. Rev. A 81 (5) (2010) 052338.
- [61] B. Bauer, P. Corboz, R. Orús, M. Troyer, Phys. Rev. B 83 (Mar) (2011) 125106.
- [62] J. Jordan, R. Orús, G. Vidal, F. Verstraete, J.I. Cirac, Phys. Rev. Lett. 101 (Dec) (2008) 250602.
- [63] R. Orús, G. Vidal, Phys. Rev. B 80 (Sep) (2009) 094403.
- [64] C.A. Müller, C. Miniatura, E. Akkermans, G. Montambaux, J. Phys. A 38 (36) (2005) 7807.
- [65] B. Buca, T. Prosen, Mar. 2012. [arXiv:1005.5486](https://arxiv.org/abs/1005.5486) V3 [quant-ph].
- [66] C. Pope, Geometry and Group Theory. Online lecture notes, Texas A&M University, 2006.
- [67] R. Gilmore, Lie groups, Lie algebras, and Some of Their Applications, Dover Publications, 2006.
- [68] M.A.A. van Leeuwen, A.M. Cohen, B. Lisser, C. Arjeh, LiE, A Package for Lie Group Computations. Computer Algebra Nederland, Amsterdam, Université de Poitiers, 1992.